

**Modeling the Effects of Projected Sea Level Rise on Water Quality in Coastal Bangladesh**

by

Morgan Leigh Shuman

A thesis submitted to the Graduate Faculty of  
Auburn University  
in partial fulfillment of the  
requirements for the Degree of  
Master of Science in Geology

Auburn, Alabama  
May 9, 2015

Approved by

Ming-Kuo Lee, Chair, Professor of Geosciences  
James Saunders, Professor of Geosciences  
Ashraf Uddin, Professor of Geosciences

## **Abstract**

Climate models show that Bangladesh will experience high rates of change in temperature, precipitation, runoff, and local sea level rise rates by 2100. Sea level rise will result in the degradation of groundwater quality by causing vertical infiltration of brackish water from tidal channels and lateral intrusion of seawater into aquifers from the ocean. It is also likely that sea level rise will cause an increase in pH and ionic concentrations of the groundwater, which may result in the mobilization of arsenic into the water as a result of ionic competition for sorbing sites. Sea level rise maps were produced using Shuttle Radar Topography Mission data for sea level rise scenarios at 1 meter, 2 meters, and 5 meters and results indicate that populations of 28 million, 39 million, and 71 million people living in inundated zones will be affected, respectively. An examination of water quality data from the Bangladesh Water Development Board (BWDB) and British Geological Survey (BGS) wells show that the water type is highly variable, with Na-Ca-Mg-HCO<sub>3</sub> as the dominant water type and Na-Cl type in some wells close to the Bay of Bengal and tidal channels. Surface water salinity shows that all locations have a higher salinity in the dry season than in the wet season; Regional Climate Models (RCMs) and Global Climate Models (GCMs) for the region suggest that the dry seasons will become drier and wet seasons will become wetter, which is likely to exacerbate the problems of water salinization during dry seasons or droughts. Groundwater salinity distribution maps were produced for both shallow and deep wells and indicate that the shallow aquifer has a higher mean (4517 mg/l) and wider range (96 to 25,422 mg/l) of TDS concentrations than the mean (1213

mg/l) and range (123 to 8814 mg/l) of the main aquifer, suggesting widespread vertical infiltration of brackish water from tidal channels. The main aquifer has some areas with TDS concentrations under the drinking water limit, located mostly in the north and east of coastal Bangladesh. The shallow aquifer has fewer areas with TDS concentrations under the drinking water limit, and none of these areas are located in the coastal districts. Lateral saltwater intrusion models were constructed for the sea level rise scenarios and results show a saltwater wedge consistent with the shape predicted by the Ghyben-Herzberg relation. Sensitivity analysis for these models shows that saltwater intrusion can be limited by an increase in the hydraulic gradients of fresh groundwater in the southern (downgradient) direction or by the presence of a confining clay layer in the coastal region. Vertical saltwater infiltration models show that small tidal channels have a local effect with a infiltration of saline surface water into the shallow layers, whereas larger tidal channels affect a larger area and can reach the deeper layers and main aquifer. Sensitivity analysis for these models shows that the presence of a confining clay layer restricts intrusion of saline water into the deeper layers, but can cause a larger zone of diffusion in both shallow and deeper strata. Arsenic concentrations were compared to  $\text{Cl}^-$  concentrations for all BWDB wells and showed no positive correlation. While the pH or salinity effect may cause additional mobilization of arsenic in this area, the pH of wells included in this study have a mean of 7.75, which is below the arsenic desorption threshold of 8.5. It is likely that other mechanisms (e.g., bacterial reduction of iron oxides, sulfate reduction, etc.) may also affect arsenic mobilization, but the pH effect could become problematic in the future should seawater intrusion continue to drive up pH and salinity in the aquifers.

## **Acknowledgments**

I would like to extend thanks to the following members of the Geosciences Department at Auburn University for their support and academic guidance: Dr. Ming-Kuo Lee, Dr. Li Dong, Dr. Chandana Mitra, Dr. James Saunders, and Dr. Ashraf Uddin. I also would like to thank the Bangladesh Water Development Board for allowing me to use their extensive data that was central to this thesis. I thank the graduate students in the Geosciences Department for their camaraderie and endless support.

I extend gratitude to my parents, Dan and Karen Shuman, for always encouraging me to chase my dreams. I also thank my husband, Yassine Annab, for his patience and his ability to turn even my worst days into moments of optimism. Above all, I thank God for allowing me to pursue a fulfilling career.

I dedicate this thesis to the people of Bangladesh and all others around the world who are suffering the consequences of climate change.

Style manual or journal used: Water Resources Research

Computer software used: Adobe Illustrator, ArcGIS, Basin2, Microsoft Excel, Microsoft Word, Petra, Rockware AqQA

## Table of Contents

Abstract .....	i
Acknowledgments.....	iii
List of Tables .....	vii
List of Figures .....	viii
List of Abbreviations .....	xi
Introduction .....	1
Background and Previous Works .....	10
Geologic Setting .....	10
Study Area .....	13
Hydrogeology and Hydrostratigraphy .....	20
Methodology .....	22
Data Acquisition .....	22
Data Processing and Modeling .....	23
Results & Discussion .....	27
Sea Level Rise.....	27
Hydrostratigraphic Cross-Sections .....	35
Water Geochemistry .....	39
Surface Water Salinity .....	45
Groundwater Salinity .....	48

Two-Dimensional Groundwater Flow Models .....	52
Lateral Saltwater Intrusion Models.....	53
Vertical Saltwater Infiltration Models .....	59
Vertical and Lateral Infiltration Model.....	66
Arsenic Contamination .....	67
Conclusions .....	70
References .....	74
Appendix 1: Basin2 Input File, Lateral Infiltration .....	82
Appendix 2: Basin2 Input File, Vertical Infiltration .....	85

## **List of Tables**

Table 1 – Sea level rise timetable for RMSL and ESLR .....	9
Table 2 – Bangladesh and WHO water quality standards .....	46
Table 3 – Surface water salinity concentrations (TDS, mg/l) for 23 surface wells during wet and dry seasons .....	47

## List of Figures

Figure 1 – Digital elevation model (DEM) map of Bangladesh.....	3
Figure 2 – Map of population density for Bangladesh .....	4
Figure 3 – Temperature and precipitation Regional Climate Models for southeast Asia.....	7
Figure 4 – Weighted GCM for change in annual mean precipitation in mm/day.....	8
Figure 5 – Weighted GCM for change in annual mean runoff in mm/day.....	8
Figure 6 – Plot showing historical global sea level rise rates from 1880 to 2010.....	9
Figure 7 – Map showing the geographic location and tectonic setting of the Bengal Basin and surrounding region.....	11
Figure 8 – Map showing the districts, major cities, and study area in southern Bangladesh .....	14
Figure 9 – Map showing the location and names of shallow wells from 2013 BWDB report...	15
Figure 10 – Map showing the location and names of deep wells from 2013 BWDB report.....	16
Figure 11 – Map showing the location and names of surface water sampling locations from 2013 BWDB report .....	17
Figure 12 – Map showing the location and names of wells from 2001 BGS report.....	18
Figure 13 – Map showing the location and names of transects used in this study.....	19
Figure 14 – Map showing a 1 meter sea level rise for Bangladesh .....	29
Figure 15 – Map showing upazilas and major cities impacted by a 1 meter sea level rise.....	30
Figure 16 – Map showing a 2 meter sea level rise for Bangladesh .....	31
Figure 17 – Map showing upazilas and major cities impacted by a 2 meter sea level rise .....	32

Figure 18 – Map showing a 5 meter sea level rise for Bangladesh .....	33
Figure 19 – Map showing upazilas and major cities impacted by a 5 meter sea level rise .....	34
Figure 20 – Cross-section showing the stratigraphy of transect EW1 .....	36
Figure 21 – Cross-section showing the stratigraphy of transect EW2.....	36
Figure 22 – Cross-section showing the stratigraphy of transect NS1 .....	38
Figure 23 – Cross-section showing the stratigraphy of transect NS2 .....	38
Figure 24 – Piper diagram for all BWDB report wells .....	40
Figure 25 – Piper diagram for all BGS report wells, showing Na-Ca-Mg-HCO <sub>3</sub> water type ....	41
Figure 26 – Piper diagram for select wells in the shallow aquifer from the BWDB report .....	43
Figure 27 – Piper diagram for select wells in the deep aquifer from the BWDB report .....	44
Figure 28 – Plot showing surface water salinity (TDS, mg/l) for 23 surface water sampling wells during the wet season and dry season.....	46
Figure 29 – Map of the salinity distribution of the main aquifer in the dry season.....	49
Figure 30 – Map of the salinity distribution of the main aquifer in the wet season .....	49
Figure 31 – Map of the salinity distribution of the shallow aquifer in the dry season .....	51
Figure 32 – Map of the salinity distribution of the shallow aquifer in the wet season.....	51
Figure 33 – Lateral infiltration model with 1000 ppm salinity contour, 1 meter sea level rise..	54
Figure 34 – Lateral infiltration model with 1000 ppm salinity contour, 2 meter sea level rise..	54
Figure 35 – Lateral infiltration model with 1000 ppm salinity contour, 5 meter sea level rise...	55
Figure 36 – Sensitivity analysis for lateral infiltration model, 5 meter sea level rise.....	55
Figure 37 – Lateral intrusion model at 5 meter sea level rise with confining clay.....	58
Figure 38 – Vertical infiltration model, transect EW1 .....	60
Figure 39 – Vertical infiltration sensitivity analysis model, transect EW1 .....	60

Figure 40 – Vertical infiltration model, transect EW2 .....	61
Figure 41 – Vertical infiltration sensitivity analysis model, transect EW2 .....	61
Figure 42 – Vertical infiltration model, transect NS1.....	63
Figure 43 – Vertical infiltration sensitivity analysis model, transect NS1 .....	63
Figure 44 – Vertical infiltration model, transect NS2.....	65
Figure 45 – Vertical infiltration sensitivity analysis model, transect NS2 .....	65
Figure 46 – Lateral and vertical infiltration model with confining clay, transect NS3 .....	67
Figure 47 – Plot of Cl <sup>-</sup> (mg/l) v. As (µg/l) for all wells in the study area.....	68
Figure 48 – Plot of pH v. As (µg/l) for all wells in the study area .....	68

## **List of Abbreviations**

BGS	British Geological Survey
BWDB	Bangladesh Water Development Board
DEM	Digital Elevation Model
DPHE	Department of Public Health Engineering
ESLR	Effective Sea Level Rise
GBM	Ganges-Brahmaputra-Meghna
GCM	Global Climate Model
IPCC	Intergovernmental Panel on Climate Change
RCM	Regional Climate Model
RMSL	Relative Mean Sea Level
SRTM	Shuttle Radar Topography Mission
TDS	Total Dissolved Solids
UNEP	United Nations Environmental Programme
WHO	World Health Organization

## **Introduction**

Sea level rise is anticipated to be one of the largest global challenges of this century, with estimates of eustatic sea level rise ranging between 0.5 meters and 2 meters in response to a 4° C temperature rise by 2100 [Nicholls et al., 2010]. The Intergovernmental Panel on Climate Change (IPCC) fifth assessment report cites two main causes of eustatic sea level rise: (1) increased water volume in the oceans resulting from melting of the Antarctic and Greenland ice sheets and (2) thermal expansion of ocean waters in response to rising global temperatures [2014]. Other factors include changes in land water storage due to excess groundwater withdrawal and melting of land glaciers [IPCC, 2014].

Regional changes in sea level are also anticipated, and result from a variety of factors, including tectonic uplift or subsidence, changes in sedimentation rates, water-mass redistribution, changes in wind patterns, changes in air-sea heat exchange, changes in air pressure, freshwater fluxes, and ocean currents [IPCC, 2014]. The locations at highest risk of sea level rise include the coastlines of Africa and southeast Asia as well as the islands of the Pacific Ocean and Indian Ocean [Nicholls and Cazenave, 2010]. The risk to the population of these areas is immense, as the majority of people live along the coastal areas. The impacts of sea level rise are extensive, and include inundation of land, increased flood events, saltwater intrusion of surface waters and groundwater, increased erosion, and subsidence [Nicholls and Cazenave, 2010], as well as adverse effects on coastal ecosystems and biogeochemical cycles of nutrients and trace elements [Lee et al., 2013].

A recent study of global climate change vulnerability by Maplecroft, a risk-analysis firm, has identified Bangladesh as the most vulnerable country in the world with regard to sea level rise [Hume, 2013]. The majority of the country is characterized by a low-elevation, flat topography located within kilometers of either the Bay of Bengal or the Ganges-Brahmaputra-Meghna (GBM) river system (Figure 1). To complicate the issue, Bangladesh is most densely populated along its coastal and floodplain region (Figure 2) with estimates by the United Nations Environmental Programme (UNEP) that 15 million people are at risk with a scenario of 1 meter sea level rise [UNEP, 2008]. Additionally, surface water pollution from human and animal waste has left the population of Bangladesh dependent upon groundwater from shallow aquifers for drinking water. This study explored the hydrodynamics of groundwater salinization resulting from vertical and lateral seawater intrusion and how these processes may pose a significant risk to the water quality of coastal aquifers.

In addition to water quality degradation resulting from increased salinity in response to seawater intrusion, both shallow (<100 m) and main aquifers (100-300 m) in Bangladesh experience arsenic (As) contamination from natural sources that has led to the World Health Organization (WHO) naming the problem as the “largest poisoning of a population in history” [Smith et al., 2000; BGS and DPHE, 2001; Ahmed et al., 2004]. Arsenic exposure is associated with a range of significant health effects, including skin lesions [Smith et al., 2000; Mitra et al., 2002], cancer [Smith et al., 2000; Vahter et al., 2002; 2007], Type II diabetes [Navas-Acien et al., 2006; 2008], fetal loss and infant death [Sohel et al., 2010], and there is evidence of links to hypertension [Abhyankar et al., 2012]. The spatial distribution of elevated As levels is unpredictable throughout the basin [BGS and DPHE, 2001; van Geen et al., 2003; Ahmed et al.,

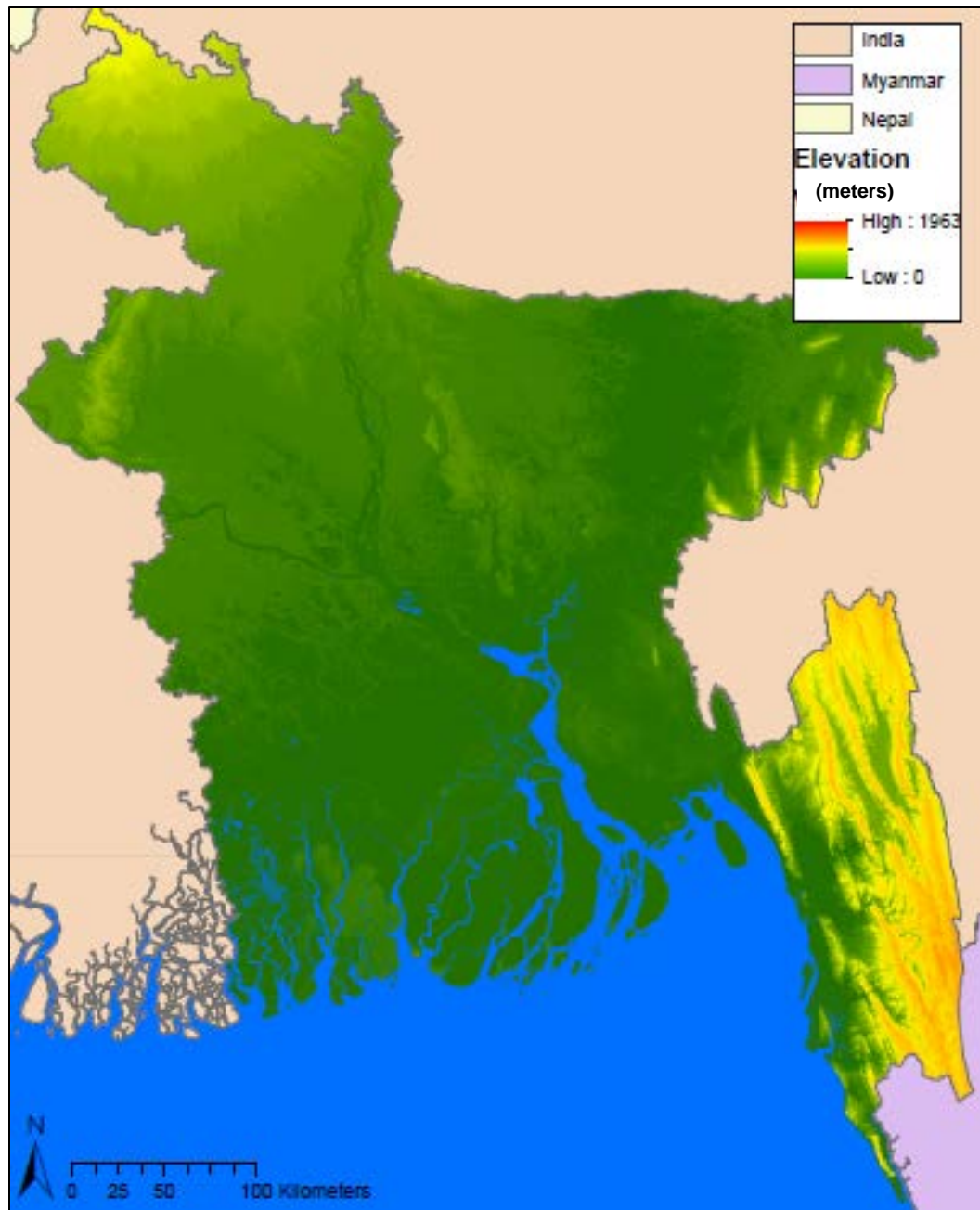


**Figure 1.** Digital elevation model (DEM) map of Bangladesh (data from WeoGeo)

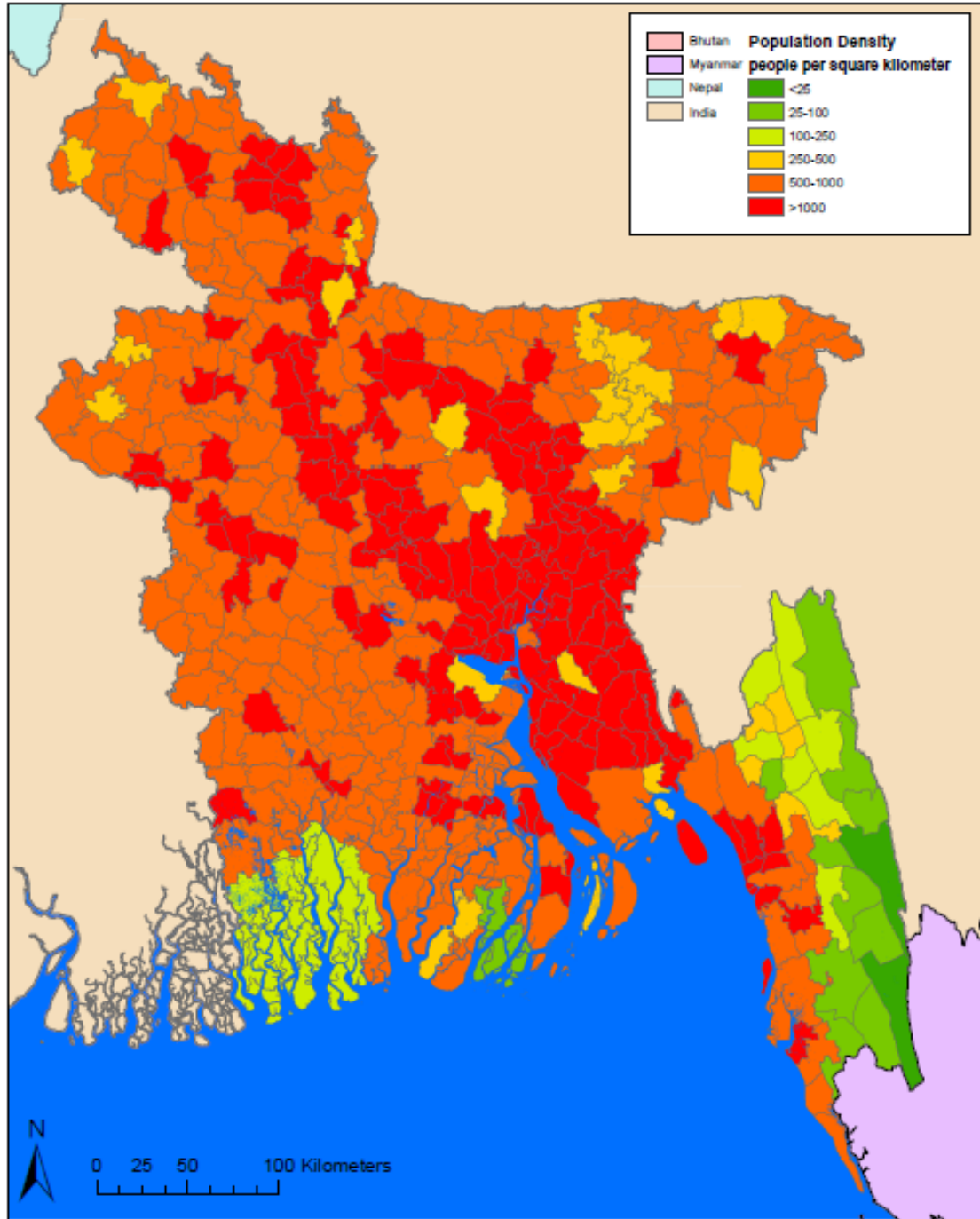


**Figure 2.** Map of population density for Bangladesh (data from WeoGeo, GADM Boundaries, and UN OCHA)

2004; Shamsudduha et al., 2009]. Variations of As concentrations that are orders of magnitude apart have been observed at different wells that are separated by only meters [BGS and DPHE, 2001; Ahmed et al., 2004]. This phenomenon has been attributed to the uneven distribution of As-rich sediments [Shamsudduha et al., 2008], the presence of Fe-reducing bacteria [Islam et al., 2004], and a shift in redox conditions over short distances [Lee et al., 2007]; however, these processes are still not fully understood [BGS and DPHE, 2001]. Lee et al. [2013] found that high ion contents in seawater lead to an increase in As mobilization due to ionic competition for sorbing sites of Fe oxides. Nath et al. [2008] also suggest that As mobilization via desorption may increase in response to pH rise and an increase in the microbial activity that drives iron reduction. This study will also focus on the potential correlation between saline groundwater in the shallow and main aquifers and As concentration.

The climate of Bangladesh is characterized by a yearly monsoon, which begins in June and ends in October and delivers 75-80% of the country's annual precipitation, with an average annual rainfall in the coastal areas of 2000 millimeters [BWDB, 2013]. The rest of the year is divided into a dry, cool season lasting from November to February and a warm, slightly wetter pre-monsoon season from March to May. Although Bangladesh is at a high risk of sea level rise, very few studies have downscaled and projected global climate models at a regional scale in the study area. The monsoon is poorly predicted in most models that otherwise perform well for southeastern Asia [Nohara et al., 2006].

A few studies based on Global climate models (GCMs) and regional climate models (RCMs) do provide some insights on climate changes in Bangladesh. Temperature is predicted to rise in a RCM for southeast Asia (Figure 3), with Bangladesh experiencing increases in excess of 2° C by 2100 [Nohara et al., 2006; Chotamonsak et al., 2011]. This estimate is consistent with

a study on the Brahmaputra basin that predicts a temperature rise of 2.3-3.5° C by 2100 [Immerzeel, 2007]. RCMs and GCMs for precipitation (Figure 3, Figure 4) and runoff (Figure 5) both predict increased trends for Bangladesh, with precipitation and runoff both increasing in excess of 1 mm/day [Nohara et al., 2006; Chotamonsak et al., 2011]. Immerzeel's work on the Brahmaputra basin supports the precipitation GCM, estimating an increase in precipitation of 14-22% by 2100 [2007]. Overall trends for the region suggest a wetter wet season and a drier dry season [Chotamonsak et al., 2011].

Local variations in sea level will depend upon regional topography, tectonics, and tides. Relative Mean Sea Level (RMSL) is a measure often used to estimate sea level rise at a local scale, and a previous study shows sea level rise increasing at a rate of 2.8 to 8.8 millimeters (mm) per year for Bangladesh [Pethick and Orford, 2013]. Effective Sea Level Rise (ESLR) is a more precise measure of sea level rise for a small region like the GBM delta, as it combines the effects of deltaic subsidence and tidal amplification with eustatic sea level rise [Pethick and Orford, 2013]. ESLR for Bangladesh ranges between 15.9 and 17.2 mm per year, which is higher than previous estimates of 14.1 mm per year [Pethick and Orford, 2013], and are much higher than the average global rate of 2-4 mm per year [Church and White, 2006] estimated from multi-century sea level records (Figure 6). Table 1 shows a timetable for RMSL and ESLR estimates for 1, 2, 5, and 10 meter rises in sea level. The authors concluded that the increase in ESLR is a direct result of anthropogenic activity, in part due to channel embankments in the Sundarbans area that increase tidal amplification.

The overarching goal of this research is to understand the relationship between climate change, sea level rise, saltwater intrusion, and groundwater quality and its implications for coastal Bangladesh.

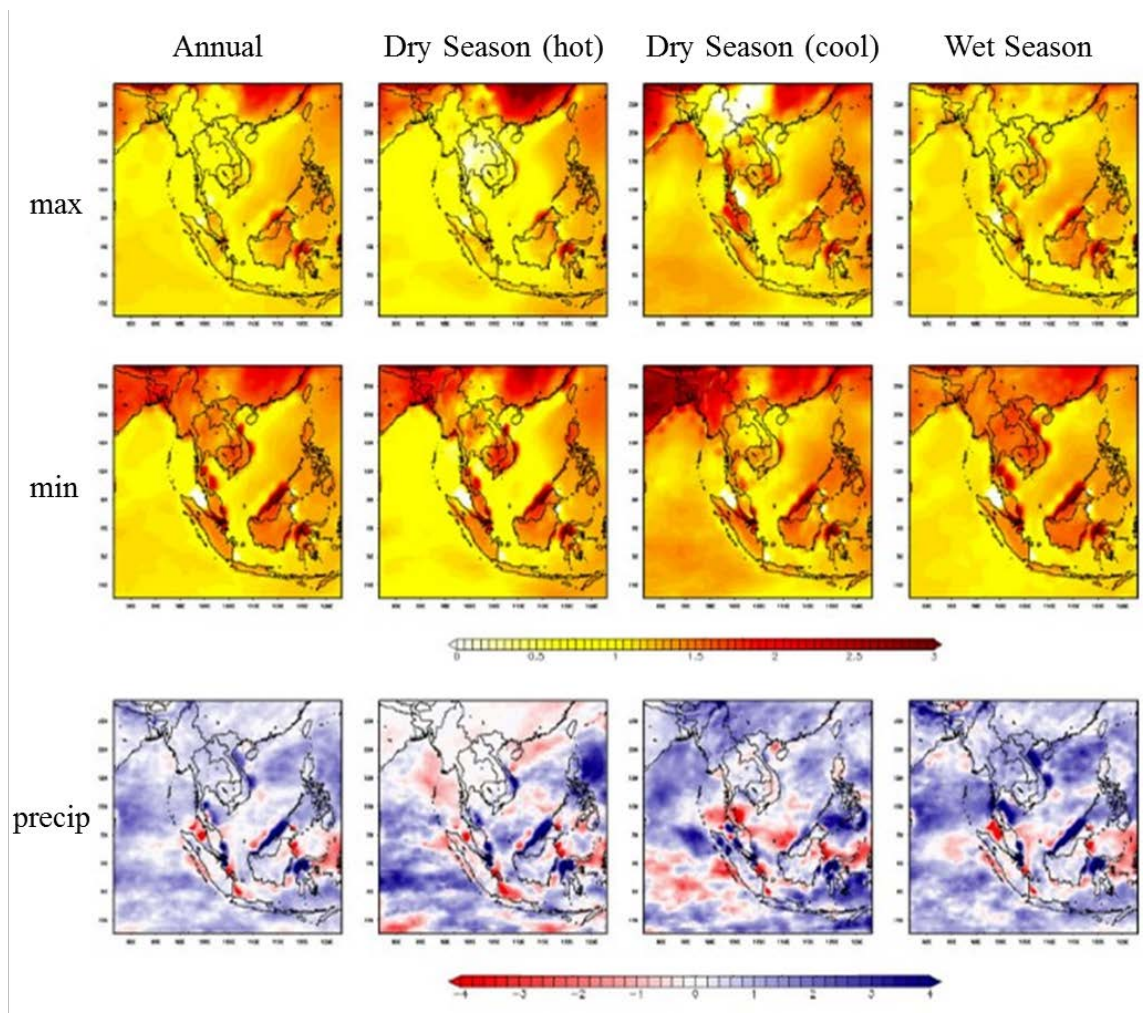


**Figure 3.** Temperature and precipitation Regional Climate Models for southeast Asia [from Chotamonsak et al., 2011]

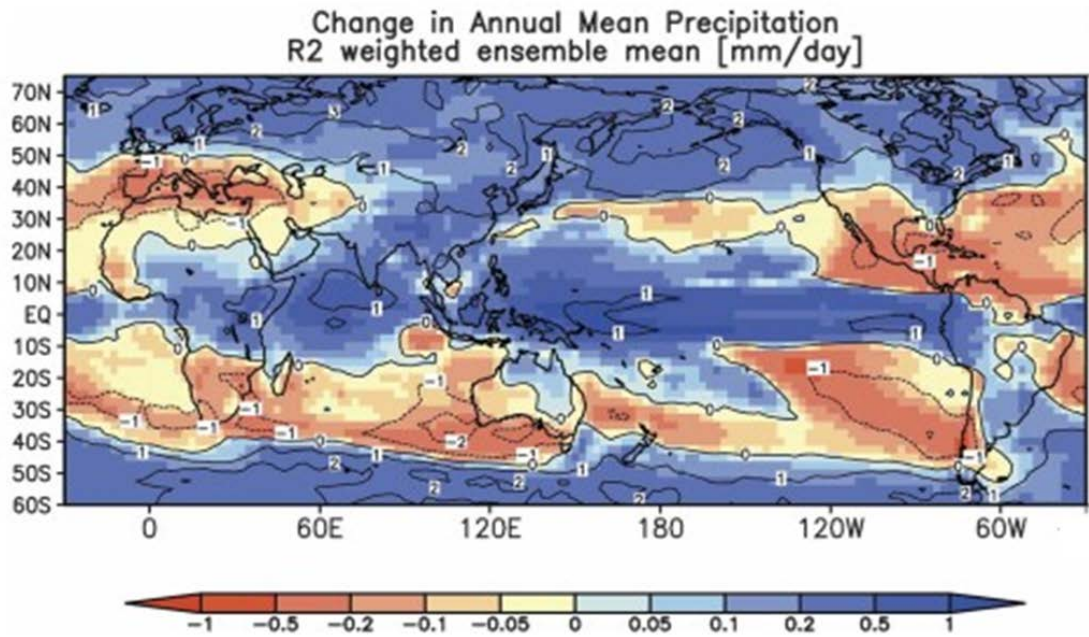
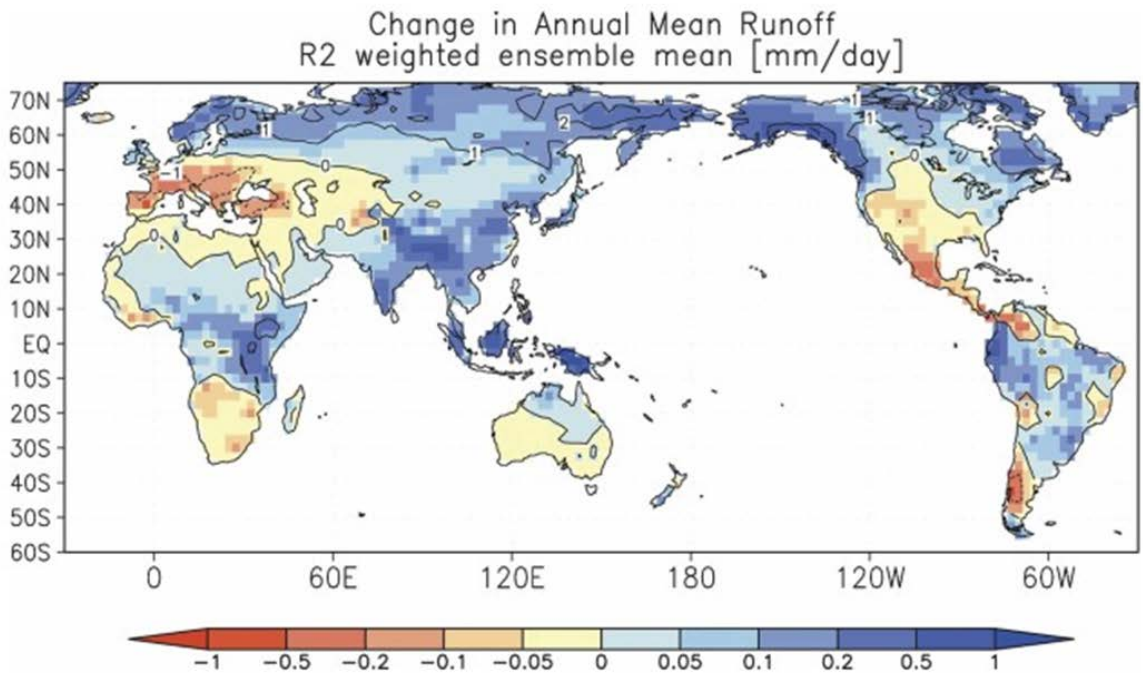


**Figure 4.** Weighted GCM for change in annual mean precipitation in mm/day [from Nohara et



al., 2006]

**Figure 5.** Weighted GCM for change in annual mean runoff in mm/day [from Nohara et al., 2006]

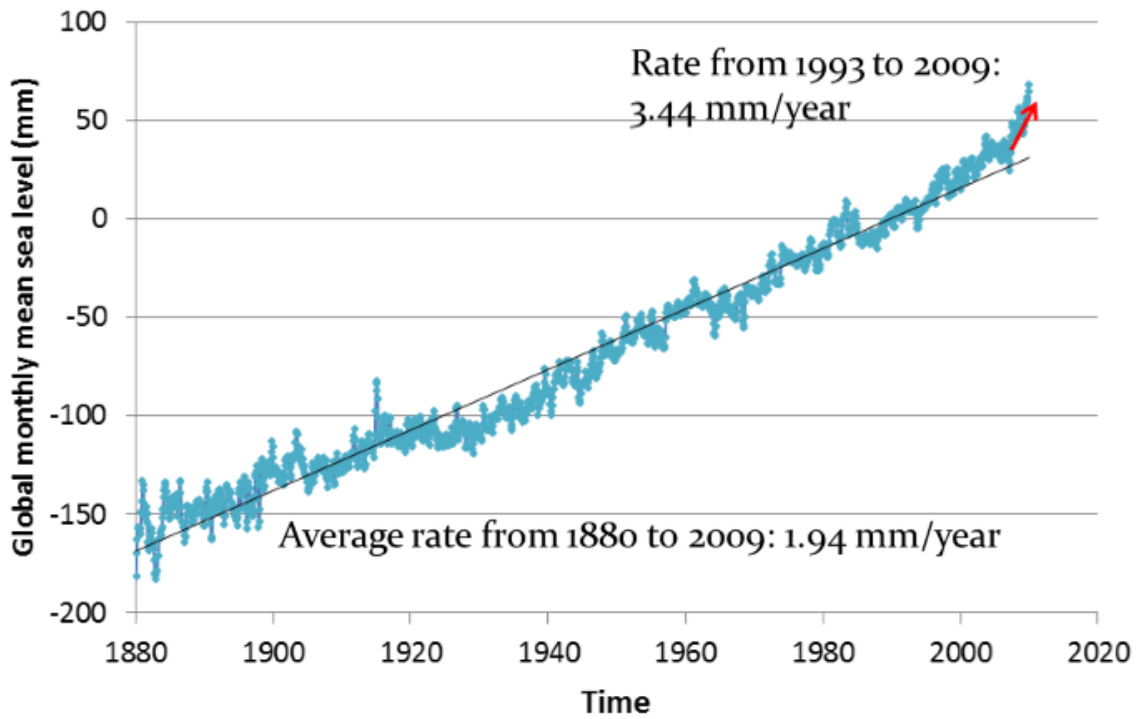


**Figure 6.** Plot showing historical global sea level rise rates from 1880 to 2010 [data from Church and White, 2006]

**Table 1.** Sea level rise timetable for RMSL and ESLR [from Pethick and Orford, 2013].

Sea Level Rise (meters)	RMSL Time (years)	ESLR Time (years)
1	110-360	58-63
2	230-710	120-130
5	570-1800	290-310
10	1100-3500	580-630

## **Background and Previous Works**

### **Geologic Setting**

The study area encompasses coastal areas of the Bengal Basin in Bangladesh (Figure 7), which is located along the active plate margin of the Indian, Tibetan (Eurasian), and Burma Plates [Uddin and Lundberg, 1998; Alam et al., 2003]. The Bengal Basin is located in eastern India and Bangladesh, bound to the north by the Shillong Plateau and to the south by the Bay of Bengal [Morgan and McIntyre, 1959; Alam et al., 2003]. The eastern limits of the basin are the Tripura and Chittagong Hills, and the western limits are defined by the Rajmahal Hills and the Indian Craton [Morgan and McIntyre, 1959; Alam et al., 2003]. The basin is subsiding as a result of tectonic activity and sediment loading from weathered Himalayan rocks [Morgan and McIntyre, 1959; Alam et al., 2003; Kuehl et al., 2005].

The Ganges, Brahmaputra, and Meghna (GBM) rivers are present in the Bengal Basin and drain into the Bay of Bengal, comprising one of the largest delta systems in the world. The country of Bangladesh is covered by 82% Holocene sediments that have been weathered from the Himalayas and transported by the GBM river system, with the remaining 18% consisting of exposed of exposed rocks that are Pliocene to Pleistocene in age and are located in the higher elevation areas in the far north and east, belonging to the Dupi Tila Group [Alam et al., 2003; BWDB, 2013]. The Ganges River originates in the Indian Himalayas and flows in a southeastern direction into Bangladesh. The Brahmaputra River originates in the Chinese Himalayas and flows parallel to the mountain range until crossing into Bangladesh, where it

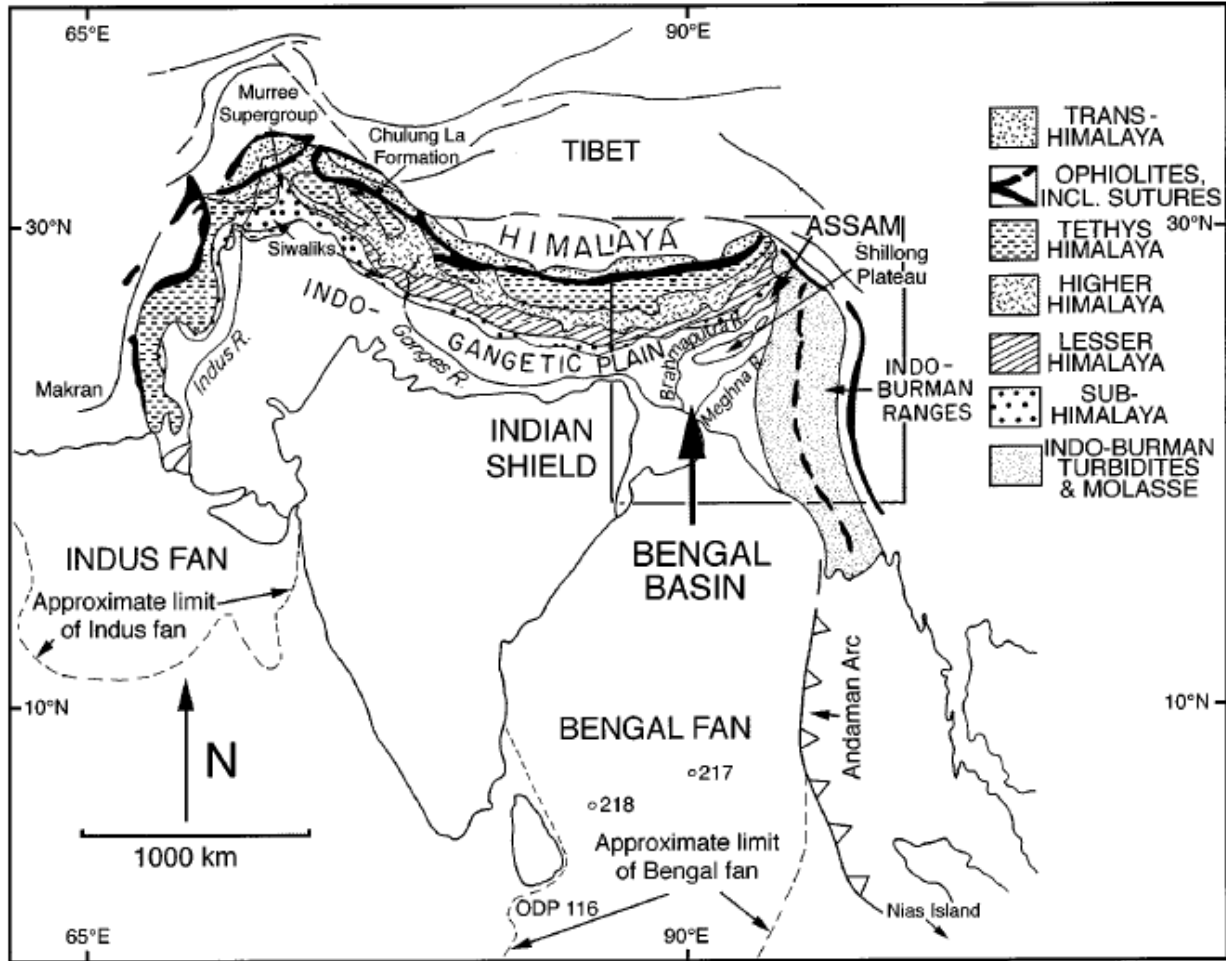


**Figure 7.** Map showing the geographic location and tectonic setting of the Bengal Basin and surrounding region [from Uddin and Lundberg, 1998]

flows south. The Meghna River originates in eastern India and flows southwest into Bangladesh. The three rivers converge south of Dhaka and drain into the Bay of Bengal through a system of smaller stream channels that are tidally-influenced. The southwestern region of the delta system includes the Sundarbans Mangrove Forest, which stretches from India to Bangladesh. The Sundarbans region is sensitive to climate change and sea level rise due to its low elevation. The region is renowned for its biodiversity, particularly because it is home to the endangered Bengal tiger species.

Deposition of As-rich Holocene sediments into the Bengal Basin from weathering of the Himalayas is considered to be the main source of As present in the groundwater [Bhattacharya et al., 1997; BGS and DPHE, 2001; Ahmed et al., 2004; Saunders et al., 2005]. Arsenic has been mobilized into the groundwater from minerals (i.e., Fe- and Mn- oxyhydroxides) due to the moderately reducing geochemical conditions present in the region. Reducing conditions have resulted from the deposition and decomposition of organic matter with weathered Himalayan material, capped by a layer of silt and/or clay [Bhattacharya et al., 1997; BGS and DPHE, 2001]. These conditions allow Fe-reducing bacteria to reduce As to trivalent arsenite [As(III)] or pentavalent arsenate [As(V)]; both chemical species are present in the groundwater of Bangladesh [BGS and DPHE, 2001]. Higher As concentrations are present in shallow aquifers that contain Holocene sediments, whereas low As concentrations are present in deeper Pliocene-Pleistocene aquifers. This inconsistency may be due to a different composition of the sediments, or a result of the slow flushing rates in shallow aquifers that have existed since the warm Holocene period with high sea level stand [BGS and DPHE, 2001; Shamsudduha et al., 2008; Lee et. al., 2013].

## Study Area

The study area for this research is located in southern coastal Bangladesh (Figure 8). The red box shown in Figure 8 is bound by latitudes 21° N to the south and 23.5° N to the north, and 89° E to the west and 92.4° E to the east. The area is characterized by a flat topography with the elevation generally below 20 meters relative to sea level, with the exception of the Chittagong Hill Tracts in the east. The GBM rivers drain through an extensive delta that is tidally-influenced. Seawater has invaded many intertidal channels and caused widespread water salinization issues. The cities of Dhaka and Chittagong are contained within the study area.

The Bangladesh Water Development Board [BWDB] has established a groundwater and surface water monitoring network along coastal Bangladesh; this network provides long-term hydrological data to monitor and assess any changes in water quality and quantity. Data from a total of 85 BWDB groundwater sampling locations from 19 districts are included in this study. These locations are split into three groups: 32 shallow wells (Figure 9), 30 deep wells (Figure 10), and 23 surface water sampling locations (Figure 11). Shallow wells are wells with a water sampling depth screened in the shallow (1<sup>st</sup>) aquifer, ranging between 20 m and 152 m; deep wells have a water sampling depth in the main (2<sup>nd</sup>) aquifer, ranging between 177 m and 335 m. Water quality and salinity data are also available for surface water samples collected from tidal channels, beaches along the Bay of Bengal, and small ponds. The British Geological Survey also conducted a large study on As contamination in southern Bangladesh and used a network of BWDB wells (Figure 12) in their report; these wells are used in the current study for piper diagrams to examine main hydrochemical facies based on major ions. Four transects and

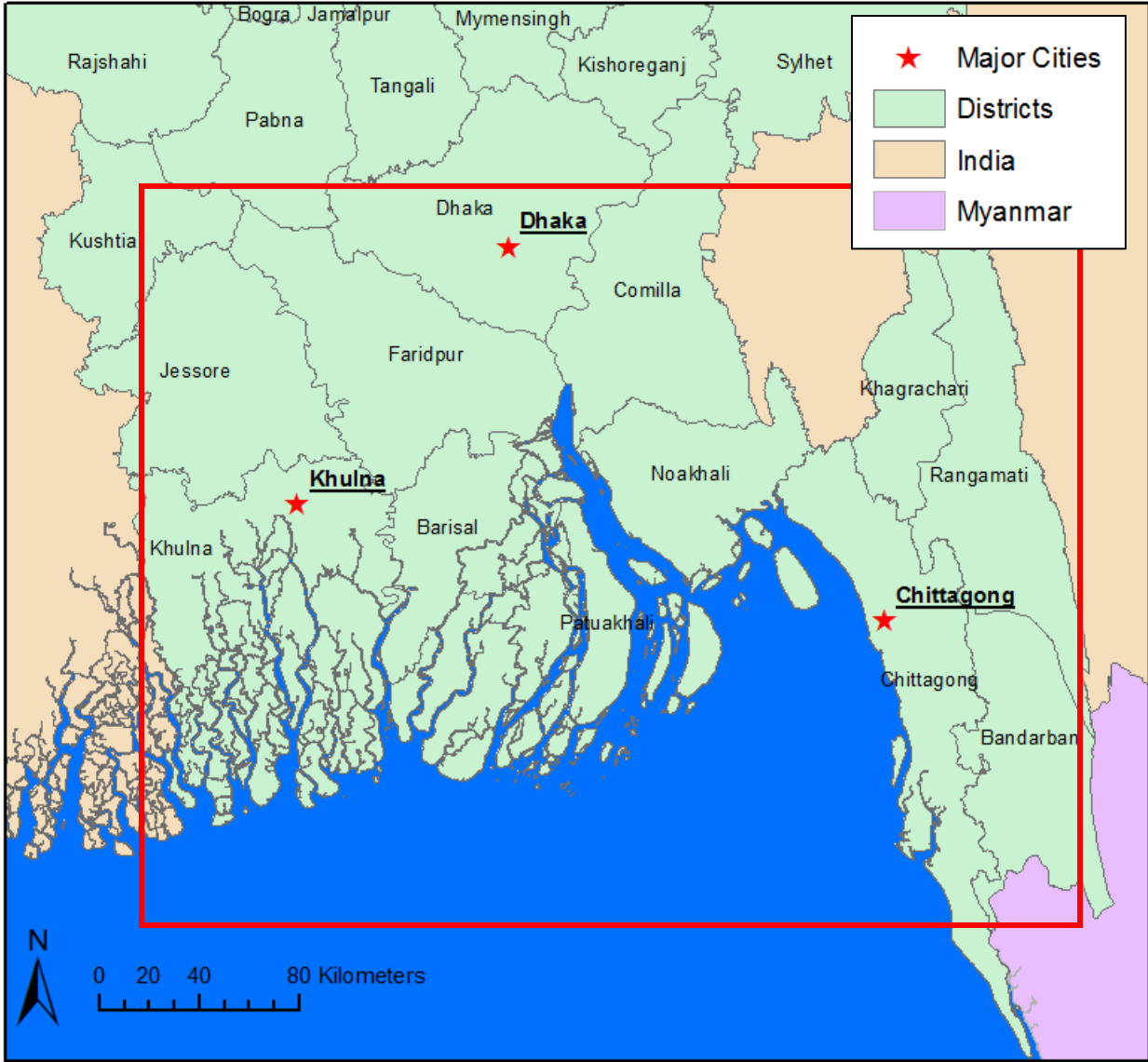


**Figure 8.** Map showing the districts, major cities, and study area in southern Bangladesh

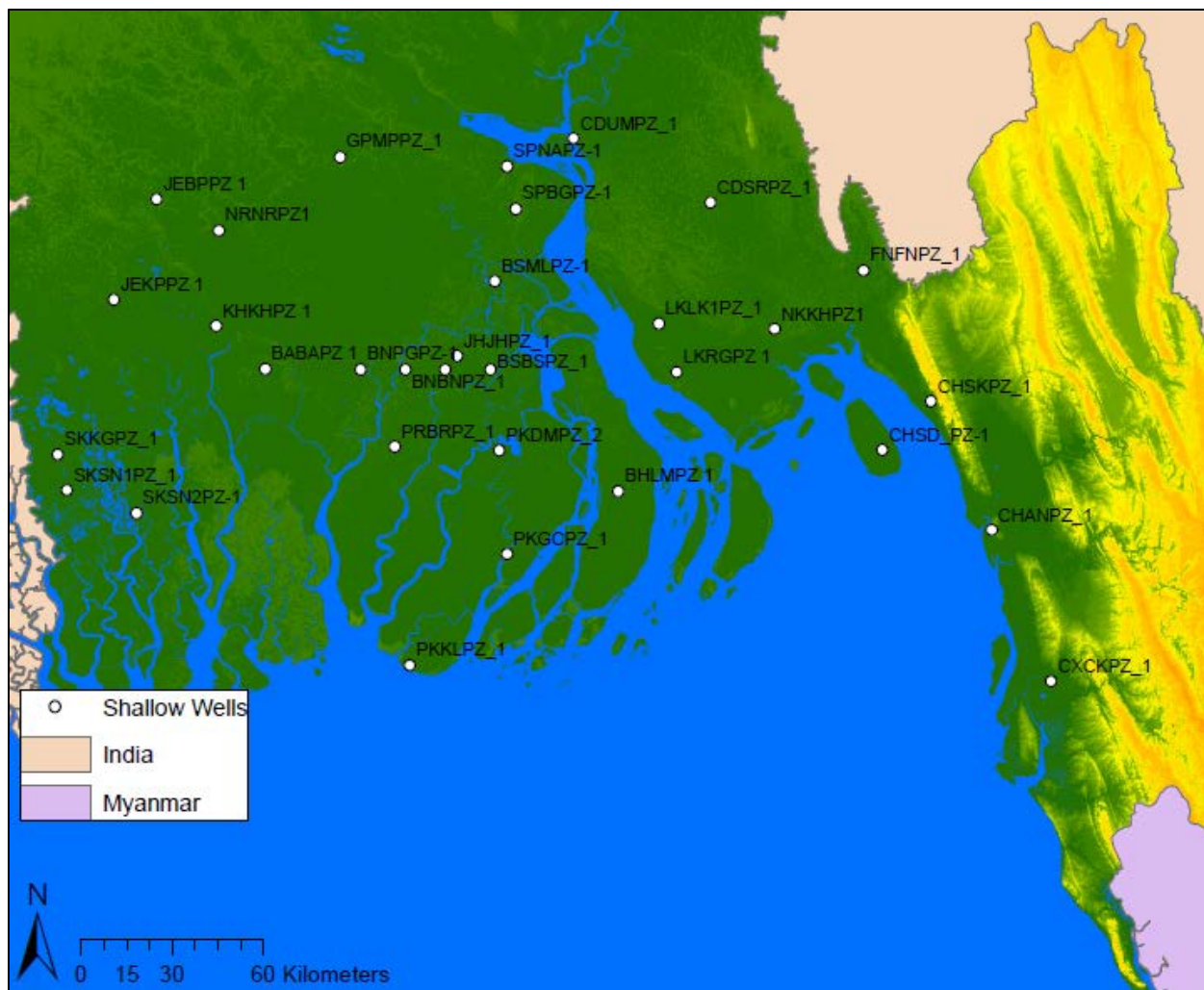


**Figure 9.** Map showing the location and names of shallow wells from 2013 BWDB report

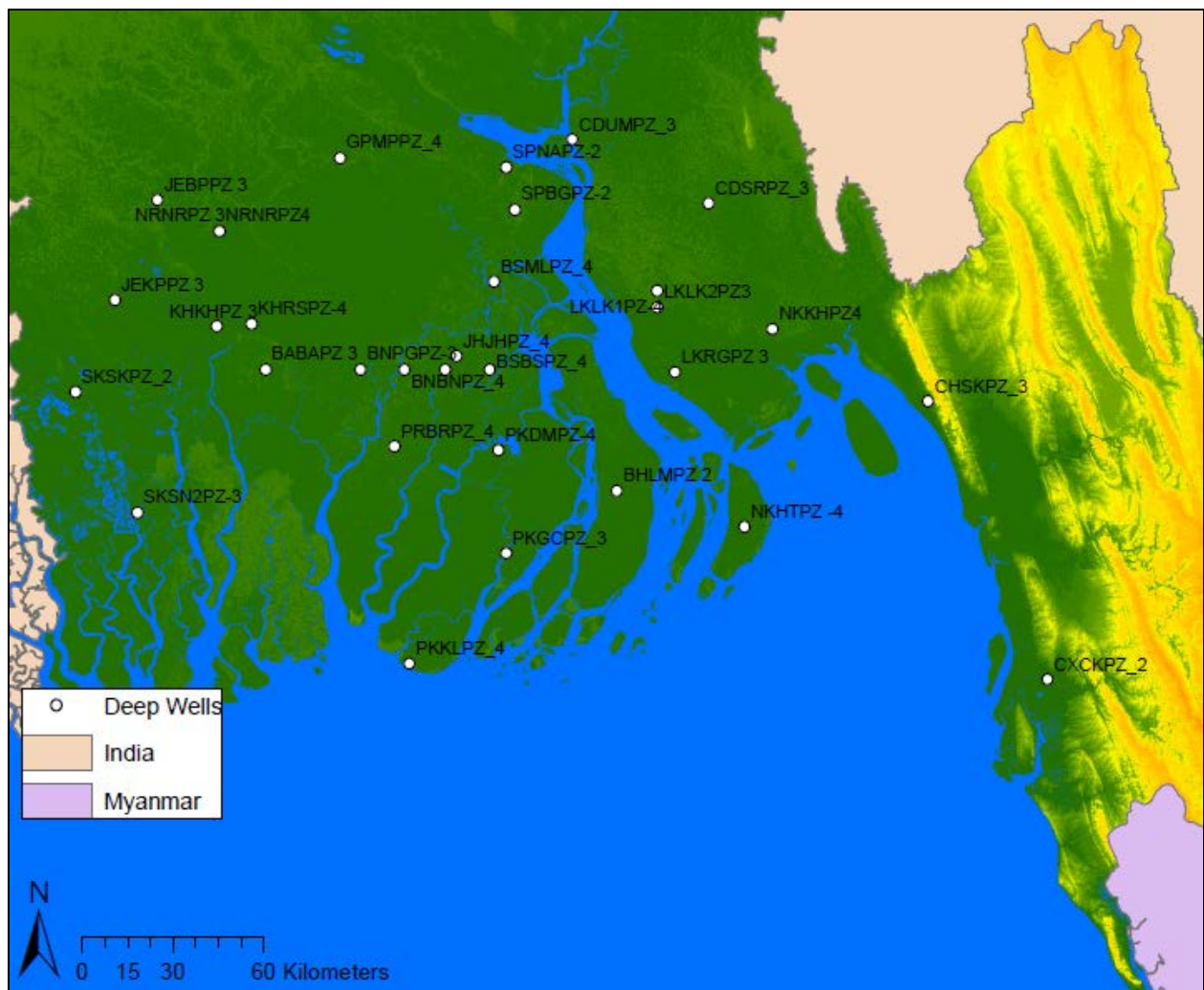


**Figure 10.** Map showing the location and names of deep wells from 2013 BWDB report

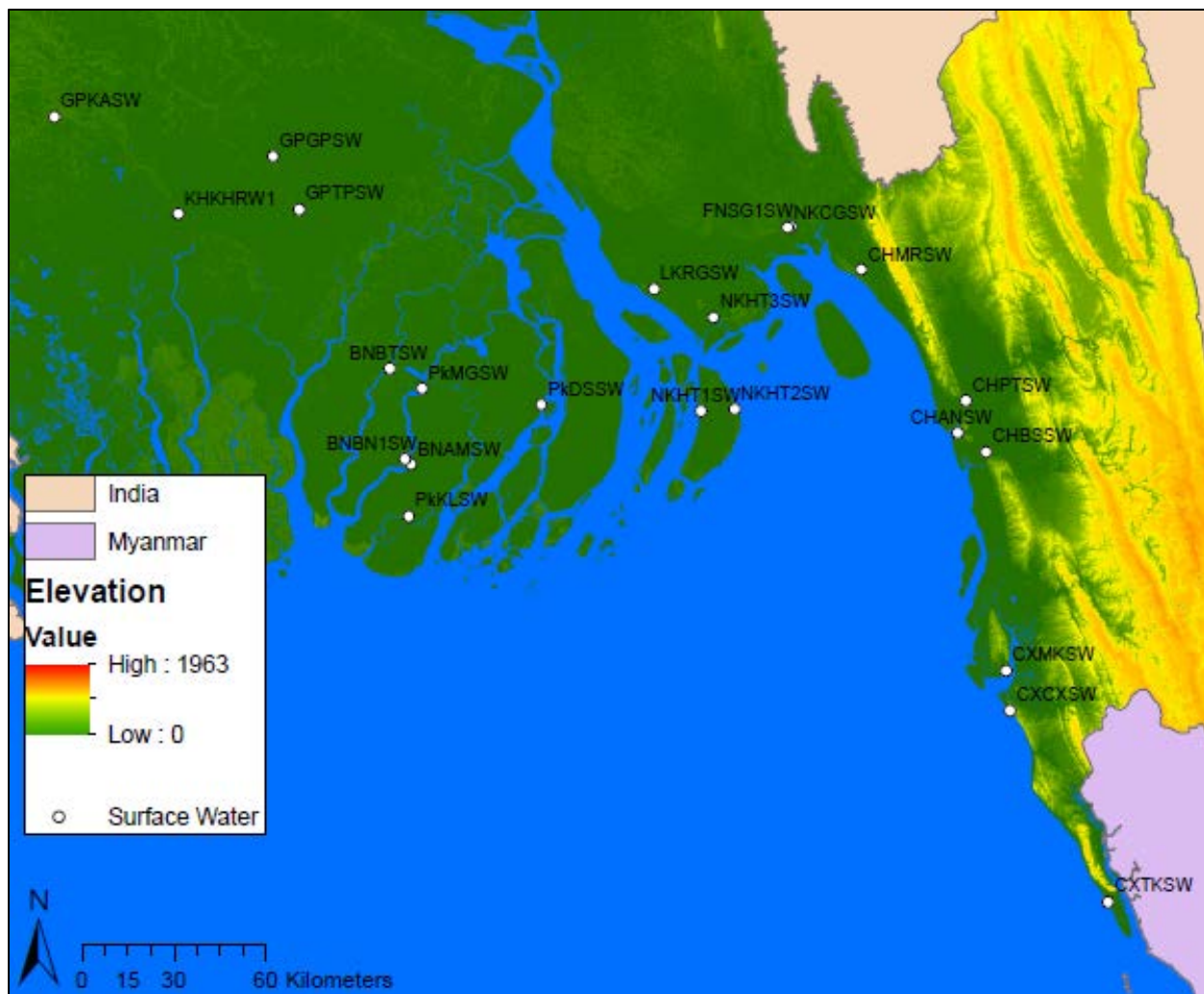


**Figure 11.** Map showing the location and names of surface water sampling locations from 2013 BWDB report

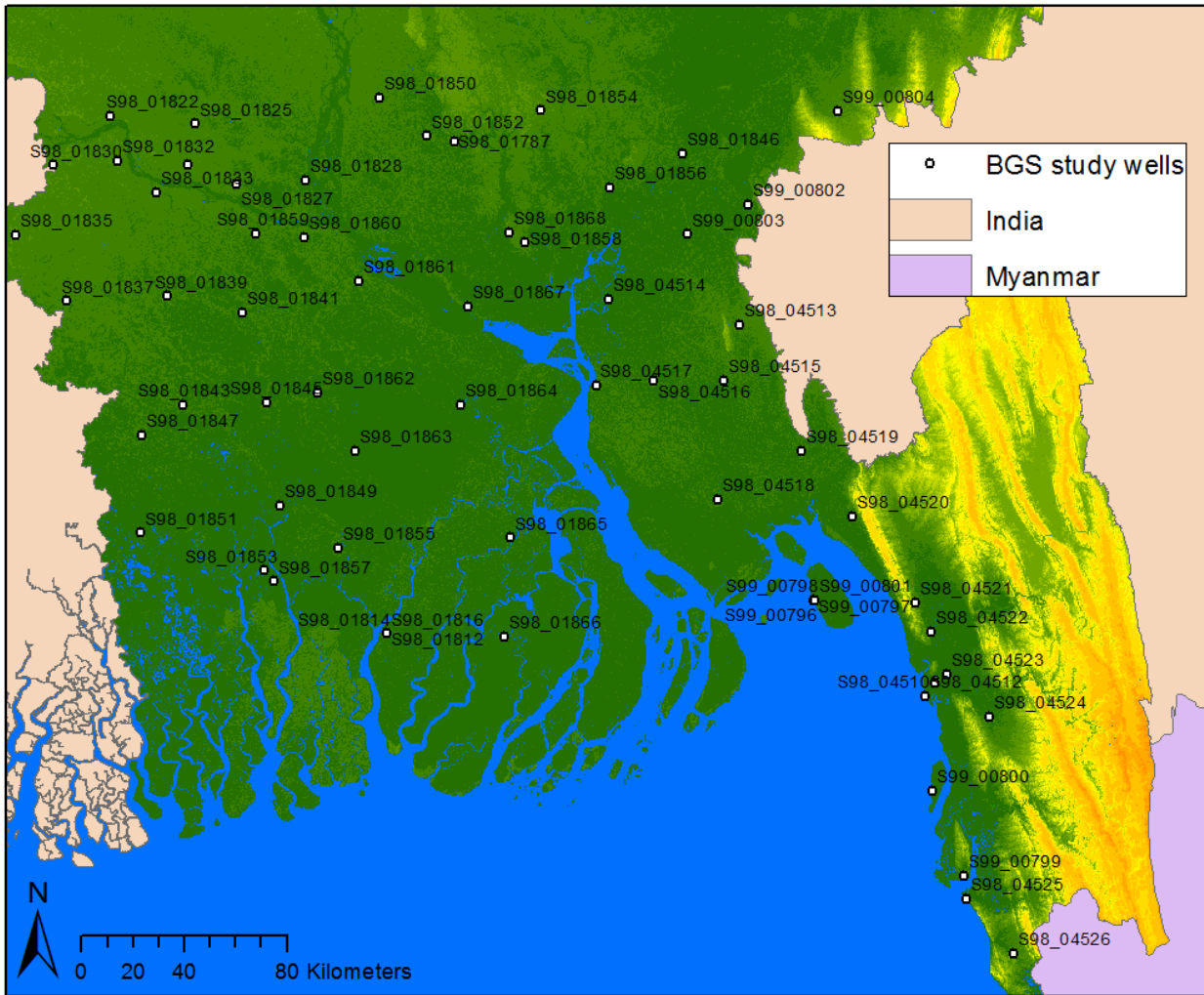


**Figure 12.** Map showing the location and names of wells from 2001 BGS report

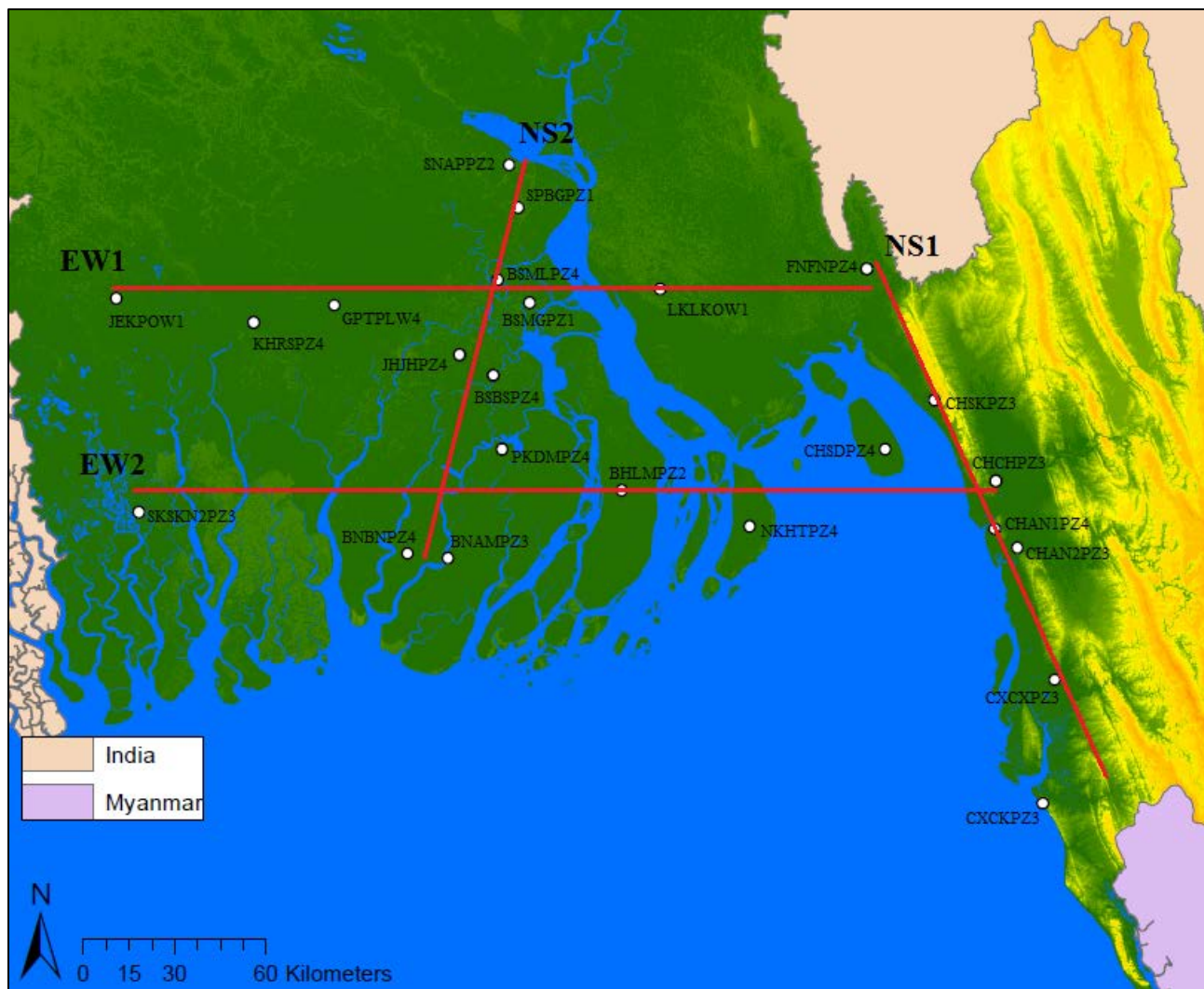


**Figure 13.** Map showing the location and names of transects used in this study

associated hydrostratigraphy were re-constructed from surface to deep wells for two-dimensional groundwater and saltwater intrusion modeling (Figure 13). These transects are named EW1, EW2, NS1, and NS2. EW1 extends from the Jessore district in the east to the Feni district in the west. The transect is 228 kilometers long and includes data from 6 wells: JEKPOW1, KHRSPZ4, GPTPLW4, BSBSPZ4, LKWKOW1, and FNFNPZ4. EW2 extends from the Satkhira district in the east to the Chittagong district in the west. The transect is 261 kilometers long and includes data from 7 wells: SKSKN2PZ3, JHJHPZ4, PKDMPZ4, BHLMPZ2, NKHTPZ4, CHSDPZ4, and CHCHPZ3. NS1 is 180 kilometers in length and extends from the Feni district in the north to the Cox's Bazar district in the south. The transect includes data from 7 wells: FNFNPZ4, CHSKPZ3, CHCHPZ3, CHAN1PZ4, CHAN2PZ3, CXCXPZ3, and CXCKPZ3. Transect NS2 is 135 kilometers long and extends from the Shariatpur district in the north to the Barguna district in the south, and NS2 includes data from 9 wells: SNAPPZ2, SPBGPZ1, BSMLPZ4, BSMGPZ1, JHJHPZ4, PKDMPZ4, BSBSPZ4, BNBNPZ4, and BNAMPZ3. The transect includes data from 7 wells: FNFNPZ4, CHSKPZ3, CHCHPZ3, CHAN1PZ4, CHAN2PZ3, CXCXPZ3, and CXCKPZ3. Transect NS2 is 135 kilometers long and extends from the Shariatpur district in the north to the Barguna district in the south, and NS2 includes data from 9 wells: SNAPPZ2, SPBGPZ1, BSMLPZ4, BSMGPZ1, JHJHPZ4, PKDMPZ4, BSBSPZ4, BNBNPZ4, and BNAMPZ3.

### **Hydrogeology and Hydrostratigraphy**

The hydrogeology of the Bengal Basin has been studied extensively, particularly with respect to the issue of arsenic contamination [BGS and DPHE, 2001]. Regional equipotential maps and groundwater models have shown that the area has groundwater flow in a general north-

to-south direction that is controlled by topography, with little influence from seasonal changes in the water level on regional groundwater movement [BGS and DPHE, 2001; Shamsudduha et al., 2008; Michael and Voss, 2009; Zahid et al., 2014]. However, local streams may change from a gaining stream to a losing stream in response to the decline of the groundwater table during dry seasons. The Bangladesh Water Development Board reports a hydraulic conductivity of 1-25 m/day for the shallow (1<sup>st</sup>) aquifer and 1-9 m/day for the main (2<sup>nd</sup>) and deep (3<sup>rd</sup>) aquifers in the coastal region [BWDB, 2013]. Transmissivity ranges between 100-2300 m<sup>2</sup>/day for the 1<sup>st</sup> aquifer, 100-2200 m<sup>2</sup>/day for the 2<sup>nd</sup> aquifer, and 100-1600 m<sup>2</sup>/day for the 3<sup>rd</sup> aquifer; values for transmissivity are highly variable due to the difficulty in estimating aquifer thicknesses throughout the region [BWDB, 2013].

The stratigraphy within the study area is highly variable and is comprised of interbedded sand, silt, and clay layers. Throughout most of the region, a clay-rich top layer of Holocene sediments overlays a Pliocene sandy layer [BWDB, 2013]. Three sandy aquifers with clay lenses have been defined, with the 1<sup>st</sup> shallow aquifer present at depths from 20 to 100 m, the 2<sup>nd</sup> main aquifer present between 100 to 250 m, and the 3<sup>rd</sup> deep aquifer locally present at depths exceeding 300m. The semi-confined aquitard between the 1<sup>st</sup> and 2<sup>nd</sup> aquifers is locally leaky and contains stratified interconnected, unconfined water-bearing zones [BWDB, 2013]. The 1<sup>st</sup> aquifer consists of mostly brackish water with isolated freshwater lenses and is rarely used for drinking water or irrigation, and the 2<sup>nd</sup> aquifer is the main source of drinking water [BWDB, 2013]. The present study focuses on the water quality of the 1<sup>st</sup> and 2<sup>nd</sup> aquifers. Several north-south and east-west cross-sections were reconstructed by Petra and Basin2 software (see Results section) based on lithological logs from the BWDB report.

## Methodology

### Data Acquisition

Geologic and hydrologic data for this study were acquired from a 2013 report by the Bangladesh Water Development Board [BWDB, 2013]. This extensive report includes geologic, hydrologic, and geochemical data for 42 nested wells, 102 line wells, 690 lithological logs, 20 aquifer pump tests, 108 slug tests, and 1100 groundwater and surface water quality samples collected from 140 upazilas along the southern coastal region of Bangladesh [BWDB, 2013]. The present study focuses on data from 62 nested and line wells and their corresponding lithological logs, as well as data from 23 surface wells.

Water quality data are also available for all of these sampling locations and were collected in both dry and wet seasons. Data used in the current study include total dissolved solids (TDS), major ions ( $\text{Ca}^{2+}$ ,  $\text{Mg}^{2+}$ ,  $\text{Na}^+$ ,  $\text{K}^+$ ,  $\text{Cl}^-$ ,  $\text{CO}_3^{2-}$ ,  $\text{HCO}_3^-$ , and  $\text{SO}_4^{2-}$ ), and arsenic concentrations in a few selected wells. Samples were analyzed for TDS and other water quality and redox-sensitive parameters (temperature, pH, Eh, and electrical conductivity) in the field using a mobile hand-held meter to avoid changes of these parameters during sample transportation and storage [BWDB, 2013]. Water samples were analyzed for major ions using atomic absorption spectrophotometry and ultraviolet-visible (UV-VIS) spectrophotometry at BWDB facilities and were cross-checked for precision at facilities of the Department of Public Health Engineering and Department of Geology at the University of Dhaka. Additional data for major ions were acquired from Phase 2 study by the British Geological Survey using the BWDB network of wells [BGS and DPHE, 2001].

Digital data for surface elevation and sea level rise maps were acquired from preprocessed data published by WeoGeo Market. The data are acquired from NASA's Shuttle Radar Topography Mission (SRTM), which conducted a near-global scale elevation mapping project since February 2000. The data are 3 arc-second (90 meter) surface elevation, and preprocessing was conducted to adjust for single pixel errors. Country border data were acquired as shapefiles from the GADM Global Administrative Areas database. Population data for Bangladesh were from the 2001 census and were obtained from the United Nations Office for the Coordination of Humanitarian Affairs [UNOCHA, 2014].

### **Data Processing and Modeling**

Data processing and hydrologic modeling were conducted using a variety of computer software programs, including ArcGIS, AqQA, Basin2, and Petra. ArcGIS was used for sea level rise analysis, Basin2 for modeling groundwater flow and lateral and vertical solute (salt) transport, AqQA for hydrochemical facies analysis, Microsoft Excel for surface water salinity distribution, and Petra for groundwater salinity distributions.

ArcGIS and digital elevation models (DEMs) from SRTM data were used to identify and quantify areas of inundation under sea level rise scenarios of 1, 2, and 5 meters. This was performed by using raster reclassification to highlight areas that would be inundated where surface elevations are lower than projected sea level. Sea level rise scenario layers were added to the map, and the populations of affected upazilas was added to find the total affected population in each sea level rise scenario.

A basin hydrology model Basin2 [Bethke et al., 2003] was used as the primary tool for constructing two-dimensional stratigraphic sections and for modeling groundwater flow and

saltwater intrusion processes. The program can model groundwater flow driven by topographic relief, compaction, density variation and solute (salt) transport by advection, diffusion, and mechanic dispersion using the following equation:

$$\frac{\partial}{\partial t}(C) = \frac{\partial}{\partial x}D_x\left(\frac{\partial C}{\partial x}\right) + \frac{\partial}{\partial z}D_z\left(\frac{\partial C}{\partial z}\right) - q_x\left(\frac{\partial C}{\partial x}\right) - q_z\left(\frac{\partial C}{\partial z}\right) \quad (1)$$

where  $C$  is concentration ( $\text{mol cm}^{-3}$ ),  $q$  is specific discharge ( $\text{cm sec}^{-1}$ ),  $t$  is time (sec), and  $D$  is hydrodynamic dispersion ( $\text{cm}^2 \text{sec}^{-1}$ ), which accounts for molecular diffusion of solutes as well as mechanical dispersion. The model calculates the coefficients of hydrodynamic dispersion  $D_x$  and  $D_z$  from the following equations:

$$D_x = D^* + \alpha_{LV_z}' + \alpha_{TV_x}' \quad (2)$$

$$D_z = D^* + \alpha_{LV_z}' + \alpha_{TV_x}' \quad (3)$$

where  $D^*$  is the diffusion constant ( $\text{cm}^2 \text{sec}^{-1}$ ),  $\alpha_L$  and  $\alpha_T$  are the dispersivities (cm) in the longitudinal and transverse directions, and  $v_x'$  and  $v_z'$  are lateral and vertical fluid flow velocities ( $\text{cm sec}^{-1}$ ) in curvilinear coordinates.

Input files for generating groundwater flow and saltwater intrusion along transects can be found in Appendices 1 and 2. The hydrologic system was simulated as steady-state conditions, assuming groundwater flow and salinity distribution has fully adjusted to defined boundary conditions, including topography relief (water table configurations) relative to sea level and fixed salinity of ocean and surface water in tidal channels. The program maps an irregular basin cross section into a finite difference grid. The modeling grid was set with 40 nodes in the x-direction (along stratigraphy) and the average width of nodes in the z-direction (perpendicular to stratigraphy) was set to 20 m. Stratigraphic units were defined based on their sediment composition, which was calculated using mathematical weighted averages from the lithological

logs from the BWDB report. The time of deposition was calculated using an average sedimentation rate of about 9.5 mm per year [Michels et al., 1998].

Rising sea level can cause lateral and vertical infiltration of saltwater into freshwater-bearing aquifers near the coast and along the tidal river channels, respectively. Lateral infiltration models were constructed along the north-south transect NS2 (Figure 16) by setting a salinity concentration of 0.5 molal of surface seawater and 0 modal for land surface exposed to freshwater recharge. In sensitivity analysis, the freshwater table heights (corresponding to surface topographic elevation), relative to sea level, were adjusted lower based on varying sea level rise scenarios of 1 meter, 2 meters, and 5 meters. Sensitivity analysis was also performed by increasing the slope of the “water depth” variable, which increase the hydraulic gradients that push the front of saltwater back toward the ocean. Vertical infiltration models were constructed for all east-west and north-south transects (Figures 13-16) by setting a salinity concentration of 0.5 molal for surface water in tidal channels (assuming seawater invades and occupy water columns along channels) that intersect the transects. Sensitivity analysis was performed by adding a low-permeability ( $k = 10^{-8}$  darcy) confining clay layer below the uppermost aquifer impacted by saline surface water. This sensitivity analysis was used to test the hypothesis that the presence of low-permeability clay confining layer may block or limit the downward vertical infiltration of saline water into deeper aquifers, which may explain higher water salinity in the shallow aquifer than in the deep aquifer. One additional sensitivity analysis was performed by combining lateral and vertical infiltration models to most accurately represent real-world conditions.

Rockware software program AqQA was used to construct piper diagrams for analyzing the distribution of groundwater hydrochemical facies influenced by sediment-water interaction

and saltwater intrusion. Four piper diagrams were constructed; one for all BWDB wells, one for all BGS wells, one for select shallow BWDB wells to show the effects of vertical infiltration, and one for select deep BWDB wells to show the effects of lateral intrusion.

Petra was used to create salinity isosurface maps to determine the salinity distribution throughout the study area. Maps were produced using data from dry and wet seasons for both shallow and deep wells. TDS values (in mg/L) were used to create zones and maps were produced using nearest neighbor interpolation to create and contour grids in the mapping module. Grids of data were exported and maps were produced using ArcGIS.

## **Results and Discussion**

### **Sea Level Rise**

Sea level rise impacted maps showing areas inundated were produced for the entire country of Bangladesh at different sea level rise scenarios of 1 meter, 2 meters, and 5 meters; the ESLR models predict these sea level rise to occur in the next 58-63 years, 120-130 years, and 290-210 years in Bangladesh, respectively (Table 1).

With a 1 meter rise in sea level, there will be significant coastal flooding, particularly in southwestern Bangladesh (Figure 14). 107 upazilas have areas that become inundated (Figure 15), and the total population living in these areas exceeds 28,000,000. Floodplains of the GBM river system away the coast also begin to show inundation, particularly along the Ganges River, and to a lesser degree, along the Meghna River. The major cities of Chittagong and Dhaka have minor areas inundated.

At 2 meters of sea level rise, much of southwestern coastal Bangladesh is inundated (Figure 16), while the coastal districts to the east of the GBM river bordered by Shillong Plateau and Indo-Burman Ranges remain largely above projected sea level due to higher surface elevation. The total estimated population in this scenario may reach as much as 39,000,000 in 149 upazilas (Figure 17). The flooding in this scenario begins to extend in the general directions to the north and northwest, with wide areas along the Ganges River and associated stream channels occupied by seawater. The islands along the Bay of Bengal also exhibit significant inundation, which would also be further complicated by increased erosion in these areas. The cities of

Chittagong and Dhaka continue to see increasing inundation in some areas. The floodplains of the three major GBM Rivers show different degree of flooding, with most significant impacts occurring along the Ganges and Meghna river channels.

At a sea level rise of 5 meters, much of southern Bangladesh is inundated in this worst case scenario (Figure 18), with over 71,000,000 people living in the 264 affected upazilas (Figure 19). All of southwestern coastal Bangladesh except for the southernmost islands is flooded, and the area of inundation extends almost completely to the Ganges. The southern and central coastal islands will also disappear. The coastal districts to the east of the GBM Rivers bordered by higher lands of Indo-Burman Ranges begin to show significant flooding. Major flooding occurs in the large cities of Dhaka and Chittagong, and the areas adjacent to the GBM rivers also experience substantial land loss. Interestingly, the eastern Sundarbans area along the southwest coast, with average land surface ranging from 6 to 11 meters, remain above sea level in this worst case scenario.

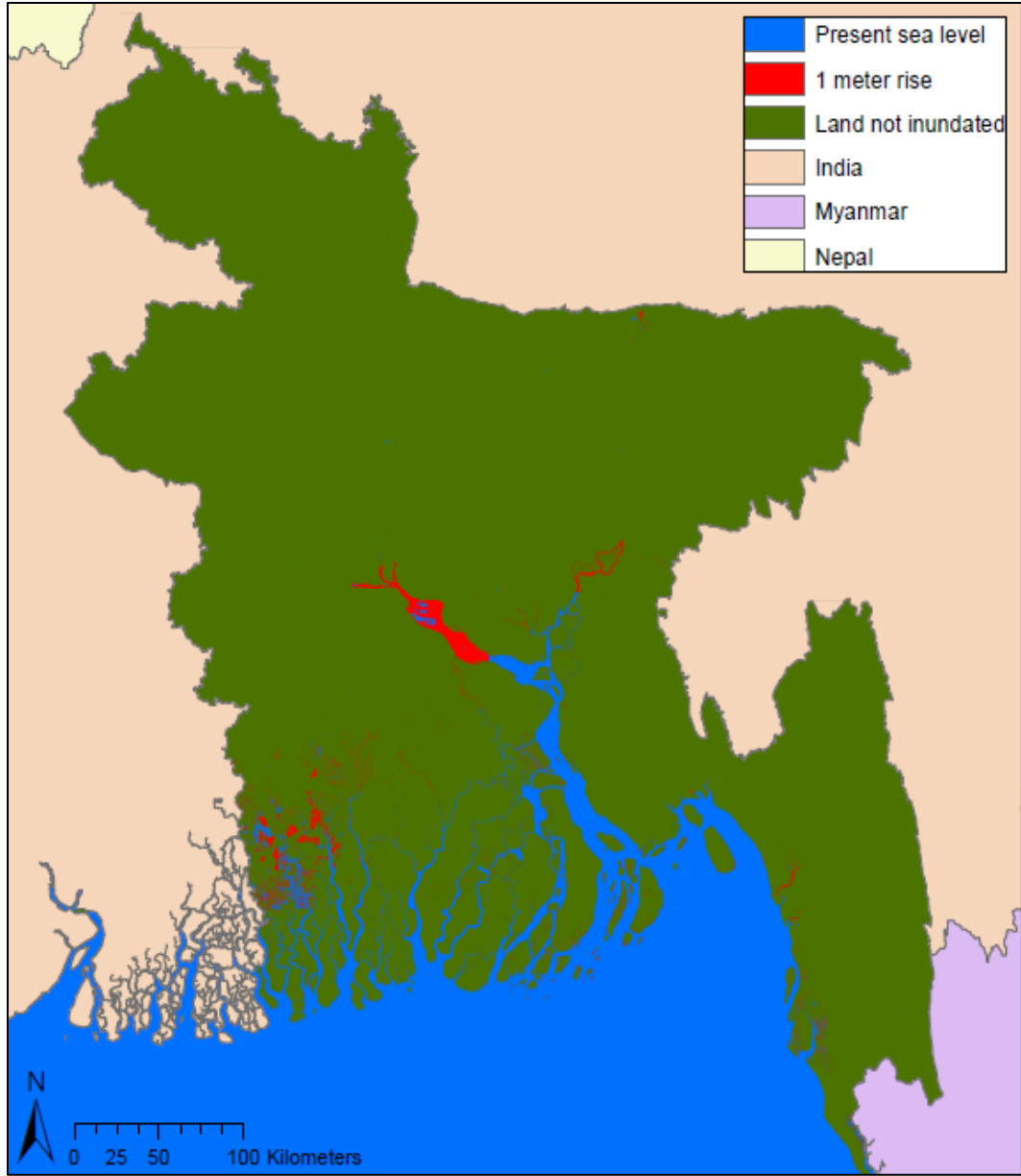


**Figure 14.** Map showing a 1 meter sea level rise for Bangladesh

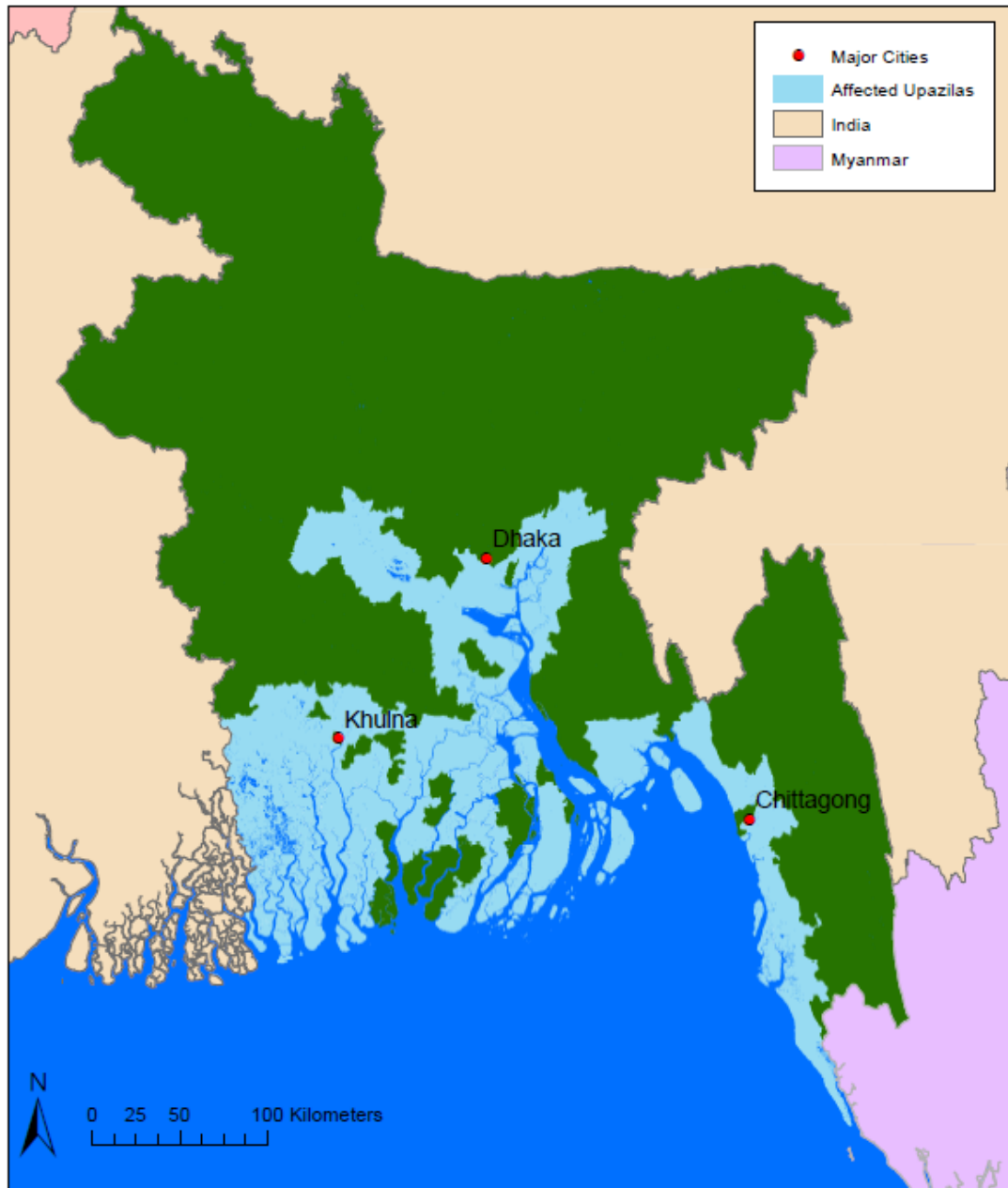


**Figure 15.** Map showing upazilas and major cities impacted by a 1 meter sea level rise

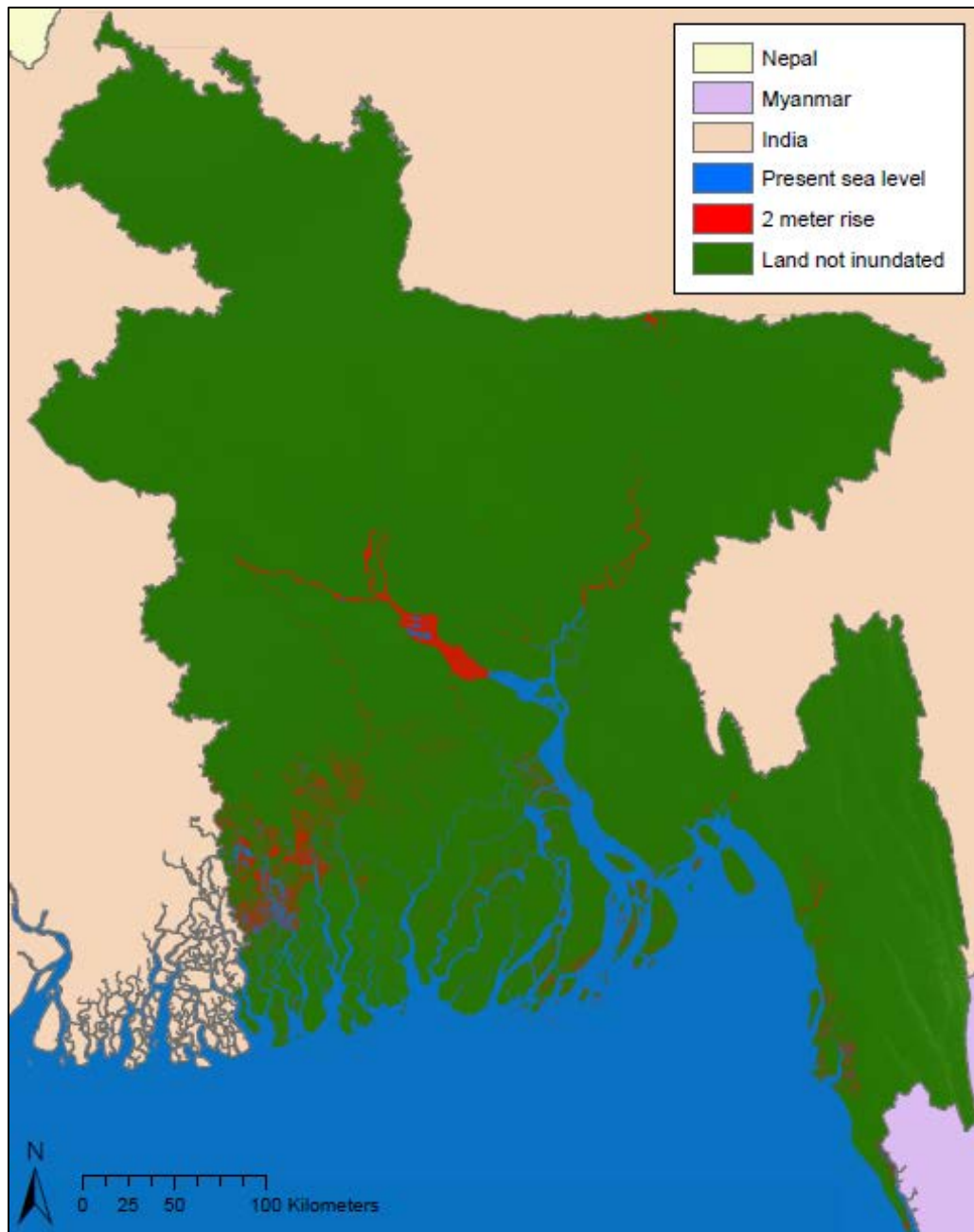


**Figure 16.** Map showing a 2 meter sea level rise for Bangladesh

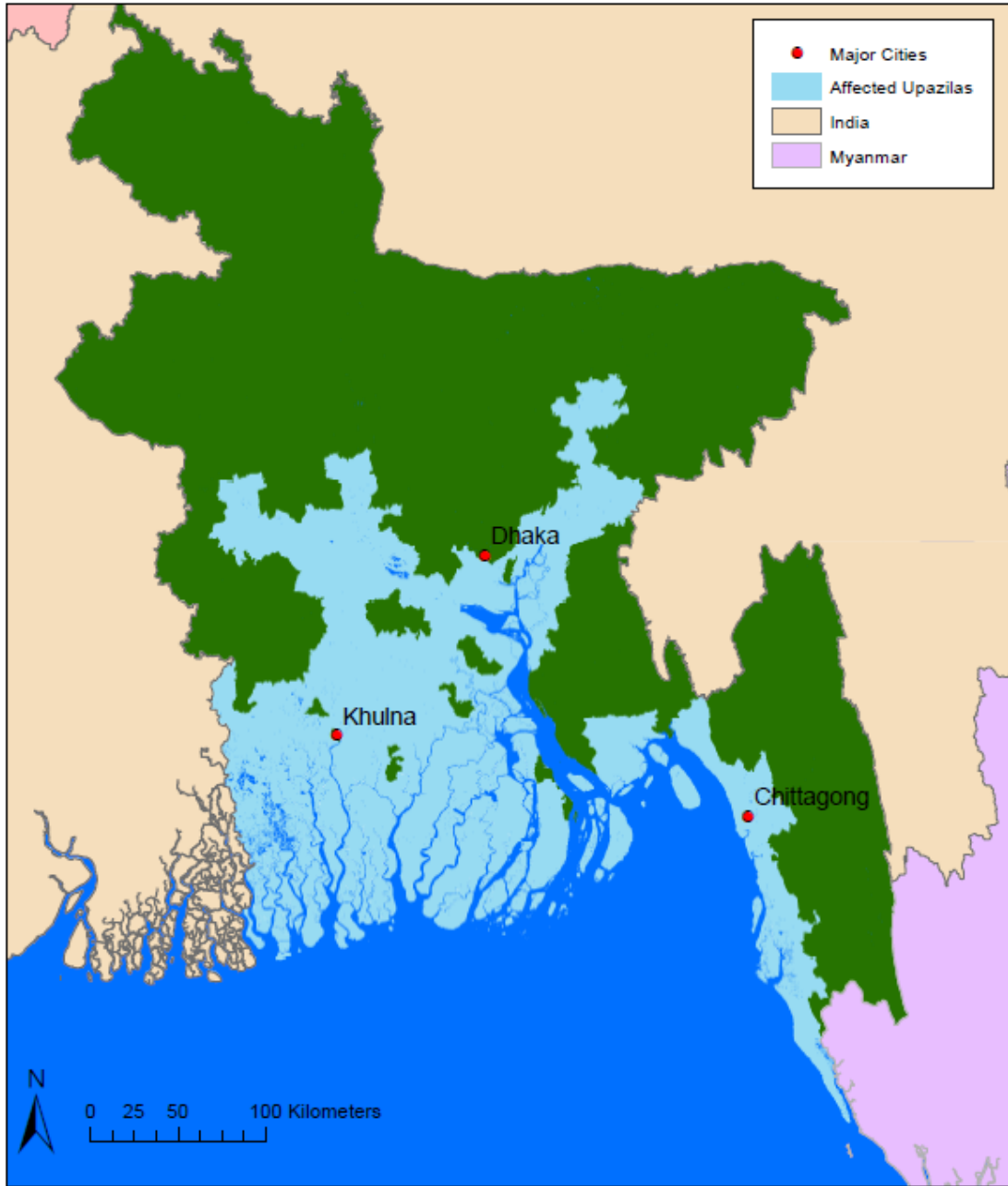


**Figure 17.** Map showing upazilas and major cities impacted by a 2 meter sea level rise

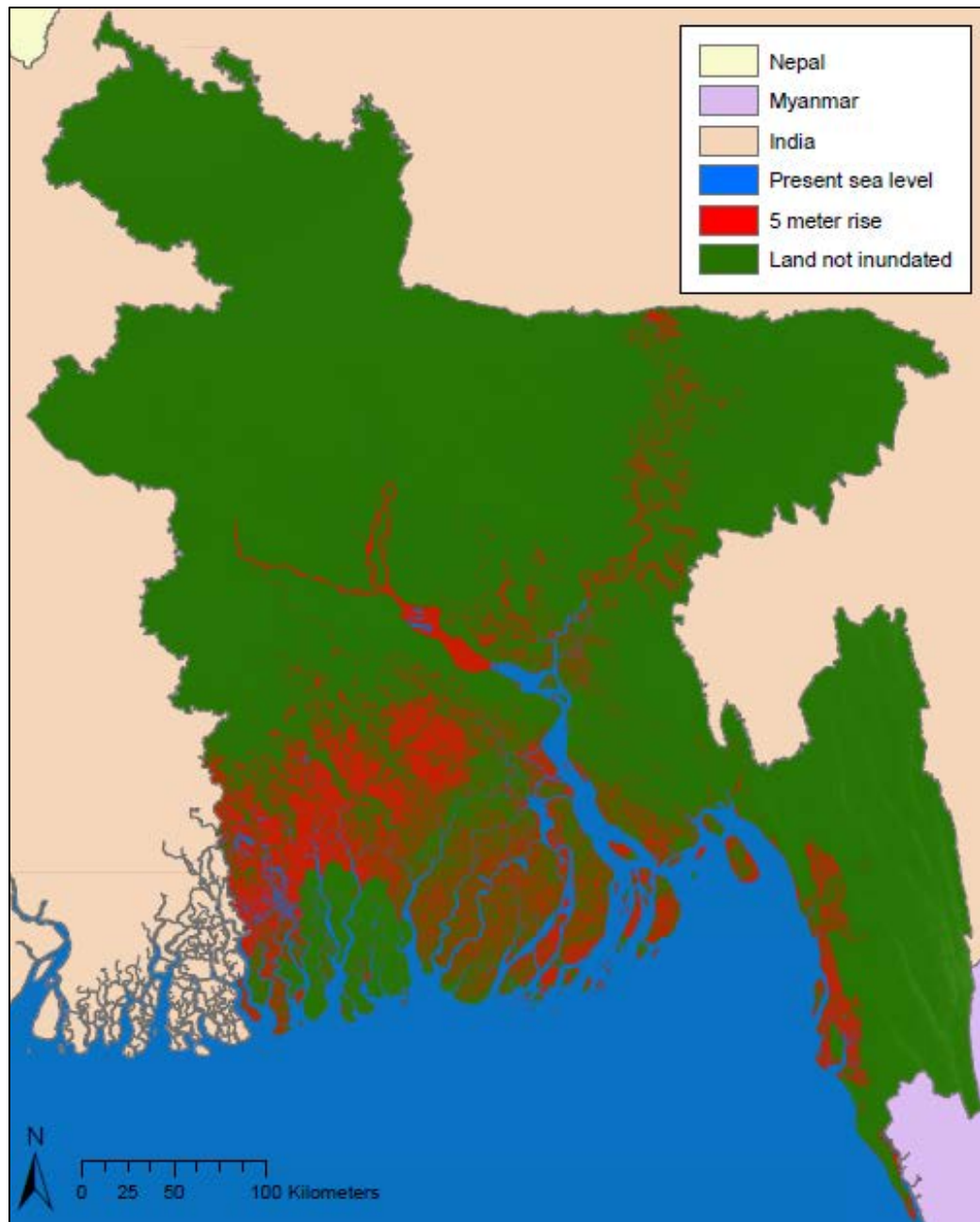


**Figure 18.** Map showing a 5 meter sea level rise for Bangladesh

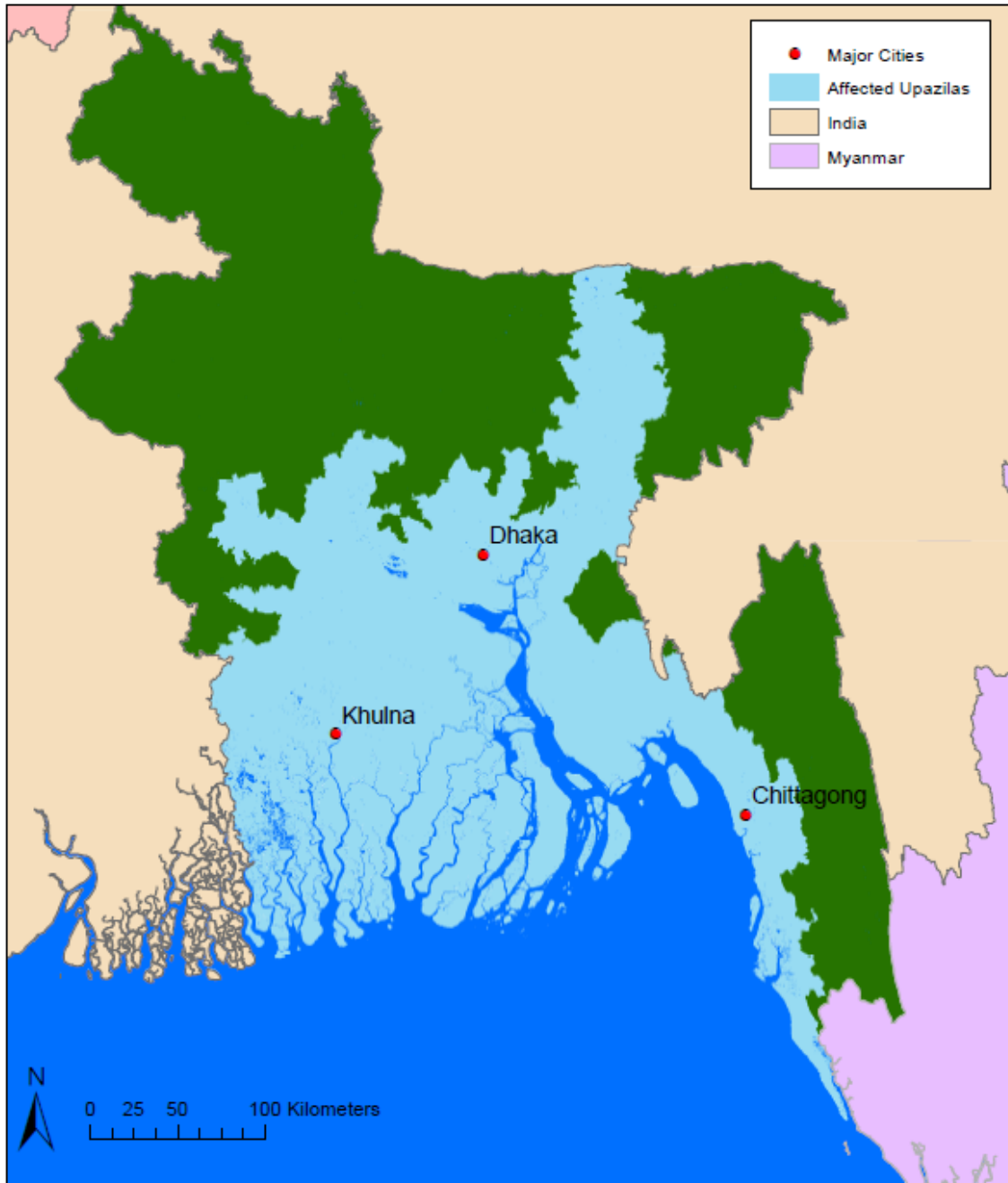


**Figure 19.** Map showing upazilas and major cities impacted by a 5 meter sea level rise

## Hydrostratigraphic Cross-Sections

Geologic cross-sections were re-constructed using lithological logs from the BWDB report for the following transects shown in Figure 13: EW1 (Figure 20), EW2 (Figure 21), NS1 (Figure 22), and NS2 (Figure 23). Lithological logs included descriptions of sediment variations every 10 feet which consist mainly of very fine sand, fine sand, medium sand, coarse sand, silt, and clay.

EW1 has a clay unit at the surface that is nearly continuous, ranging in thickness from 0 to 61 m. Across the transect, the top layer is 64-100% clay with some silt and little fine sand. Below the clay is a sandy unit (1<sup>st</sup> aquifer) that has a thickness ranging between 15 to 95 meters. This layer is 57-100% sand with up to 40% silt in some locations and contains minor clay lenses. A silty clay layer is present to the west and east of this transect, but is not present at wells BSBSPZ4 and LCLKOW1, containing between 65-100% clay. The bottom layer of EW1 is interbedded clay and sand and extends to the depths of all wells, up to 280 meters. This layer is clay-rich to the east and west and is sandy with silt and clay lenses in the center.

EW2 has a thin silty clay layer present at most locations with a thickness between 3 and 12 m. An interbedded silty layer is present between wells JHJHPZ4 and CHSDPZ4, which is an area dominated by tidal channels and the mouth to the Bay of Bengal. Below these top two layers is a sand-rich layer (1<sup>st</sup> aquifer) with a thickness ranging between 30 to 122 m; this layer is not present at well BHLMPZ4. The sand layer is 61-100% fine sand with some silt and minor clay lenses. A continuous interbedded layer is present below the 1<sup>st</sup> aquifer and has a thickness ranging between 61 to 155 meters. The bottom layer of EW2 is a continuous sand layer extending to a depth of 287 meters. The bottom sand, as with other layers, is much more clay-rich toward the center beneath the tidal channels.

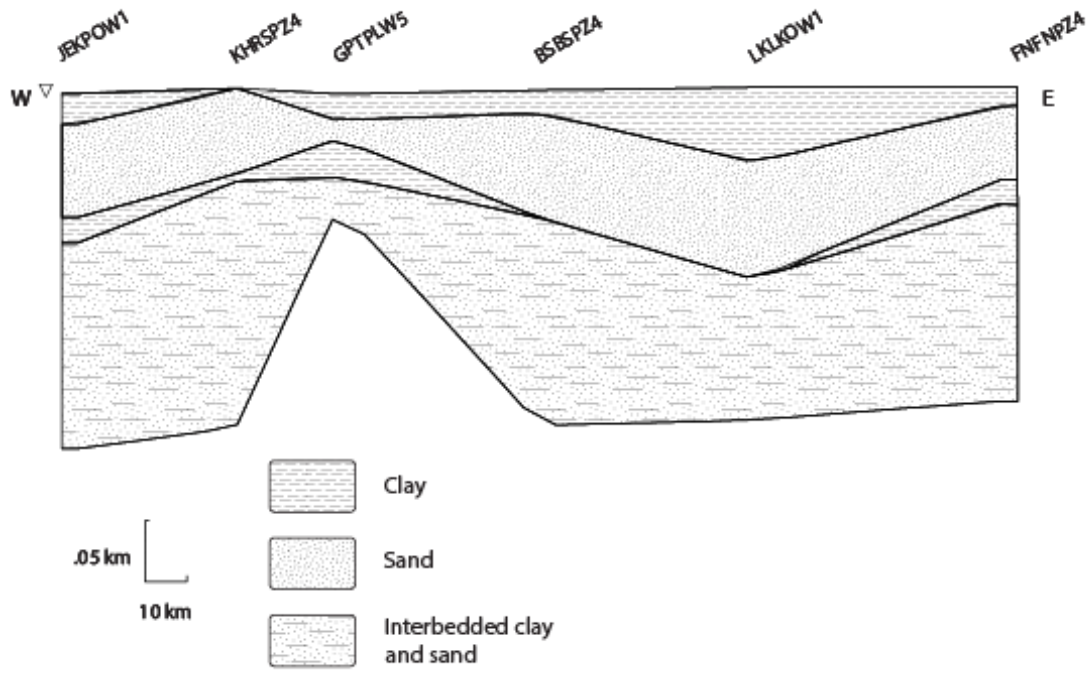


**Figure 20.** Cross-section showing the stratigraphy of transect EW1

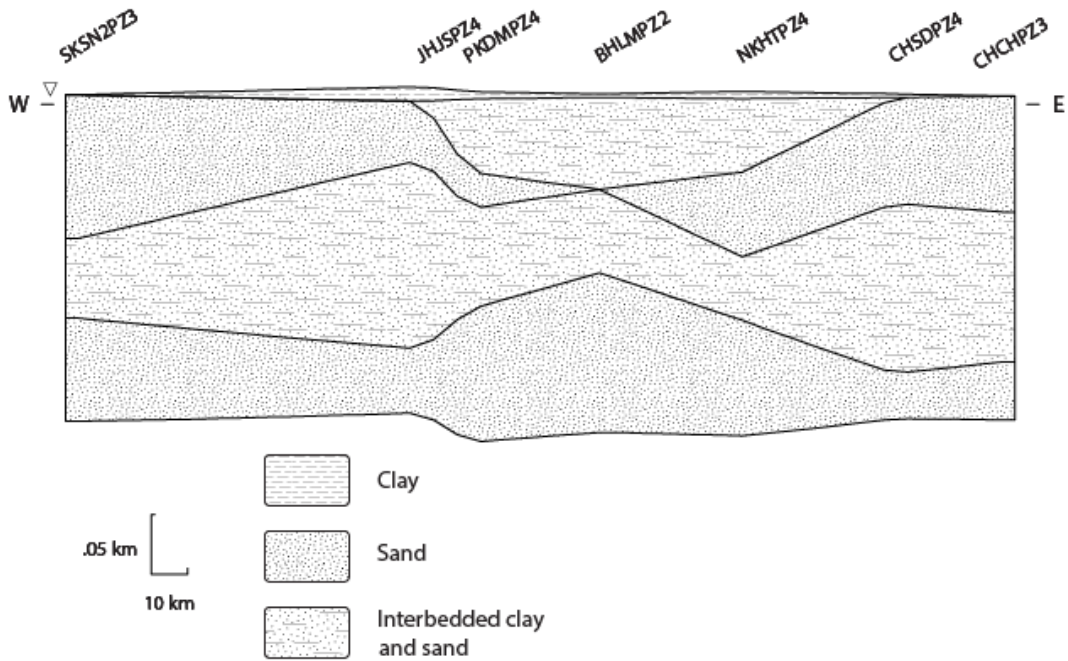


**Figure 21.** Cross-section showing the stratigraphy of transect EW2

NS1 has a top clay layer to the far north and far south, but it is absent throughout the Chittagong district. Below the clay is a sandy layer (1<sup>st</sup> aquifer) with a thickness ranging between 51 to 98 meters. This layer is between 89-100% fine sand with few isolated, thin clay lenses. A thin clay layer with a thickness not exceeding 21 meters is present locally throughout this transect. Below the clay layer, a discontinuous interbedded sand and clay layer is present that is mostly sand and silt with some clay; this layer is more clay-rich to the far north and far south. A sandy layer (2<sup>nd</sup> aquifer) is present below and contains up to 100% fine sand with some clay lenses present in Cox's Bazar district. Below the sand is another interbedded layer that is approximately 50% sand and 50% silty clay.

NS2 has a continuous top silty clay layer with a thickness between 6 and 24 meters. An interbedded unit of fine sand, silt, and clay is present in the transect south of well JHJHPZ4. A sandy layer (1<sup>st</sup> aquifer) extends below these top two layers and is upwards of 75% fine sand with some silt and medium to coarse sand. A continuous interbedded layer is present below the 1<sup>st</sup> aquifer and ranges from being clay-rich to sandy with clay lenses. Below the interbedded layer is another sandy layer (2<sup>nd</sup> aquifer) that is continuous and is mostly fine sand with few clay lenses to the north and larger medium to coarse-grained sand in the south.

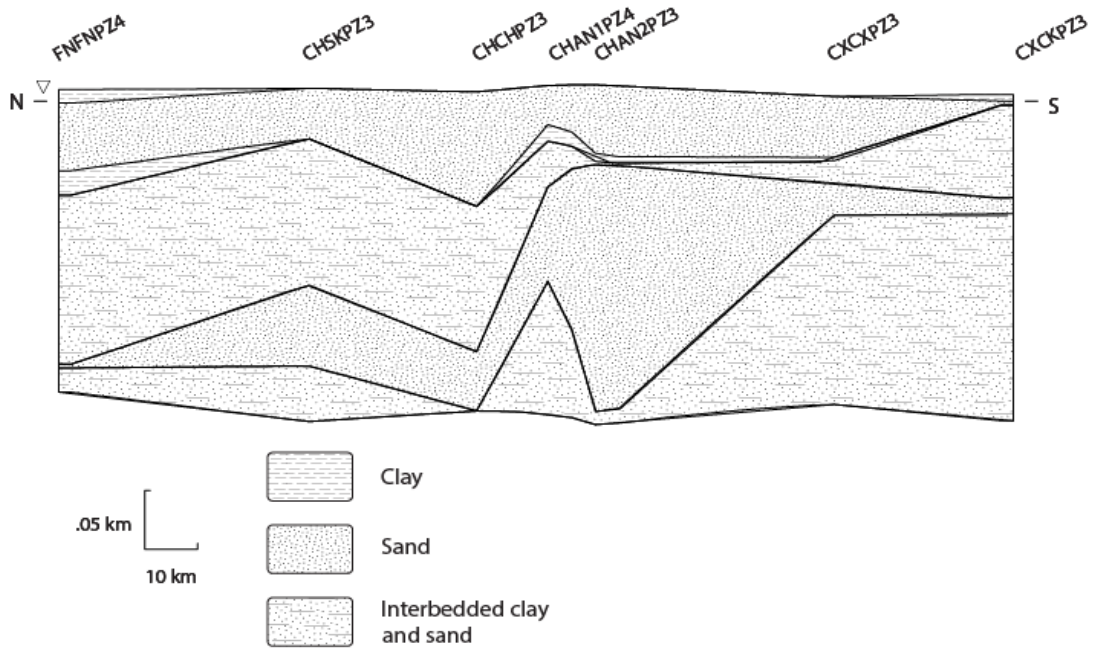


**Figure 22.** Cross-section showing the stratigraphy of transect NS1

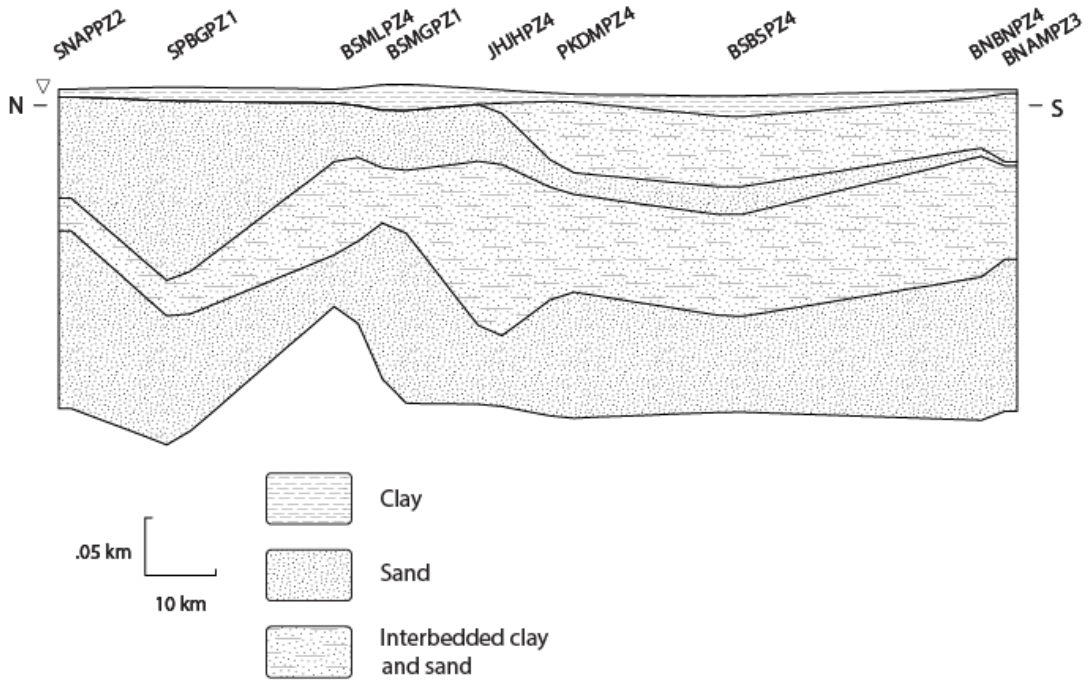


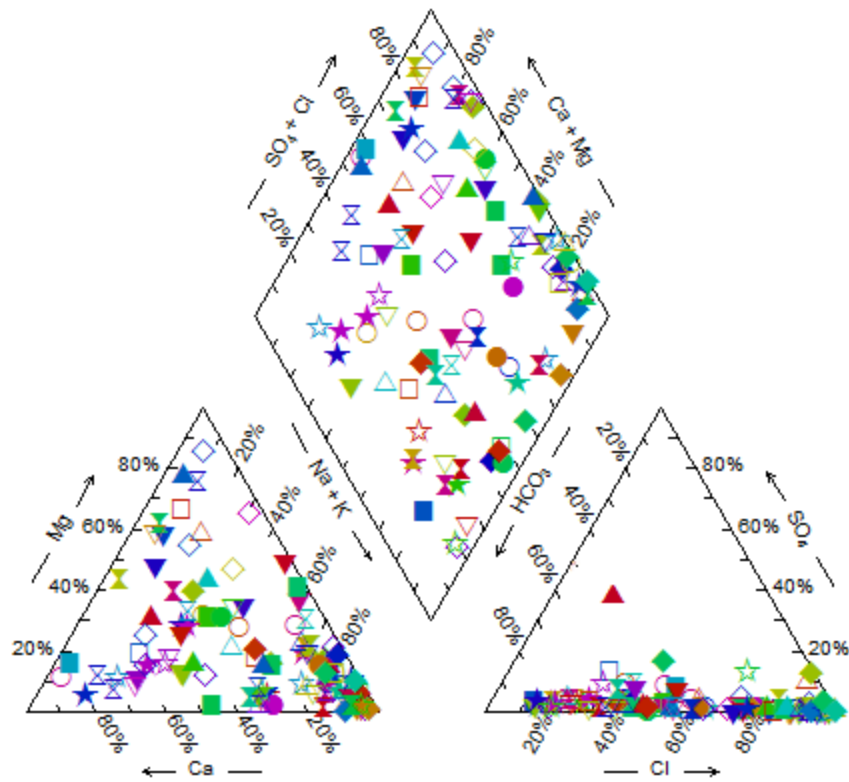
**Figure 23.** Cross-section showing the stratigraphy of transect NS2

## Water Geochemistry

Piper diagrams were constructed for groundwater from all wells in the BWDB (Figure 24) and BGS reports (Figure 25) to assess the groundwater geochemistry. Select wells were used to construct additional piper diagrams for shallow (Figure 26) and deep (Figure 27) wells to show how the spatial distribution of water types may be connected to vertical infiltration of saline water. It is expected that waters experiencing saltwater intrusion will be of Na-Cl type. The water type in the study area is highly variable, with the most dominant water type as Na-Ca-Mg-HCO<sub>3</sub>.

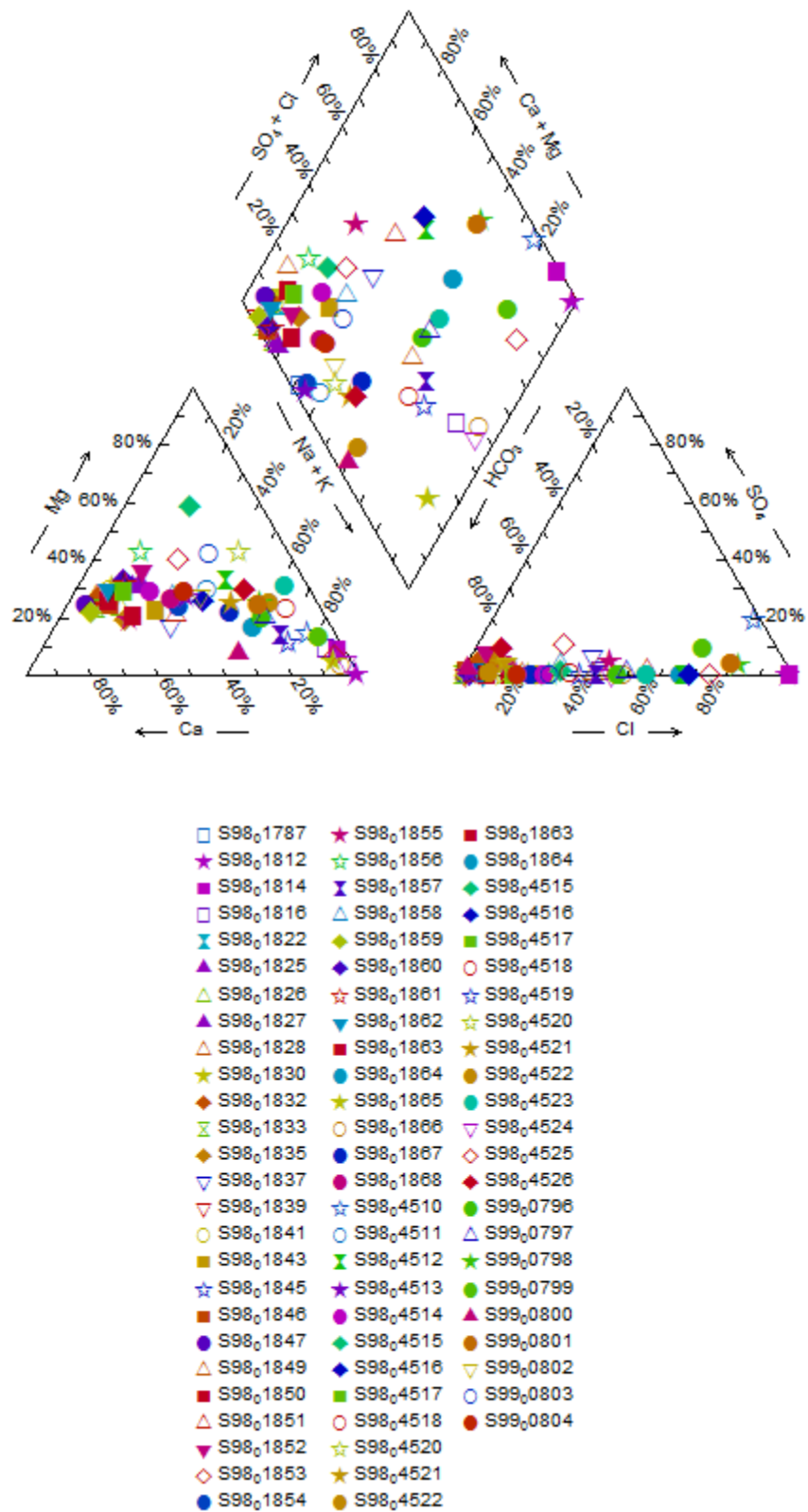
Figure 24 represents geochemical data from both shallow and deep wells in the BWDB report, and shows that there is no distinct water type in the study area, although nearly all waters are strongly HCO<sub>3</sub> type with the exception of one outlier, well CHSKPZ1 from Chittagong district. There is a cluster of some wells that display major ion trends of the Na-Cl type, but there is no distinct spatial trend to explain the distribution of these hydrochemical facies. Figure 25 shows geochemical data from wells included in the 2001 BGS study. These data show more clustering and have a distinct trend toward Na-Ca-Mg-HCO<sub>3</sub> type, with a few wells exhibiting Na-Cl type. The Na-Cl type wells are named S98<sub>0</sub>1812, S98<sub>0</sub>1814, S98<sub>0</sub>1853, S99<sub>0</sub>0799, and S98<sub>0</sub>4510. All of these are located either on the southernmost coastal islands, along tidal channels, or along the Bay of Bengal and are in the shallow aquifer.

Figure 26 includes geochemical data from 11 wells in western Bangladesh and illustrates how the water type varies spatially. The wells that are farthest to the north (JEBPPZ1, NRRNPZ1, and GPMPPZ1) and are not close to any tidal channels or water bodies have a Ca-Mg-HCO<sub>3</sub> water type and are low in the Na<sup>+</sup> and Cl<sup>-</sup> ions that indicate seawater intrusion.



- |                         |                         |                       |                         |                         |
|-------------------------|-------------------------|-----------------------|-------------------------|-------------------------|
| □ CHANPZ <sub>1</sub>   | ★ CHSD <sub>p</sub> Z-3 | ▽ JEKPPZ 1            | ◇ BSMLPZ <sub>3</sub>   | ⋈ SKSKPZ <sub>2</sub>   |
| ★ CHCHPZ <sub>4</sub>   | ▽ CDSRPZ <sub>2</sub>   | ■ BNBPNZ <sub>2</sub> | ◇ JHJHPZ <sub>3</sub>   | ◇ BSBSBP <sub>1</sub>   |
| ▲ CHSKPZ <sub>1</sub>   | □ CHSD <sub>p</sub> Z-4 | ⋈ KHKHPZ 1            | ◆ BSMLPZ-2              | ◇ BSBSBP <sub>2</sub>   |
| △ LKLK1PZ <sub>3</sub>  | ■ NRNPZ1                | ● CDSRPZ <sub>3</sub> | ⋈ SKSKPZ <sub>2</sub>   | ■ NKKHPZ1               |
| ○ CHSKPZ <sub>3</sub>   | ⋈ JHJHPZ <sub>4</sub>   | ● GPMPPZ <sub>1</sub> | ◇ BSBSBP <sub>1</sub>   | ⋈ PRBRPZ <sub>3</sub>   |
| ◆ CXCKPZ <sub>2</sub>   | ▽ CHSKPZ <sub>2</sub>   | ★ CDUMPZ <sub>1</sub> | ◇ BSBSBP <sub>2</sub>   | ⋈ SKSN2PZ-1             |
| ■ CXCKPZ <sub>1</sub>   | ◆ PKDMPZ-4              | ⋈ CDUMPZ <sub>3</sub> | ■ NKKHPZ1               | ▲ PRBRPZ <sub>1</sub>   |
| ⋈ SPNAPZ-3              | ◆ BSBSBP <sub>3</sub>   | ⋈ BNAMPZ <sub>2</sub> | ⋈ PRBRPZ <sub>3</sub>   | ◇ JHJHPZ <sub>2</sub>   |
| ○ LKLK2PW               | △ BNAMPZ <sub>4</sub>   | ★ KHKHPZ 3            | ⋈ SKSN2PZ-1             | ⋈ SKSN2PZ-2             |
| ○ LKLK1PZ-4             | ▽ PKDMPZ <sub>3</sub>   | ▼ PKKLPZ <sub>3</sub> | ▲ PRBRPZ <sub>1</sub>   | ◆ PRBRPZ <sub>5</sub>   |
| ■ FNFNPZ <sub>3</sub>   | ◇ NKKHPZ3               | ▼ GPMPPZ <sub>3</sub> | ◇ JHJHPZ <sub>2</sub>   | ◇ SKKGPZ <sub>1</sub>   |
| ★ NKKHPZ2               | ○ BABAPZ 1              | ⋈ PKKLPZ <sub>4</sub> | ⋈ SKSN2PZ-2             | ▽ LKLK1PZ <sub>2</sub>  |
| ★ LKLK2PZ1              | ◇ BNAMPZ <sub>3</sub>   | ◆ CDSRPZ <sub>1</sub> | ◆ PRBRPZ <sub>5</sub>   | ▽ BNP GPZ-3             |
| ■ NRNPZ3                | ▽ LKLK2PW               | ◇ SPBGPZ-1            | △ SKKGPZ <sub>1</sub>   | ⋈ CHSD <sub>p</sub> Z-1 |
| ★ FNFNPZ <sub>2</sub>   | ● BSMLPZ <sub>4</sub>   | ▽ BNBPNZ <sub>3</sub> | ▽ LKLK1PZ <sub>2</sub>  | ◆ SKSN1PZ <sub>1</sub>  |
| ○ SPNAPZ-2              | ★ CDUMPZ <sub>2</sub>   | ▽ NRNPZ2              | ▽ BNP GPZ-3             | ▲ BNAMPZ <sub>1</sub>   |
| ⋈ NKHTPZ -4             | ▲ BSMLPZ-1              | ▼ JHJHPZ <sub>1</sub> | ⋈ CHSD <sub>p</sub> Z-1 | ★ PKGCPZ <sub>3</sub>   |
| ★ JEBPPZ 1              | ● BSBSBP <sub>4</sub>   | ▲ SKSN2PZ-3           | ◆ SKSN1PZ <sub>1</sub>  | ⋈ BHLMPZ 1              |
| ▼ JEBPPZ 2              | □ BABAPZ 2              | ★ JEKPPZ 2            | ▲ BNAMPZ <sub>1</sub>   | ⋈ LKLK1PZ <sub>1</sub>  |
| ★ JEBPPZ 3              | ◆ BABAPZ 3              | ▼ PKGCPZ <sub>2</sub> | ★ PKGCPZ <sub>3</sub>   | ★ PRBRPZ <sub>2</sub>   |
| ⋈ LKLK2PZ1              | ▽ BNBPNZ <sub>4</sub>   | ⋈ SKSKPZ <sub>1</sub> | ⋈ BHLMPZ 1              | ○ BNBPNZ <sub>1</sub>   |
| △ CHSD <sub>p</sub> Z-2 | ◇ NRNPZ 2               | □ GPMPPZ <sub>2</sub> | ⋈ LKLK1PZ <sub>1</sub>  | ★ PKKLPZ <sub>1</sub>   |
| ◆ NKHTPZ -3             | ▽ PKDMPZ <sub>2</sub>   | ▽ SPBGPZ-2            | ★ PRBRPZ <sub>2</sub>   | ◆ PKKLPZ <sub>2</sub>   |
| ★ LKLK2PZ1/1            | ▼ PKGCPZ <sub>1</sub>   | ◇ GPMPPZ <sub>4</sub> | ○ BNBPNZ <sub>1</sub>   | ▲ BNP GPZ-2             |
| ◆ BHLMPZ 2              | ▽ NRNPZ 1               | ▼ FNFNPZ <sub>1</sub> | ★ PKKLPZ <sub>1</sub>   | ◆ BNP GPZ-1             |
| ⋈ CXCX1PZ <sub>1</sub>  | ▲ SPNAPZ-1              | ● PRBRPZ <sub>4</sub> | ◆ PKKLPZ <sub>2</sub>   |                         |

Figure 24. Piper diagram for all BWDB report wells



**Figure 25.** Piper diagram for all BGS report wells, showing Na-Ca-Mg-HCO<sub>3</sub> water type

Moving in a southward direction, the water type begins to move toward Na-Cl type with wells JEKPPZ1 and KHKHPZ1. The remaining wells on this diagram are located along tidal channels or adjacent to the Bay of Bengal, and they are all Na-Cl type water, which suggests that vertical infiltration of seawater is responsible for the change in water type.

Figure 27 displays geochemical data for 14 wells in the main aquifer. As with the shallow aquifer, the wells that are not close to any water bodies (JEBPPZ3, NRNRZ3, JEKPPZ3) are lower in  $\text{Na}^+$  and  $\text{Cl}^-$  ions than other wells that are located near tidal channels (BNPGPZ3, SKSKPZ2, KHRSPZ4). On the other hand, this diagram shows more outliers that do not fit the pattern; GPMPPZ4 is located north and inland from any water bodies but has Na-Cl water type, while PKKLPZ4 is located far south along the Bay of Bengal but is low in  $\text{Na}^+$  and  $\text{Cl}^-$  ions. It is possible that pumping of the main aquifer is responsible for a distribution of Na-Cl water type that is unexpected. The unpredictable spatial distribution of confining clay layers and freshwater lenses in the study area can also explain the outliers that are seen in BWDB data.

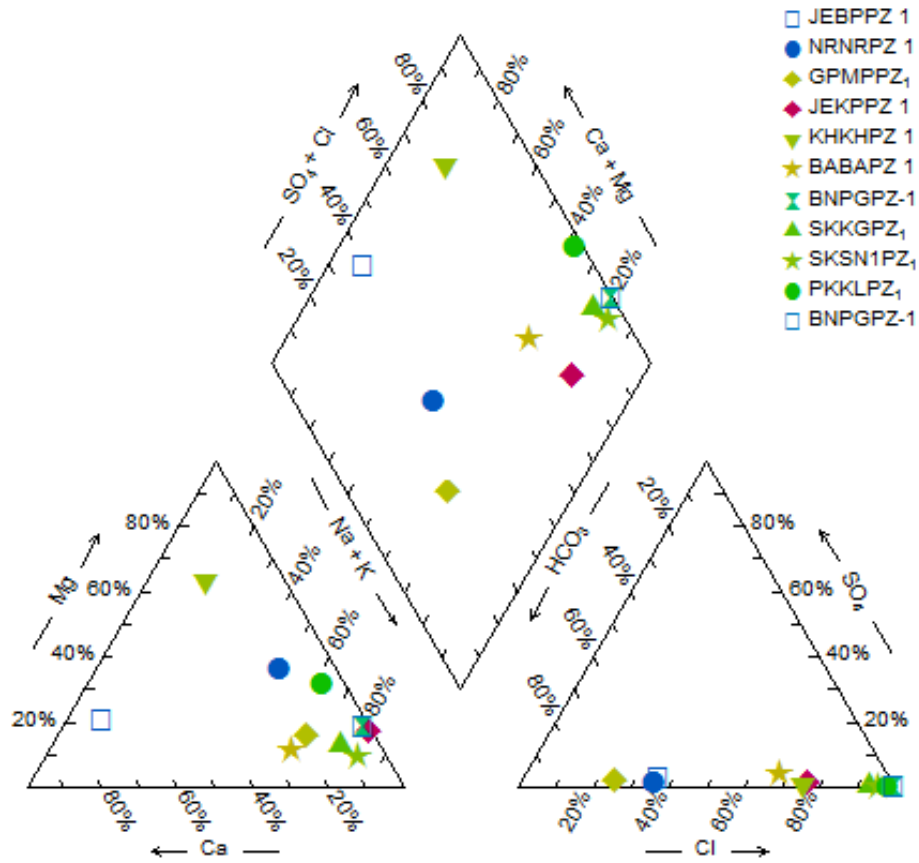


**Figure 26.** Piper diagram for select wells in the shallow aquifer from the BWDB report

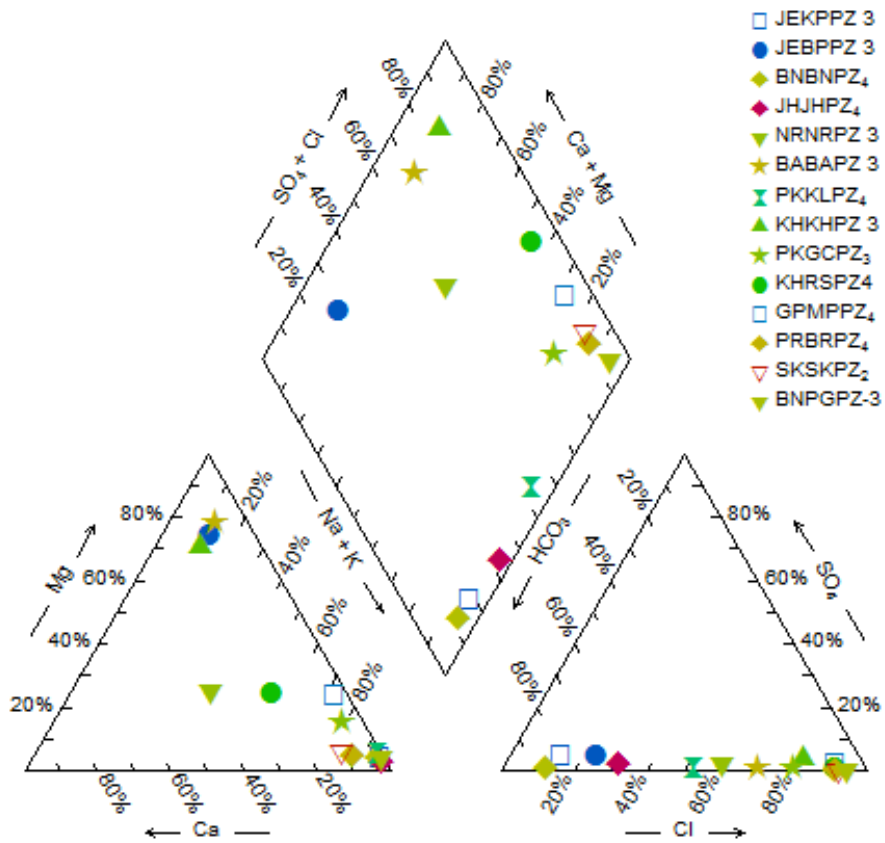


**Figure 27.** Piper diagram for select wells in the deep aquifer from the BWDB report

## Surface Water Salinity

The BWDB data show that surface water in much of southern coastal Bangladesh is saline and exceeds both the WHO recommended drinking water standard of TDS < 500 mg/l and the Bangladesh drinking water standard of TDS < 1000 mg/l (Table 2). Although most surface water in Bangladesh is not used as potable water, this is still very problematic due to its hydrologic connection to the upper aquifers that are used for water consumption. Seawater intrusion through vertical infiltration from brackish tidal channels and from storm events will lead to the degradation of water quality of the aquifers, and understanding the distribution of surface water salinity can give insight into this process..

Figure 28 shows TDS concentrations (mg/l) for 23 surface water sampling locations across the study area, with the blue line illustrating dry season concentrations and the orange line illustrating wet season conditions. Salinity at certain locations approach that of seawater (about 35,000 mg/l), due to lateral intrusion of seawater through open tidal channels. All sample locations have a salinity that is significantly higher in the dry season than in the wet season, particularly in the eastern districts of Chittagong, Cox's Bazar, and Feni. Southern districts of Noakhali and Patuakhali also have a wide range of TDS concentrations throughout the year. Areas farther to the west and north that have a TDS within the drinking water range still experience the seasonal fluctuation in salinity (Table 3).

Both GCMs and RCMs indicate that Bangladesh will suffer the consequences of climate change, with the wet (monsoon) season becoming wetter and the dry season becoming drier [Nohara et al., 2006; Chotamonsak et al., 2011; IPCC 2014]. This pattern of seasonal change will likely lead to a wider range of TDS concentrations in coastal Bangladesh. The water salinization issues and hydrologic stress will get worse during the dry seasons or droughts.

Excess overland flow during the wet seasons may enhance the transport of dissolved salts that formed during dry months into river channels. RCMs that fully account for the monsoon dynamics need to be developed to gain a clearer picture of water sustainability in Coastal Bangladesh, as an increase in storm events will also lead to flooding upstream and allows transport of more dissolved salt or saline water farther downstream, which may compromise the water quality in additional districts where drinking water salinity currently are within the drinking water standards.

**Table 2.** Bangladesh and WHO water quality standards [from BWDB, 2013]

Parameters	Units	Bangladesh standards		WHO
		Drinking limit	Irrigation limit	Drinking limit
pH		6.5 - 8.5	6.0 - 9.0	6.5 – 8.5
TDS	mg/l	1000	2100	500 - 1000
Chloride	mg/l	150 - 600	600	200 - 600
Arsenic	µg/l	50	1000	10

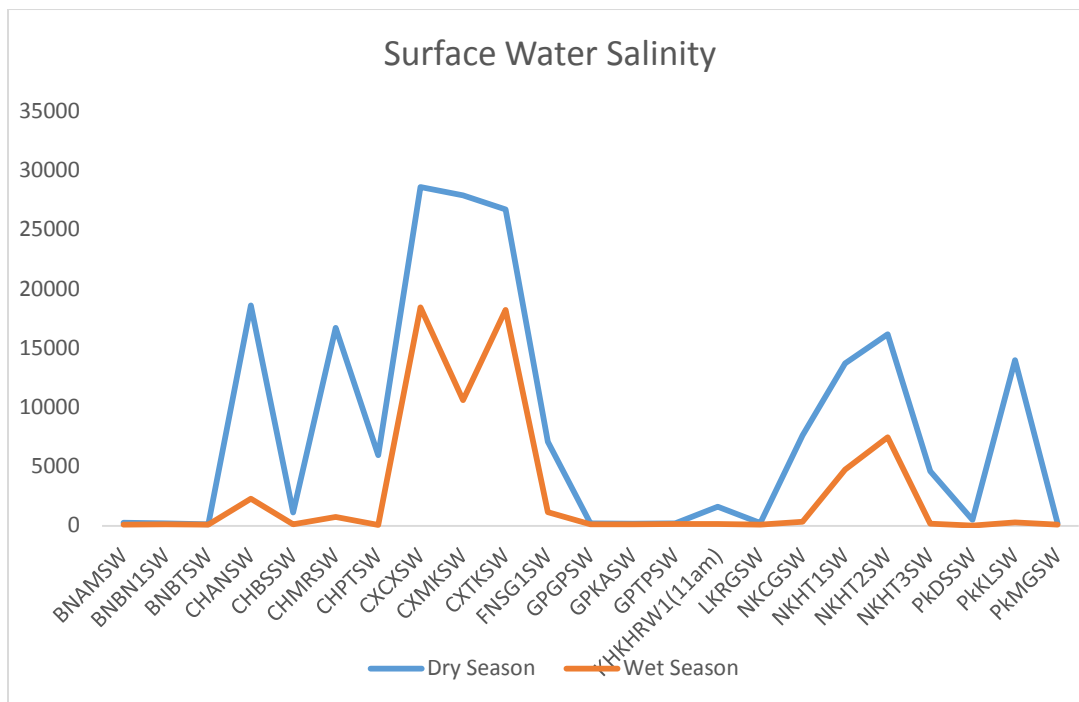


**Figure 28.** Plot showing surface water salinity (TDS, mg/l) for 23 surface water sampling wells during the wet season and dry season.

**Table 3.** Surface water salinity concentrations (TDS, mg/l) for 23 surface wells during wet and dry seasons [from BWDB, 2013].

Sample ID	Dry Season TDS (mg/l)	Wet Season TDS (mg/l)
BNAMSW	258	101
BNBN1SW	201	113
BNBTSW	128.7	100
CHANSW	18600	2277
CHBSSW	1135	121
CHMRSW	16700	753
CHPTSW	5950	70
CXCXSW	28600	18440
CXMKSW	27900	10610
CXTKSW	26700	18230
FNSG1SW	7090	1141
GPGPSW	194.2	125
GPKASW	187.8	125
GPTPSW	203	150
KHKHRW1	1598	143
LKRGSW	232	92
NKCGSW	7620	333
NKHT1SW	13710	4730
NKHT2SW	16160	7480
NKHT3SW	4620	175
PKDSSW	494	25
PKKLSW	13970	281
PKMGSW	211	110

## Groundwater Salinity

Understanding the spatial distribution of groundwater salinity is useful for determining the extent of both vertical and lateral saltwater intrusion. Examining the fluctuation between wet and dry seasons also provides insight into the response of water quality in the shallow and main aquifers to seasonal changes. Maps were produced for four scenarios: dry season main aquifer (Figure 29), wet season main aquifer (Figure 30), dry season shallow aquifer (Figure 31), and wet season shallow aquifer (Figure 32). A purple contour line denotes a TDS concentration of 500 mg/l corresponding to the WHO recommended drinking water standard, and a black contour line denotes a TDS concentration of 1000 mg/l corresponding to the Bangladesh drinking water standard (Table 2). No data were available in the southwestern Sundarbans Wildlife Sanctuary, and elevated salinity levels in this area are a result of interpolation and do not reflect observed data.

The main aquifer has TDS concentrations ranging between 128 and 7861 mg/l in the wet season and 123 and 5820 mg/l in the dry season. The poor correlation between salinity and surface precipitation suggest that the main aquifer is not well hydraulically connected to surface water. During the dry season (Figure 29), the area with highest salinity is in southwestern coastal Bangladesh near the Sundarbans area, extending in a northeastern direction toward the city of Dhaka. The highest concentration occurs in the Patharghata upazila of the southern Patuakhali district. There are also small areas in the upazilas of Borguna Sadar, Bagerhat Sadar, Fakirhat, and Rampal in southwestern Bangladesh of lower (<1000 mg/l) salinity. The districts of Khulna, Dhaka, and Chittagong are largely within the Bangladesh drinking water standards for the main aquifer. During the wet season (Figure 30), the Sundarbans area also has a high

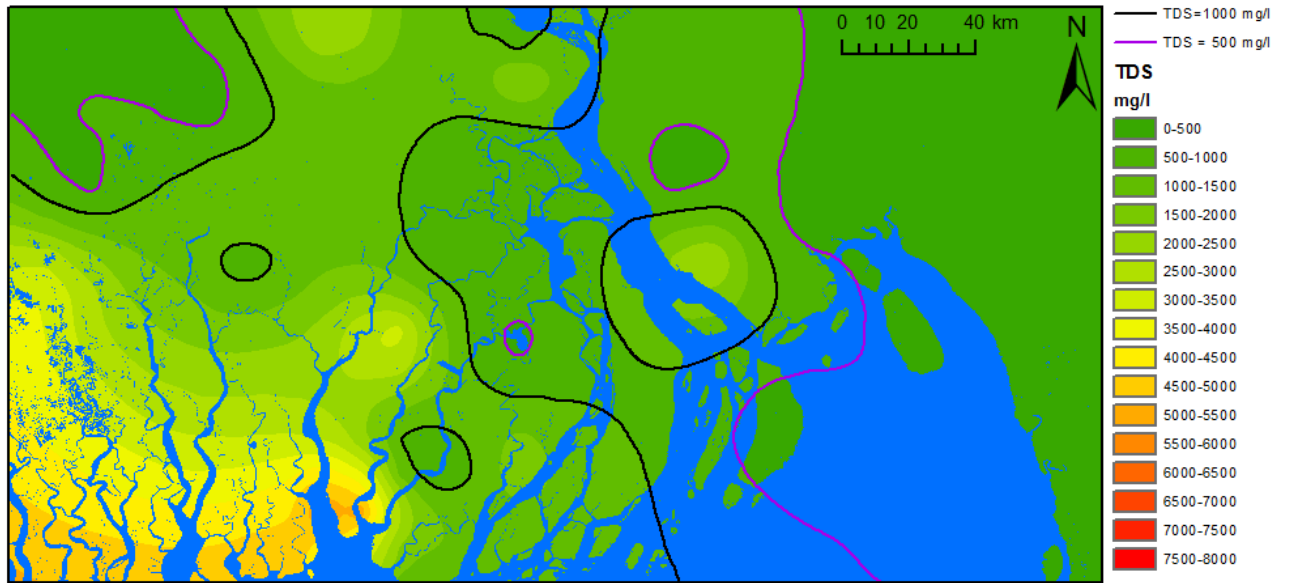


**Figure 29.** Map of the salinity distribution of the main aquifer in the dry season

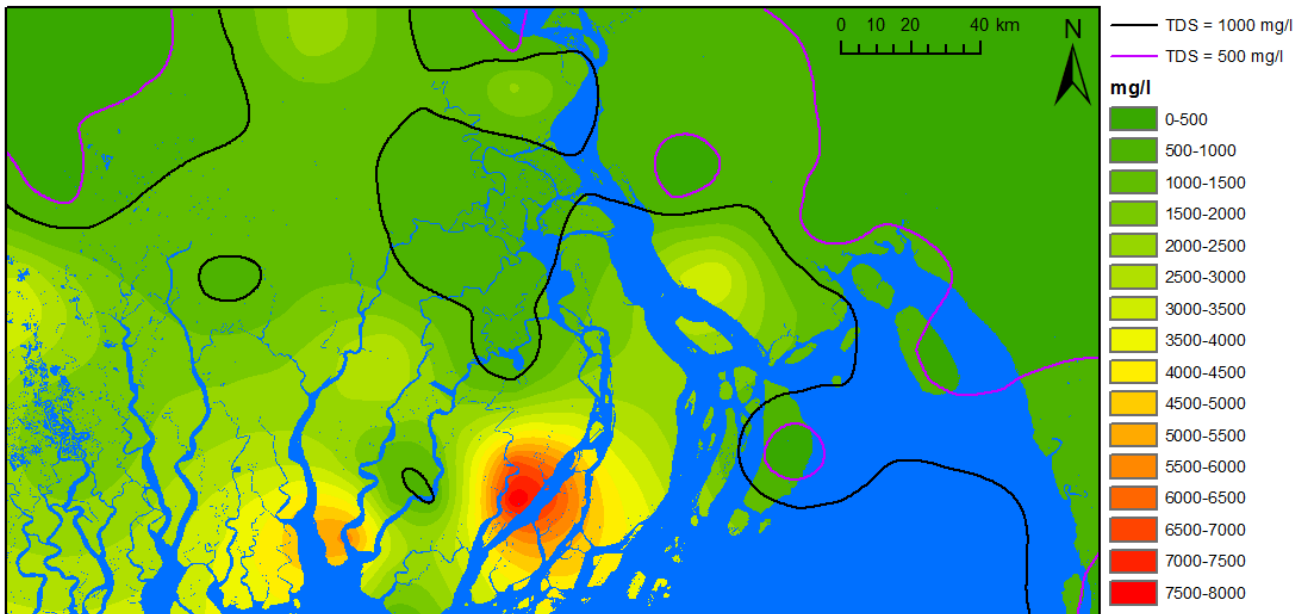


**Figure 30.** Map of the salinity distribution of the main aquifer in the wet season

salinity, but the highest salinity can be found in the Patharghata and Galachipa upazilas of the Patuakhali division. Pumping of wells in this area may be responsible for the increase in salinity within these upazilas. The 1000 mg/l line is similar to that of the dry season, with a slight northward shift in the southern Patuakhali and Noakhali districts.

The shallow aquifer has TDS concentrations ranging between 165 and 22,600 mg/l in the dry season and 96 and 15,390 mg/l in the wet season, generally higher than those in the deeper main aquifers. Lower salinity in wet seasons implies that the shallow aquifer is well-connected to surface recharge precipitation. Higher salinity in the dry season likely reflects stronger evaporation, less inputs from precipitation, and enhanced vertical infiltration of high-salinity waters from the tidal channels into the shallow aquifers. During the dry season, the tidal channels behave more as a losing stream where saline surface water recharges from channels to underlying aquifers; however, during the wet season, these tidal channels may become gaining streams to receive groundwater discharge with lower salinity. During the dry season (Figure 31), the highest TDS concentrations are found in the southern districts adjacent to the Bay of Bengal, with the highest concentration located in the Patharghata upazila of the Patuakhali district. All coastal districts have TDS in excess of the Bangladesh drinking water standard. The 1000 mg/l TDS line runs through the southern parts of the Jessore, Faridpur, and Comilla districts. One small area with TDS < 1000 mg/l is located in the Khulna district. The shallow aquifer does not contain potable water with TDS within the drinking standard in the Chittagong, Noakhali, Patuakhali, and Barisal districts.

The spatial distribution of salinity during the wet season (Figure 32) is very similar to the dry season, with high TDS concentrations located in the same upazilas. There is a noticeably westward shift in the contour lines for TDS concentrations of 500 and 1000 mg/l, particularly in

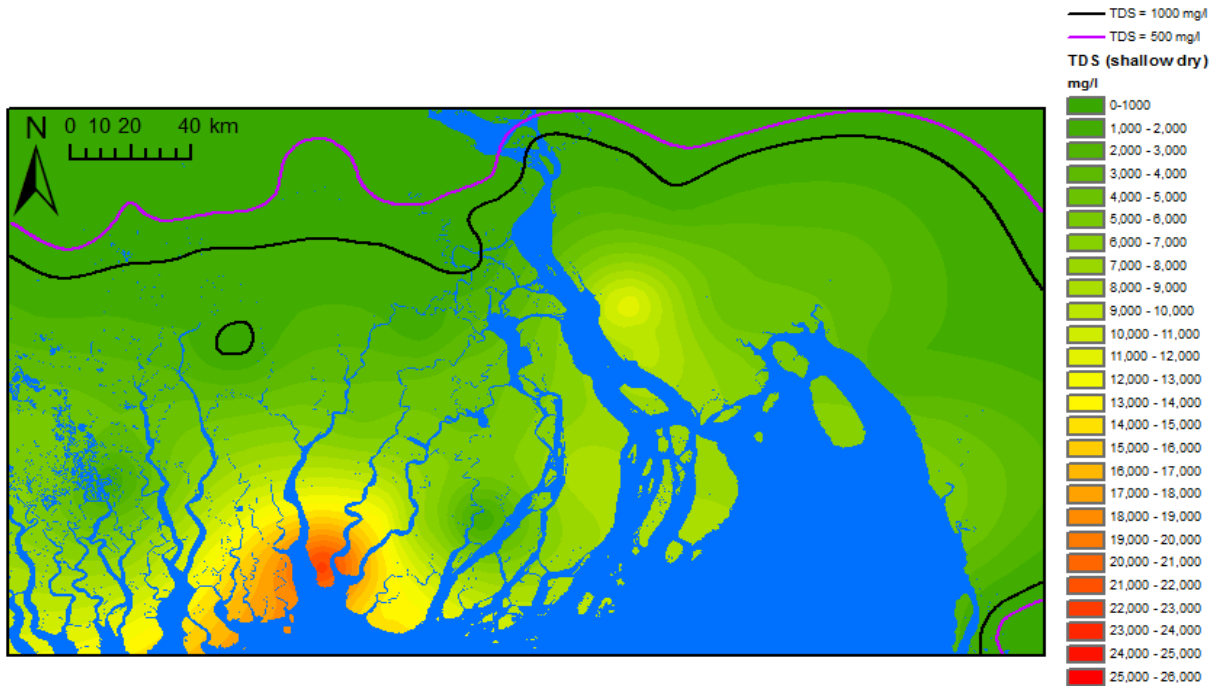


**Figure 31.** Map of the salinity distribution of the shallow aquifer in the dry season

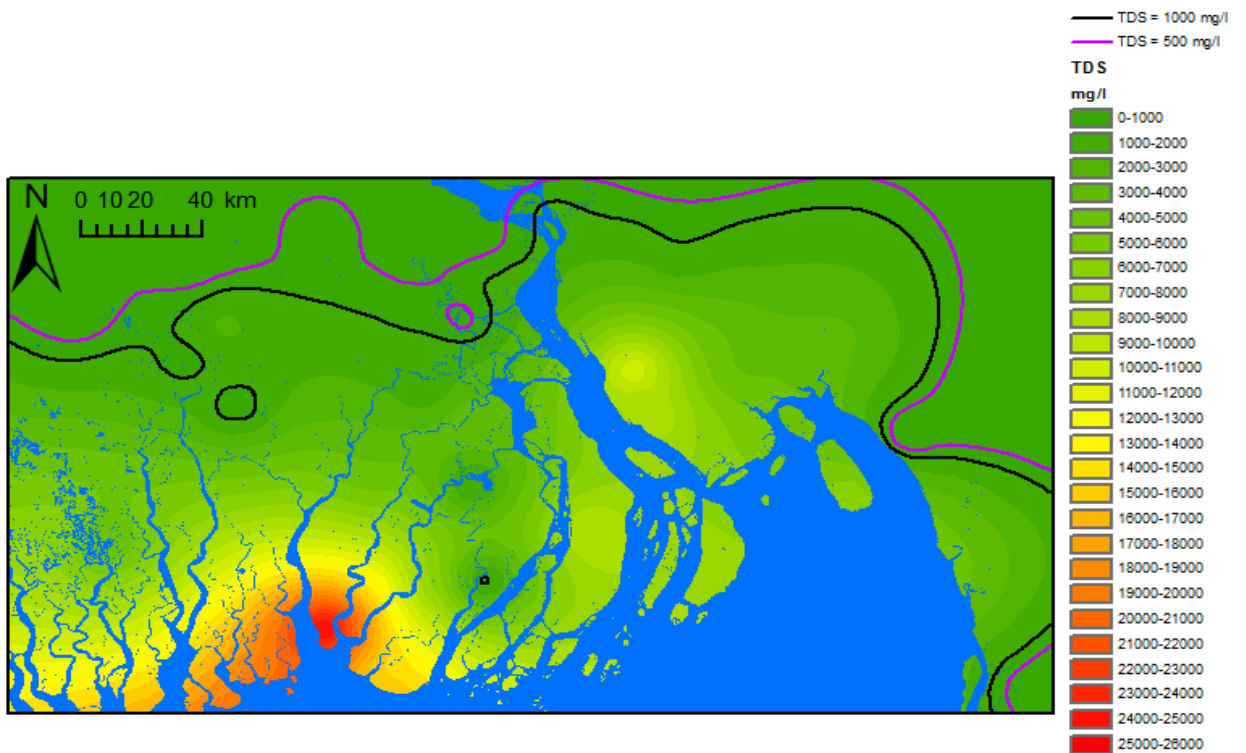


**Figure 32.** Map of the salinity distribution of the shallow aquifer in the wet season

the western Chittagong district. The lines move toward the west in response to greater hydraulic gradients established during the wet seasons, which provide potable water to the district. The Chittagong area has greater hydraulic gradients than the rest of coastal Bangladesh due to the mountains located in the Chittagong Hill Tracts [Zahid et al., 2014], and an increase in precipitation from the monsoon season may increase flushing of the aquifer and result in lower observed TDS concentrations near the coastal areas.

In summary, the salinity distribution shows that the shallow aquifer has a higher mean (4517 mg/l) and wider range (96 to 25,422 mg/l) of TDS concentrations than the mean (1213 mg/l) and range (123 to 8814 mg/l) of the main aquifer, reflecting strong inputs from both surface precipitation and vertical infiltration of saline surface water. The main aquifer has some areas with TDS concentrations under the drinking water limit, located mostly in the north and east of Bangladesh. The shallow aquifer has fewer areas with TDS concentrations under the drinking water limit, and none of these areas are located in the coastal districts. In the eastern Chittagong district, the distribution of low-salinity (500-1000 mg/l) shifts seaward during the wet season in response to faster flushing rates from monsoon precipitation.

### **Two-Dimensional Groundwater Flow Models**

Variable-density groundwater flow and solute (salt) transport simulations were conducted along several west-east and north-south cross sections in coastal Bangladesh. For the purpose of hydrologic modeling, coastal sediments in the study area are divided into 4 to 5 hydrostratigraphic units, containing both shallow and main aquifers with a depth less than 300 meters (Figures 20 to 23). The simulations aim at evaluating effects of lateral saltwater intrusion along the coast and vertical infiltration of saline surface water from intertidal channels. The

modeling results (Figures 33 to 45) show that the groundwater flow in coastal Bangladesh is dominated by a local rather than a regional system, with undulations in the water table controlled by local topographic highs and lows. Recharge areas occur mainly at local topographic highs, and discharge areas occur at nearby topographic lows. These recharge and discharge zones are represented in the Basin2 models by flow arrows; downward flow arrows denote recharge areas, and upward flow arrows denote discharge areas. The maximum flow velocity predicted by this model is on the order of 13.6 m/yr near the recharge and discharge areas. Deep regional groundwater flow is not examined by this study, as only the shallow aquifers are investigated.

Density-driven groundwater flow occurs where there is a contrast in groundwater salinity in the aquifers, where saltwater migrates vertically or laterally in response to pressure gradients exerted by the density variation between saline water and freshwater [Bethke et al., 2003; Penny et al., 2003]. Density-driven groundwater flow predicted in the study area is associated with lateral intrusion and vertical infiltration of high salinity water.

### **Lateral Saltwater Intrusion Models**

The first set of modeling simulates groundwater flow and solute (salt) transport influenced by lateral saltwater intrusion for three sea level rise scenarios at 1 meter (Figure 33), 2 meters (Figure 34), and 5 meters (Figure 35). In the model, salinity of seawater and groundwater along the land surface was set to 0.5 molal and 0, respectively. The model calculates a steady state solution for coupled groundwater flow and salt transport by advection and dispersion. Both topographically and density-driven flow are included in the simulations. Each graphic output displays simulated groundwater flow, salinity distribution, a salinity contour at 1000 ppm, and a

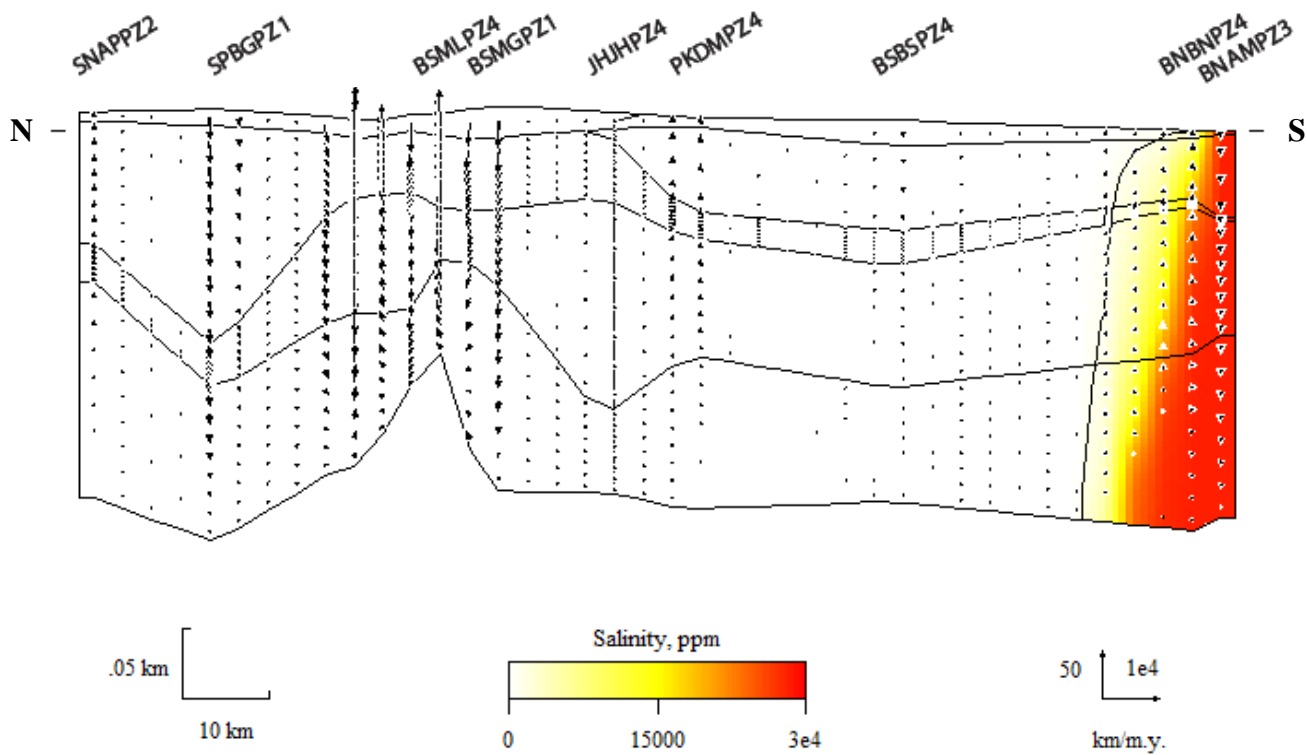


**Figure 33.** Lateral infiltration model with 1000 ppm salinity contour, 1 meter sea level rise

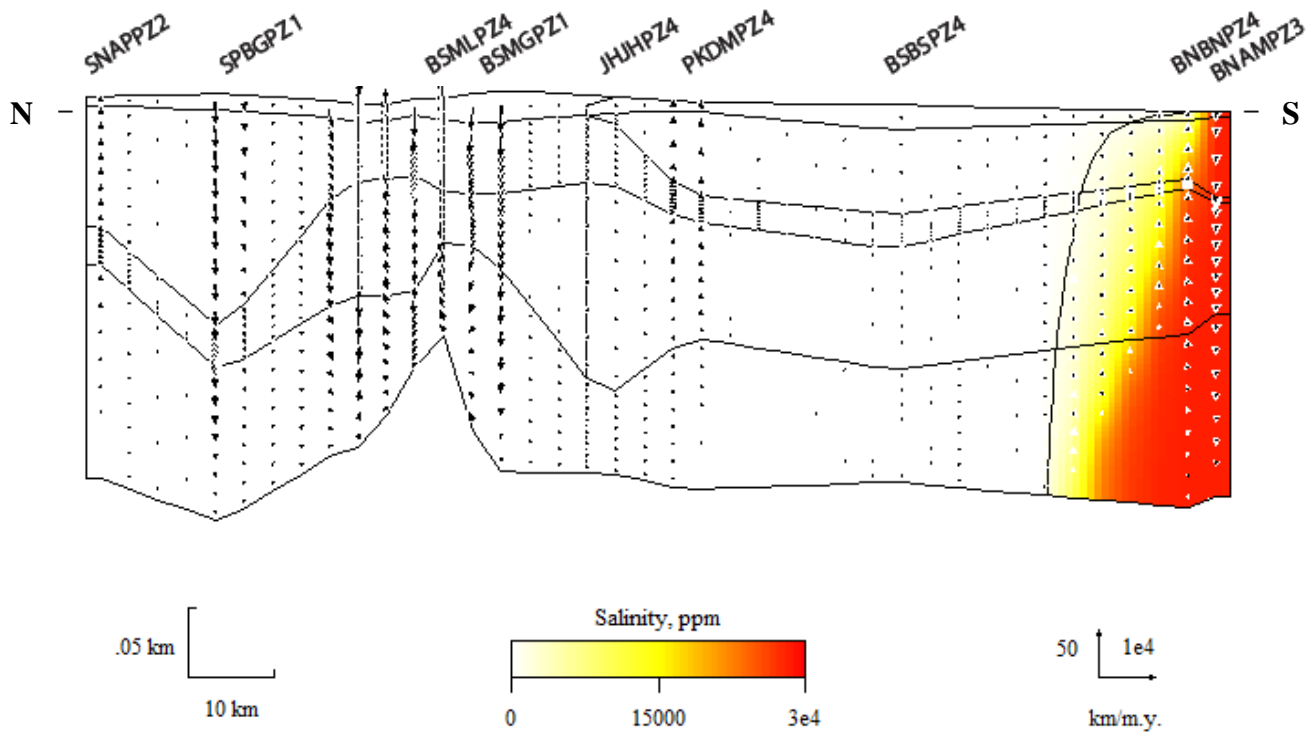


**Figure 34.** Lateral infiltration model with 1000 ppm salinity contour, 2 meter sea level rise

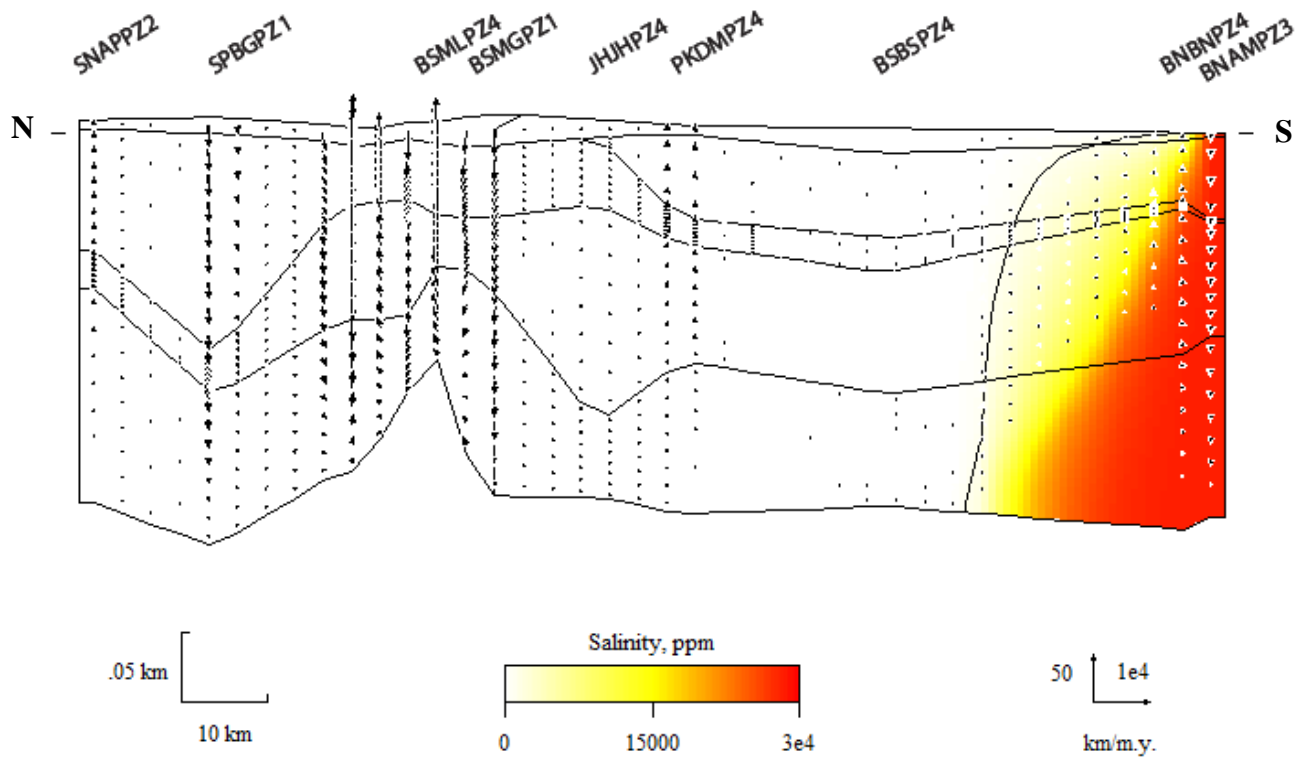


**Figure 35.** Lateral infiltration model with 1000 ppm salinity contour, 5 meter sea level rise

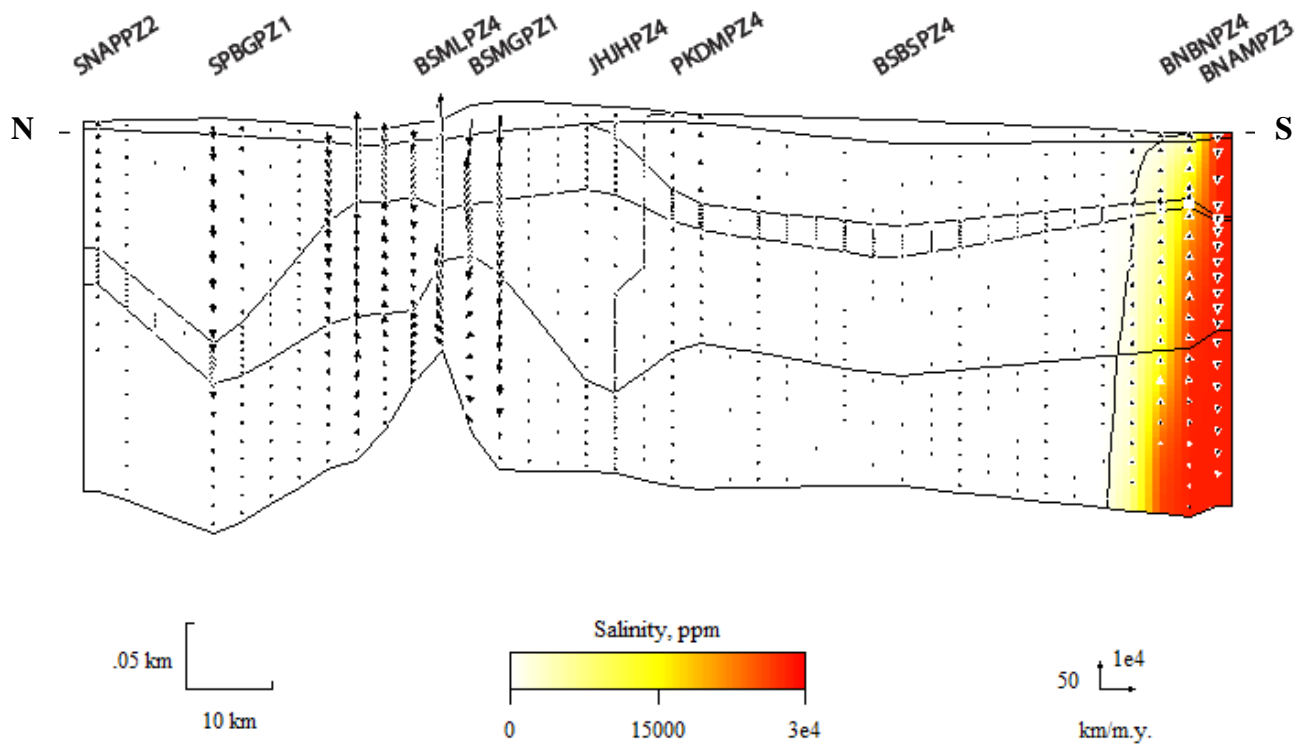


**Figure 36.** Sensitivity analysis for lateral infiltration model, 5 meter sea level rise

saltwater-freshwater interface, with a salinity of 0.5 molal (of seawater) represented by red, 0 molal (of freshwater) denoted by white, and a zone of mixing and diffusion along the interface displayed in yellow. The size of the zone of diffusion is controlled by the dispersive characteristics (see equations 2 and 3) of the geologic layers [Freeze and Cherry, 1979]. The diffusion coefficient  $D^*$  is assumed to be  $1.5 \times 10^{-5} \text{ cm}^2/\text{sec}$  in the simulations. The values of dispersivity and permeability tend to increase with the scale of observation due to geologic heterogeneity [Wheatcraft and Tyler, 1988; Gelhar et al., 1992], thus the variations in dispersivity and permeability represent sources of uncertainty in modeling salinity distribution in aquifers. These dispersivity values used in the model (about 10% of the width of cross sections) are in the same range as those used in the simulations of large-scale migration of salt plumes [Konikow and Bredehoeft, 1974; Domenico and Robbins, 1985; Person and Garven, 1994].

The lateral infiltration models shown in figures 33, 34, and 35 are for transect NS2, which runs in a northeastern to southwestern direction in central coastal Bangladesh (Figure 12). Figures 33-35 show various degrees of lateral saltwater intrusion with the saltwater-freshwater interface dipping landward, which is consistent with the shape of the saltwater wedge predicted by the Ghyben-Herzberg relation [Ghyben, 1888; Herzberg, 1901]:

$$z_s = 40z_w$$

where  $z_s$  is the depth of the saltwater interface below sea level and  $z_w$  is the height of freshwater above sea level. According to this principle, the depth to the saltwater interface is approximately 40 times the height of the freshwater table above sea level. The Ghyben-Herzberg relationship represents a simplified hydrostatic balance model of lateral inturusion, as it does not take into account dynamic groundwater flow influenced by hydraulic gradients or hydaulic conductivity. In the 1m scenario, the predicted saltwater-freshwater interface, defined as groundwater salinity

of 1000 ppm, is located approximately 18 kilometers inland at the bottom of the main aquifer. The interface is located approximately 15 kilometers inland at the bottom of the shallow aquifer. At a 2 meter sea level rise (Figure 34), the saltwater-freshwater interface is moving landward and upward, located approximately 22 kilometers inland at the bottom of the main aquifer and approximately 18 kilometers inland at the bottom of the shallow aquifer. Figure 35 shows a 5 meter sea level rise, where the saltwater-freshwater interface moves farther landward and extends approximately 30 kilometers inland at the bottom of the main aquifer and approximately 25 kilometers inland at the bottom of the shallow aquifer. According to actual field salinity data (Figures 29-32), the contours of 1000 mg/L TDS are located farther inland (in many locations more than 100 km from coast line) as compared to those predicted by lateral intrusion models, indicating that water salinization processes may be influenced by other mechanisms (i.e., vertical infiltration via tidal channels or groundwater pumping). The predicted saltwater freshwater interfaces in Figures 33-35 only consider lateral saltwater intrusion from oceans and reflect a steady state which has fully adjusted to specified boundary conditions of freshwater table and sea level.

Figure 36 shows results of the sensitivity analysis for lateral intrusion models, which was performed to illustrate how a higher hydraulic gradient of freshwater may control the front of lateral intrusion. This was done by raising the elevation of the existing topographic high by 5 meters and creating steeper hydraulic gradients in the downgradient (southward) direction of fresh groundwater flow. The sensitivity analysis was performed on the 5 meter sea level rise scenario. Flow arrows in Figure 36 show that the higher hydraulic gradient allows fresh groundwater to move farther toward the south, which helps to push the front of saltwater

oceanward and results in a smaller saltwater wedge, a steeper slope of the saltwater-freshwater interface, and a smaller zone of diffusion.

Lateral seawater intrusion is very problematic for Bangladesh, as a 1 meter sea level rise is predicted to occur in the next 58-63 years (Table 1). In the southern areas of coastal Bangladesh, the shallow aquifer does not meet drinking water quality standards, so the main aquifer that is currently used for potable water will begin to be contaminated with saline water. A deeper aquifer (>300 m) is being investigated as a potential drinking water source for Bangladesh [BWDB, 2013], but lateral intrusion may have already impacted the deep aquifer in the southern areas.

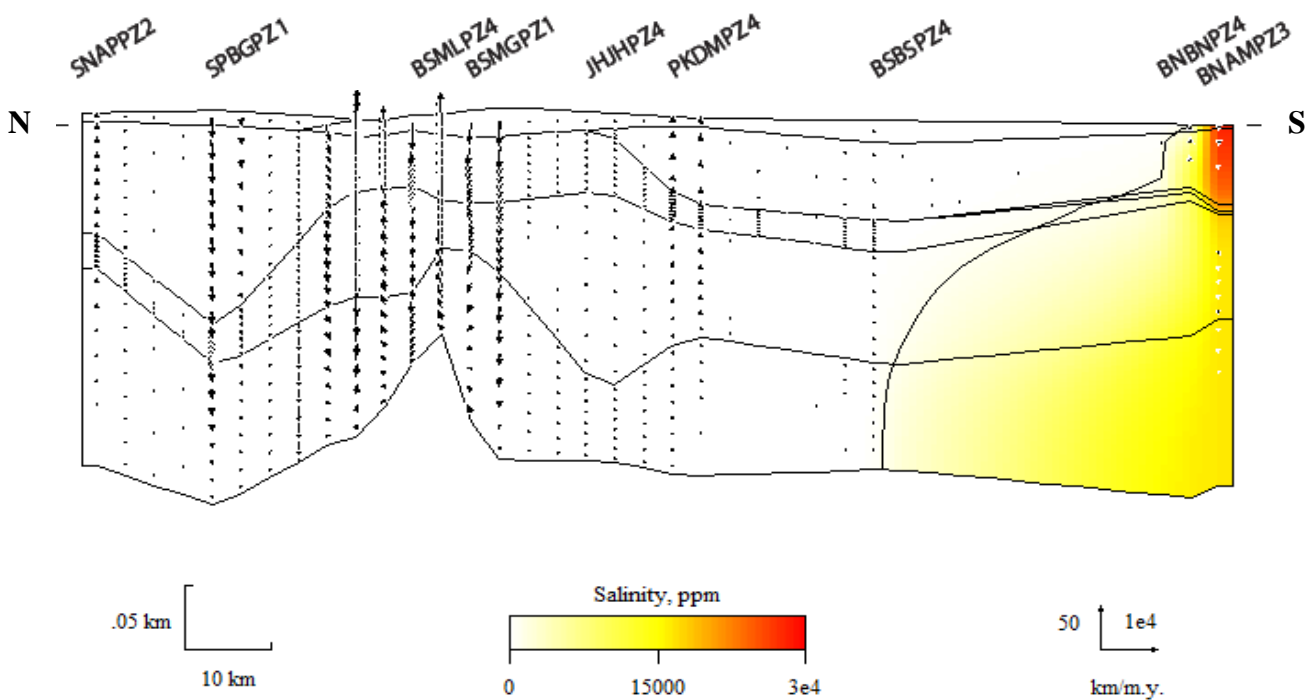


**Figure 37.** Lateral intrusion model at 5 meter sea level rise with confining clay

It should be noted that the groundwater and salinity distribution models cannot fully account for the complexity of discontinuous and interbedded layers present in coastal

Bangladesh. The actual stratigraphy is much more interbedded than the models are able to define, and stratigraphy complexity may not be captured by existing well logs. A sensitivity analysis shows that the presence of a confining clay layer in the coastal area could restrict the saltwater to the shallow layers and shows a large landward zone of diffusion in the deep layers (Figure 37). More deep monitoring wells in the coastal areas would also be useful for better defining the strata and corresponding porosities and permeabilities. Nevertheless, the models presented in this study represent a first order effort to examine the effects of sea level rise on the potential extent of lateral saltwater intrusion in coastal Bangladesh.

### **Vertical Saltwater Infiltration Models**

Vertical infiltration of saline surface water in the study area is a result of density-driven downward flow from brackish tidal channels into the layers below, and models of groundwater flow and salinity distribution were constructed along four transects: EW1 (Figure 38), EW2 (Figure 40), NS1 (Figure 42), NS2 (Figure 44). There is evidence that vertical infiltration of saline water is already occurring in southern Bangladesh, which was shown by high TDS concentrations in tidal channels (Figure 28) and in the underlying shallow aquifer (Figure 31 and Figure 32). Sensitivity analysis was also performed by adding a confining clay layer below the shallow aquifer in the area of the tidal channels for the four transects: EW1 (Figure 39), EW2 (Figure 41), NS1 (Figure 43), and NS2 (Figure 45). The salinity distribution maps and water quality data indicate that the salinity is much higher in the shallow aquifer (up to 22,600 mg/l) than in the deep aquifer (up to 7,861 mg/l), indicating that the downward infiltration of saline water may be locally blocked by the presence of a confining layer between shallow and deeper aquifers.

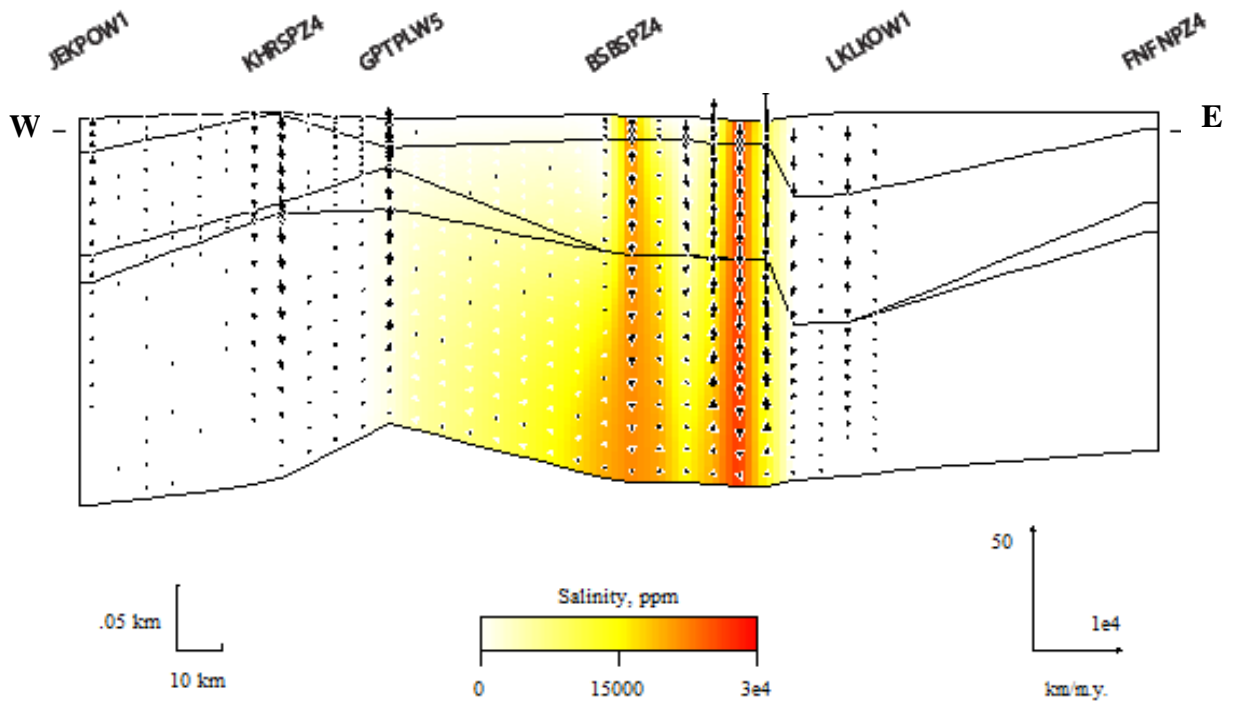


Figure 38. Vertical infiltration model, transect EW1

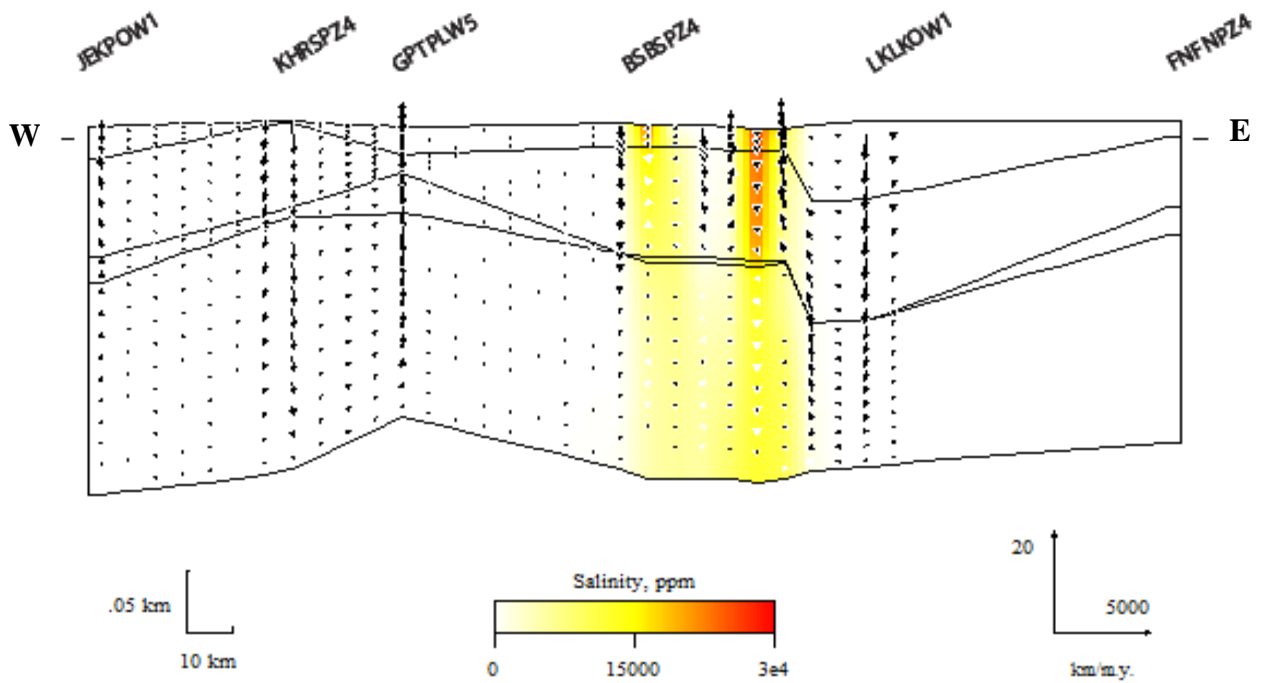
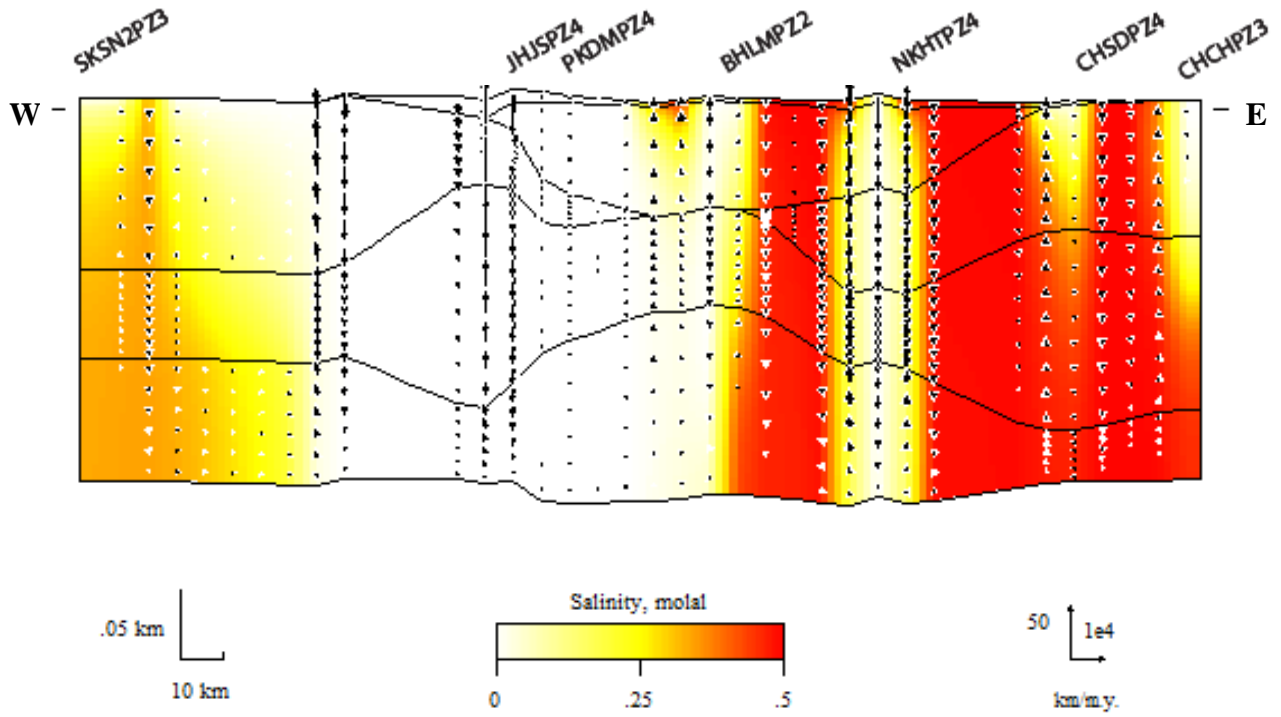
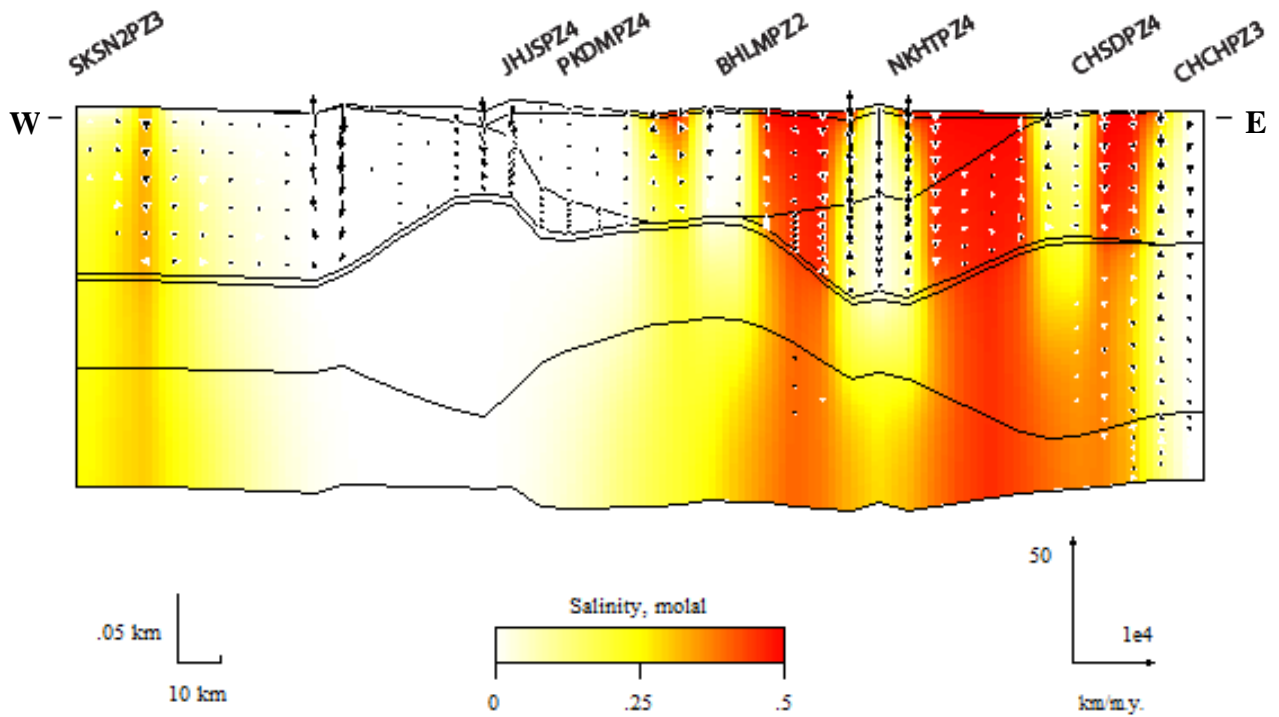


Figure 39. Vertical infiltration sensitivity analysis model, transect EW1



**Figure 40.** Vertical infiltration model, transect EW2



**Figure 41.** Vertical infiltration sensitivity analysis model, transect EW2

Transect EW1 (Figure 38) crosses two tidal channels, including the main distributary of the delta, between the Barisal and Noakhali districts. The modeling results show that freshwater groundwater recharges downward from local topographic highs and travels short-distance laterally before it discharges back to the surface. Saline surface water infiltrates downward from tidal channels in topographically low areas. Topographically low areas usually host upward groundwater discharge in a gravity-flow regime; however, in this simulation, the low elevation tidal channels host downward density-driven flow. High salinity sourced from the larger tidal channel extends from the surface to the bottom of the main aquifer, with a diffusion zone extending in a westward direction toward the Jessore district. Freshwater recharges to the east of the channel near a local topographic high, and as a result the high salinity plume originated from the smaller tidal channel extends only to the bottom of the shallow aquifer to the west. The sensitivity analysis model for this transect (Figure 39) shows the highest concentrations of salinity restricted to the shallow aquifer by the presence of a confining clay layer, which blocks the downward penetration of the saline plume to the deeper aquifer.

Transect EW2 crosses at least 4 to 5 small tidal channels in the west and the northernmost part of the Bay of Bengal in the east (Figure 40). The model of this transect shows saline water to the east along the Bay of Bengal, where small islands have isolated freshwater lenses surrounded by brackish water in the diffusion zone. To the west, one small tidal channel shows intrusion of brackish water to the bottom of the main aquifer with a wide zone of diffusion. The sensitivity analysis for this model (Figure 41) again shows that the presence of a local confining clay layer prevents the infiltration of some saltwater into the deeper layers in the eastern districts, but the area still has a very large diffusion zone and saltwater in the main aquifer. In the west,

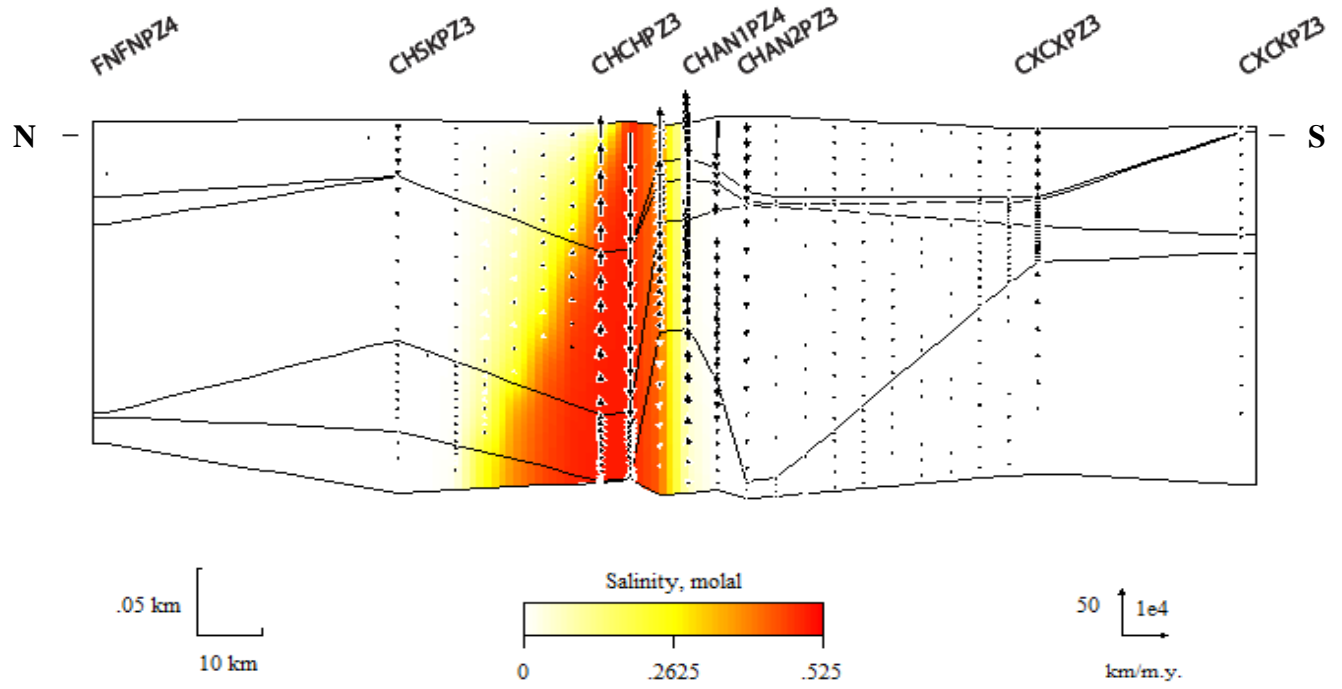


**Figure 42.** Vertical infiltration model, transect NS1

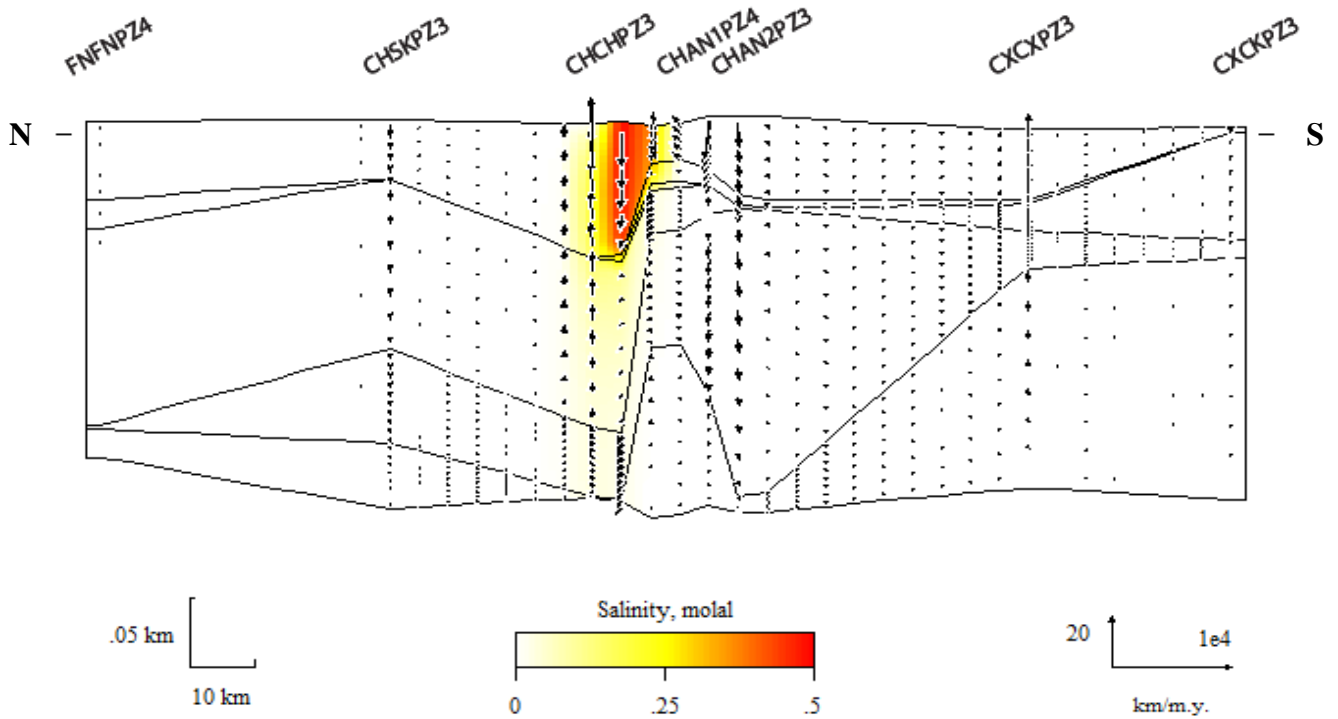


**Figure 43.** Vertical infiltration sensitivity analysis model, transect NS1

brackish water still reaches the bottom of the main aquifer, but the confining clay layer minimizes the size of the dispersion area.

Transect NS1 crosses only one tidal channel in the Chittagong district. The vertical intrusion model (Figure 42) shows vertical intrusion with the wedge shape that spreads laterally. The wedge extends in the northern direction, with a small zone of diffusion on both the northern and southern sides. The sensitivity analysis model for this transect (Figure 43) shows that the confining clay layer below the shallow aquifer changes the shape of the saltwater intrusion from a large wedge to a narrow plume and restricts the highest concentrations to the shallow aquifer. The zone of diffusion remains close to the intrusion and does not reach the underlying main aquifer. This model is consistent with the salinity distribution maps showing higher salinity in the shallow aquifer as compared to the main aquifer.

Transect NS3 crosses five tidal channels as it runs in a northeast to southwest direction in central coastal Bangladesh. The vertical intrusion model (Figure 44) shows that three of the smaller tidal channels have little to no intrusion into the shallow aquifer with small zones of diffusion immediately around the tidal channels. Two larger, wider tidal channels show substantial saltwater intrusion in a vertical direction extending to the bottom of the main aquifer, with zones of diffusion on both sides of the intrusions. The sensitivity analysis model (Figure 45) shows that a confining clay layer restricts the highest concentrations of saline water to the shallow aquifer, and causes the zone of diffusion to extend in both a northern and southern direction in the main aquifer.

In summary, all transects show some degree of vertical intrusion occurring around the tidal channels. Small tidal channels show that saltwater intrusion is restricted mainly to the top layers with a small zone of diffusion, while larger tidal channels show that saltwater intrusion

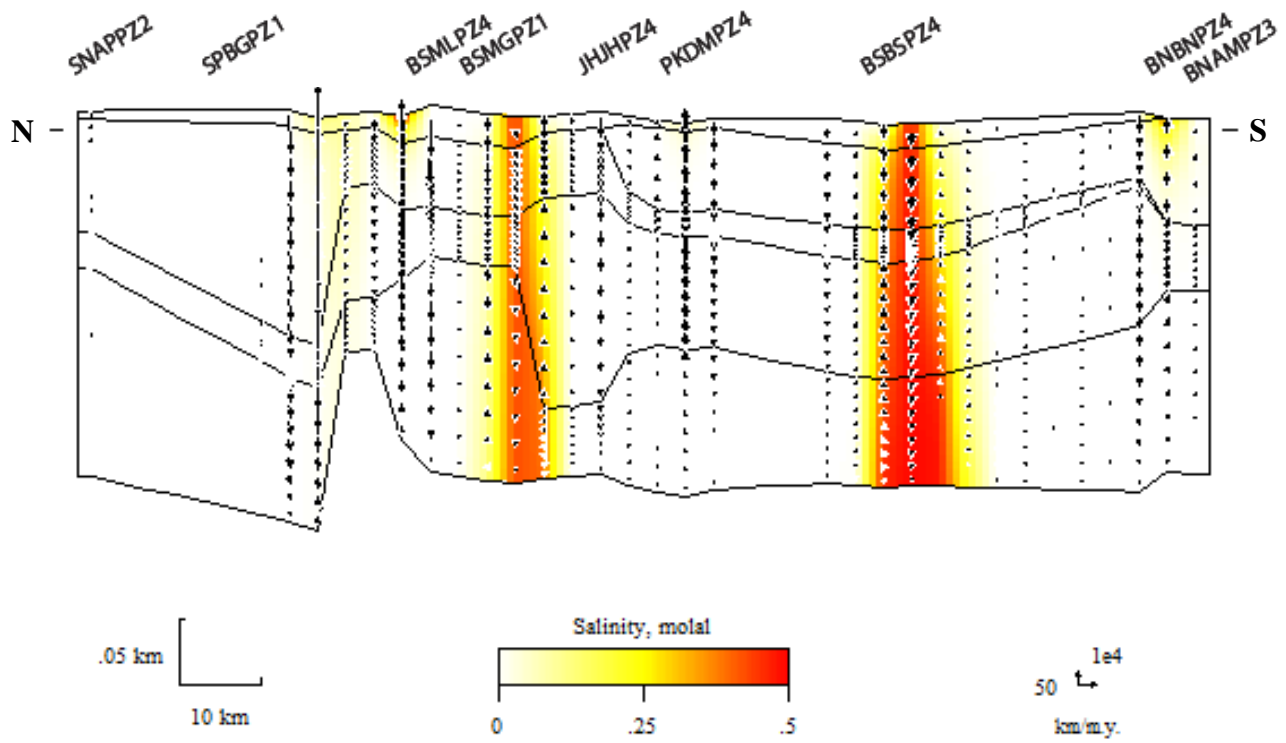


**Figure 44.** Vertical infiltration model, transect NS2

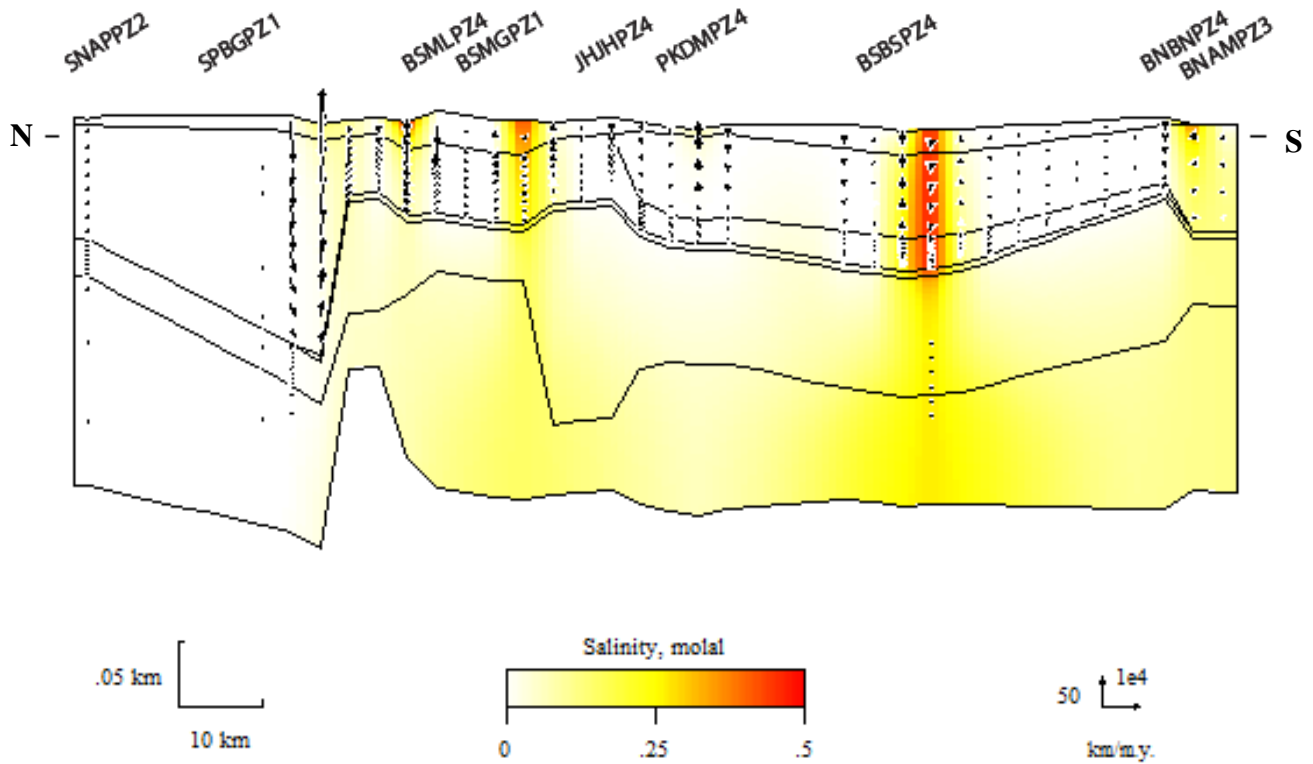


**Figure 45.** Vertical infiltration sensitivity analysis model, transect NS2

can extend to the deepest layers with zones of diffusion extending in a north-to-south or east-to-west direction. Sensitivity analysis for these models was performed by adding a confining clay layer beneath the shallow aquifer to simulate the interbedded nature of coastal hydrostratigraphy. The addition of a confining clay layer effectively prevents the highest concentrations of saltwater from reaching the deep layers and main aquifer, although in some scenarios can result in a wider zone of diffusion. More information about the distribution of confining clay lenses throughout the basin would be helpful in creating a more accurate model of vertical saltwater intrusion.

### **Vertical and Lateral Infiltration Model**

One model was created along the transect NS3 to examine the combined effects of both vertical and lateral infiltration (Figure 46). This model includes vertical infiltration from four a confining clay layer that extends below the shallow aquifer. These conditions are most likely to represent field conditions based on water quality data and salinity distribution maps. This model shows that high salinity plumes from vertical intrusion are restricted to the shallow clay, interbedded, and sandy layers with localized zones of diffusion. The largest tidal channels shows a zone of diffusion that extends below the confining clay and into the deeper layers and main aquifer, where it travels in a southern direction following the local hydraulic gradients. Lateral intrusion from the ocean shows a saltwater wedge reaching the deepest layers with a zone of diffusion in the northern direction.

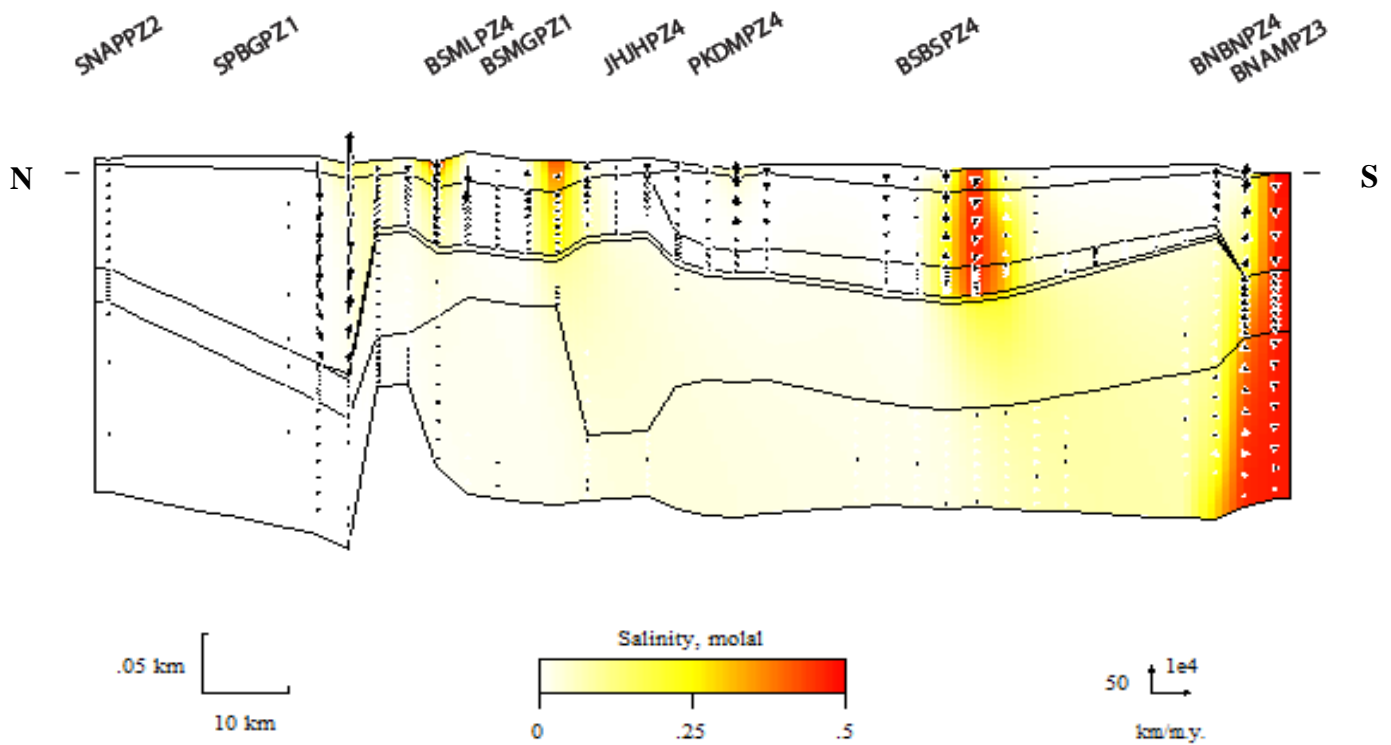


**Figure 46.** Lateral and vertical infiltration model with confining clay, transect NS3

### Arsenic Contamination

Previous studies have suggested that one mechanism for As release in the Bengal Basin may be from pH effects, as a pH exceeding 8.5 may lead to substantial desorption of adsorbed As, particularly As(V) in the anion form [Smedley and Kinniburgh, 2001], or may prevent sorbing from occurring due to ionic competition for sorbing sites [Smedley and Kinniburgh, 2001; Lee et al., 2013]. One objective of the current study is to determine if saltwater intrusion is causing As release in the study area as a result of the pH and salinity effect.

Figure 47 shows the relationship between As ( $\mu\text{g/l}$ ) and  $\text{Cl}^-$  ( $\text{mg/l}$ ) for all wells from the BWDB report. There appears to be no positive correlation between As and  $\text{Cl}^-$  in the study area; most wells with the highest As concentrations ( $>50 \mu\text{g/l}$ ) have relatively low  $\text{Cl}^-$  concentrations ( $<2500 \text{ mg/l}$ ). Data also show that the pH of the samples in the study area have an average of

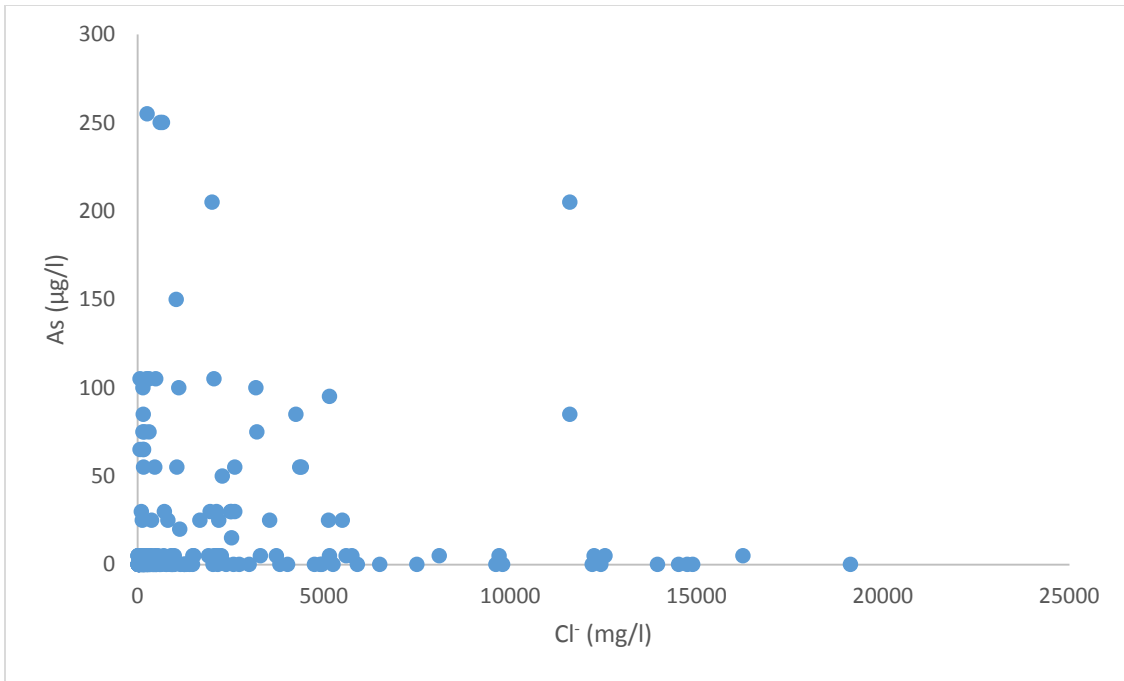


**Figure 47.** Plot of  $\text{Cl}^-$  (mg/l) v. As ( $\mu\text{g/l}$ ) for all wells in the study area

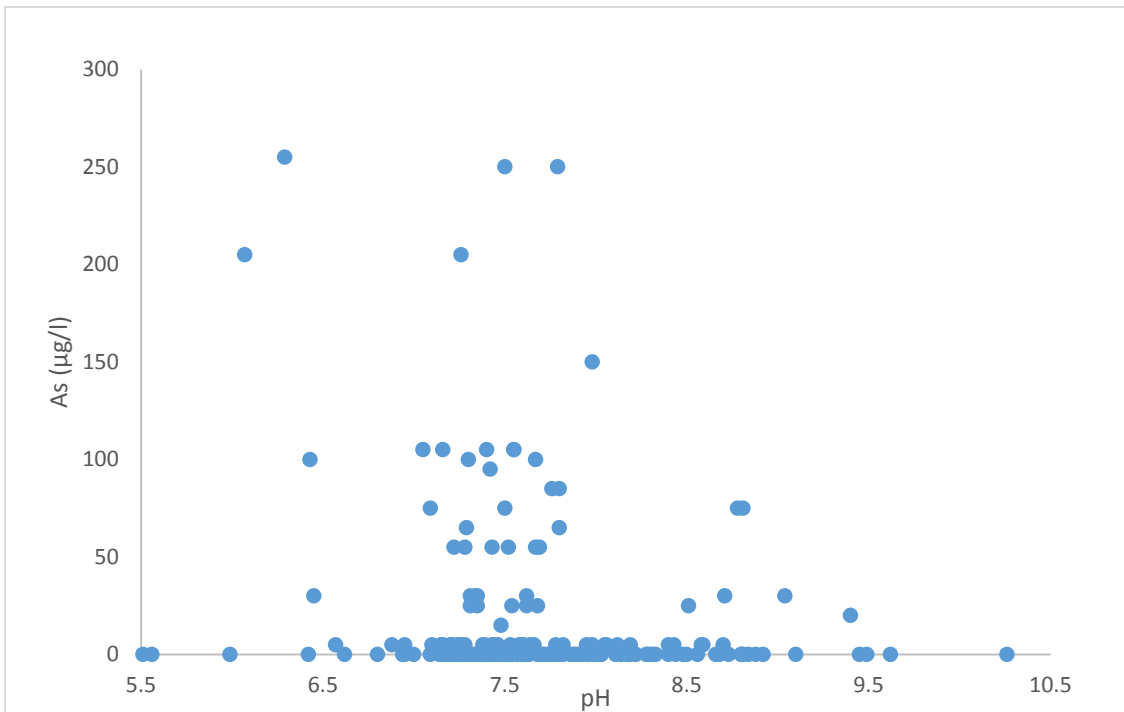


**Figure 48.** Plot of pH v. As ( $\mu\text{g/l}$ ) for all wells in the study area

7.75. Although data do not show a strong trend supporting the pH or salinity effect on As mobilization (Figure 48), it is likely that it will occur in the future as seawater intrusion continues to result in higher groundwater pH and salinity throughout the basin. It must also be noted that the mechanisms of As release are still not fully understood. Concentrations of As are widely variable [Smedley and Kinniburgh, 2001; Shamsudduha et al., 2009] and are influenced by a variety of processes and factors, including the presence of strongly-reducing conditions at neutral pH, the presence and distribution of Fe(III)-reducing bacteria and organic matter, bacterial sulfate reduction in S-rich marine environments, the abundance of As-enriched minerals, and rates of groundwater flow [Smedley and Kinniburgh, 2001; Ahmed et al., 2004; Saunders et al., 2005; Shamsudduha et al., 2009].

## Conclusions

In this study, the effects of sea level rise on water quality were assessed for coastal Bangladesh. Climate studies indicate that Bangladesh will experience high rates of change in temperature, precipitation, and runoff, as well as local sea level rise rates faster than the eustatic sea level rise projections. Groundwater is the main source for drinking water in Bangladesh, but As contamination from natural sources and water salinization from saltwater intrusion have severely degraded the water quality in the southern region. Sea level rise will complicate this problem by causing vertical infiltration of brackish water from tidal channels and lateral intrusion of seawater from the ocean into the aquifers. It is also likely that sea level rise will cause an increase in pH and salinity of the groundwater, which may result in the mobilization of more arsenic into the water as a result of ionic competition for sorbing sites or desorption of arsenate in anion form.

Sea level rise maps were produced using SRTM data for sea level rise scenarios at 1 meter, 2 meters, and 5 meters. At 1 meter of sea level rise, inundation occurs mostly in southwestern Bangladesh and along the Ganges River floodplain, with 107 upazilas affected and up to 28 million people living in the area. At 2 meters of sea level rise, inundation extends from the southwestern area in a northeastern direction toward Dhaka, as well as along the Ganges floodplain and along tidal channels in the southern area. There are 149 upazilas affected in this scenario and over 39 million people living in the affected area. At 5 meters of sea level rise, most of southwestern Bangladesh experiences land loss, as well as the floodplains of all three

GBM Rivers. 264 upazilas experience some degree of inundation, with over 71 million people living in the affected areas.

Cross-sections and hydrostratigraphy were reconstructed for two east-west transects and two north-south transects for groundwater and salt transport modeling. The hydrostratigraphy of the region shows that there is a shallow (1<sup>st</sup>) aquifer with a depth ranging between 0-125 m and a main (2<sup>nd</sup>) aquifer with a depth ranging between 60 and 200 meters. The layers are mostly fine sand and clay, with isolated medium to coarse-grained sand and silt. The stratigraphy is highly interbedded, and layers are rarely continuous or well-defined throughout the study area. Isolated clay lenses occur throughout the region and can act as confining layers above or below the aquifers.

Hydrochemical facies of major ions were analyzed using piper diagrams for wells from both the 2013 BWDB and 2001 BGS studies. The water type is highly variable, with Na-Ca-Mg-HCO<sub>3</sub> as the dominant water type and Na-Cl type in some areas impacted by saltwater intrusion. Wells from both the shallow and deep layers show that there is a trend toward Na-Cl type water in wells close to the Bay of Bengal and tidal channels; however, not all data are explained by this trend. It is likely that pumping of drinking water wells and the distribution of clay lenses and freshwater lenses causes outliers.

Water salinity was examined for surface water sampling locations, shallow wells, and deep wells. Surface water salinity shows that all locations have a higher salinity in the dry season than in the wet season; RCMs and GCMs for the region suggest that the dry seasons will become drier and wet seasons will become wetter, which is likely to exacerbate the problems of water salinization during dry seasons or droughts. Groundwater salinity distribution maps were produced for both shallow and deep wells and indicate that the shallow aquifer has a higher mean

(4517 mg/l) and wider range (96 to 25,422 mg/l) of TDS concentrations than the mean (1213 mg/l) and range (123 to 8814 mg/l) of the main aquifer, likely reflecting widespread vertical infiltration of brackish water from tidal channels. The main aquifer has some areas with TDS concentrations under the drinking water limit, located mostly in the north and east of coastal Bangladesh. The shallow aquifer has fewer areas with TDS concentrations under the drinking water limit, and none of these areas are located in the coastal districts. The distribution of salinity in the lower range (500-1000 mg/l) during the wet season in the eastern Chittagong district indicates faster flushing rates that result from the monsoon.

Lateral saltwater intrusion models were constructed for the sea level rise scenarios of 1 meter, 2 meters, and 5 meters for transect NS2. These models show a saltwater wedge consistent with the shape predicted by the Ghyben-Herzberg relation. The saltwater wedge extends 12 kilometers inland in the 1 meter rise scenario, 18 kilometers inland in the 2 meter rise scenario, and 25 kilometers inland in the 5 meter rise scenario. Sensitivity analysis for these models shows that saltwater intrusion can be limited by an increase in the freshwater hydraulic gradients in the southern direction or by the presence of a confining clay layer in the coastal region.

Vertical saltwater infiltration models were constructed for 4 transects by setting a salinity of 0.5 molal in all tidal channels that cross the transect. All models show that small tidal channels have a local effect with a infiltration into the shallow layers, while larger tidal channels affect a larger area and can reach the deeper layers and main aquifer. Sensitivity analysis for these models shows that the presence of a confining clay layer restricts intrusion of saline water into the deeper layers, but can cause a larger zone of diffusion in both shallow and deeper strata. One sensitivity analysis model combining lateral and vertical infiltration shows that saline water

is restricted to the areas adjacent to tidal channels and the Bay of Bengal, while a mixing zone is extensive throughout the area in both shallow and deep layers.

Lastly, As concentrations were compared to  $\text{Cl}^-$  concentrations for all BWDB wells and showed no positive correlation. Whereas the pH and salinity effect from saltwater intrusion can cause the mobilization of As in this area, the pH of wells included in this study have a mean of 7.75, which is below the arsenate desorption threshold of 8.5 where the pH effect becomes apparent. It is likely that other mechanisms (e.g., bacterial reduction of iron oxides, chemical weathering, and bacterial sulfate reduction) are responsible for As release [Saunders et al., 2008], but the pH effect could become problematic in the future should seawater intrusion continue to drive up pH in the aquifers.

Continuing to monitor the wells in the BWDB network is necessary for fully understanding how groundwater quality will respond to the effects of climate change and sea level rise. More wells would be useful for gaining a complete picture of spatial and temporal variations in subsurface geology water quality.

## References

- Abhyankar, L.N., M.R. Jones, E. Guallar, and A. Navas-Acien (2012), Arsenic exposure and hypertension: a systematic review, *Environmental Health Perspectives*, 120 (4), 494-500. doi: 10.1289/ehp.1103988.
- Ahmed, K.M., P. Bhattacharya, M.A. Hasan, S.H. Akhter, S.M.M. Alam, M.A.H. Bhuyian, M.B. Imam, A.A. Khan, and O. Sracek (2004), Arsenic enrichment in groundwater of the alluvial aquifers in Bangladesh: an overview, *Applied Geochemistry*, 19 (2), 181-200, doi:10.1016/j.apgeochem.2003.09.006.
- Alam, M., M.M. Alam, J.R. Curray, M.L.R. Chowdhury, and M.R. Gani (2003), An overview of the sedimentary geology of the Bengal Basin in relation to the regional tectonic framework and basin-fill history, *Sedimentary Geology*, 155 (3-4), 179-208, doi:10.1016/S0037-0738(02)00180-X.
- Bethke, C.M., M.-K. Lee, H.A.M. Quinodoz, and W.N. Kreiling (2003), Basin modeling with Basin2: A guide to using Basin2, B2plot, B2video, and B2view, Hydrogeology Program, University of Illinois, Urbana.
- Bhattacharya, P., D. Chatterjee, and G. Jacks (1997), Occurrence of arsenic-contaminated groundwater in alluvial aquifers from delta plains, eastern India: options for safe drinking water supply, *International Journal of Water Resources Development*, 13(1), 79-92, doi: 10.1080/07900629749944.
- Bangladesh Water Development Board (2013), Hydro-geological study and mathematical modelling to identify sites for installation of observation well nests, selection on model

- boundary, supervision of pumping test, slug test, assessment of different hydro-geological parameters, collection and conduct chemical analysis of surface water and groundwater, Tech. Report, 7 volumes, BWDB, Dhaka, Bangladesh.
- British Geological Survey and Department of Public Health Engineering (2001), Arsenic Contamination of Groundwater in Bangladesh, Vol. 2., BGS Technical Report, 630 pp.
- Chotamonsak, C., E. Salathe, Jr., J. Kreasuwan, S. Chantara, and K. Siriwitayakom (2011), Projected climate change over Southeast Asia simulated using a WRF regional climate model, *Atmospheric Science Letters*, 12(2), 213-219, doi: 10.1002/asl.313.
- Church, J.A., and N.J. White (2006), A 20th century acceleration in global sea-level rise, *Geophysical Research Letters*, 33(1), L01602, doi:10.1029/2005GL024826.
- Domenico, P.A., and G.A. Robbins (1985), The displacement of connate water from aquifers, *Geological Society of America Bulletin.*, 96(2), 328-335, doi: 10.1130/0016-7606(1985)96.
- Dowling, C.B., R.J. Poreda, A.R. Basu, S.L. Peters, and P.K. Aggarwal (2002), Geochemical study of arsenic release mechanisms in the Bengal Basin groundwater. *Water Resources Research*, 38(9), 12-18 , doi: 10.1029/2001WR000968.
- Freeze, R.A., and J.A. Cherry (1969), *Groundwater*, 1st ed., Prentice Hall, Upper Saddle River, NJ, USA.
- Gelhar, L.W., C. Welty, and K.R. Rehfeldt (1992), A critical review of data of field-scale dispersion in aquifers, *Water Resources Research*, 28(7), 1955-1974, doi: 10.1029/92WR00607.

- Ghyben W. B. (1888), Nota in verband met de voorgenomen putboring nabij Amsterdam (Notes on the probably results of proposed well drilling near Amsterdam, in Dutch), Tijdschrift van het Koninklijk Inst. van Ing.
- Herzberg, A (1901), Die Wasserversorgung einiger Nordseebäder (The water supply of part of the North Sea coast in Germany, in German), *J. Gasbeleucht, Wasserversorg*, 44, 815-819.
- Hume, T. (2013), Report: Climate change may pose threat to economic growth, CNN.
- Immerzeel, W. (2007), Historical trends and future predictions of climate variability in the Brahmaputra basin, *International Journal of Climatology*, 28(2), 243-254, doi: 10.1002/joc.1528.
- IPCC (2014), *Climate Change 2014: Impacts, Adaptation, and Vulnerability, Part A: Global and Sectoral Aspects, Contribution of Working Group II to the Fifth Assessment Report of the Intergovernmental Panel on Climate Change*, edited by C.B. Field et al., Cambridge University Press, Cambridge, United Kingdom and New York, NY, USA, 1132 pp.
- Islam, F., A. Gault, C. Boothman, D. Polya, J. Charnock, D. Chatterjee, and J. Lloyd (2004), Role of metal-reducing bacteria in arsenic release from Bengal delta sediments, *Nature*, 430, 68-71, doi: 10.1038/nature02638.
- Konikow, L.F., and J.D. Bredehoeft (1974), Modeling flow and chemical quality changes in an irrigated aquifer system, *Water Resources Research*, 10(3), 546-562, doi: 10.1029/WR010i003p00546.
- Kuehl, S.A., M.A. Allison, S.L. Goodbred, and H. Kudrass (2005), The Ganges-Brahmaputra Delta, In: *River Deltas – Concepts, Models, and Examples*, SEPM Special Publication

- No. 83, edited by L. Gosian and J. Bhattacharya, p. 413-434, Society for Sedimentary Geology.
- Lee, M.-K., J. Griffin, J.A. Saunders, Y. Wang, J. Jean (2007), Reactive transport of trace elements and isotopes in Alabama coastal plain aquifers, *Journal of Geophysical Research*, 112, G02026, doi:10.1029/2006JG000238.
- Lee, M.-K., M. Natter, J. Keevan, K. Guerra, J. Saunders, A. Uddin, M. Humayun, Y. Wang, and A. R. Keimowitz (2013), Assessing effects of climate change on biogeochemical cycling of trace metals in alluvial and coastal watersheds, *British Journal of Environment & Climate Change*, 3, 44-66, doi: 10.9734/BJECC/2013/3061.
- Michael, H.A. and C.I. Voss (2009), Controls on groundwater flow in the Bengal Basin of India and Bangladesh: regional modeling analysis, *Hydrogeology Journal*, 17(7), 1561-1577, doi:10.1007/s10040-008-0429-4.
- Michels, K.H., H. R. Kudrass, C. Hubscher, A. Suckow, M. Wiedicke (1998), The submarine delta of the Ganges-Brahmaputra: cyclone-dominated sedimentation patterns, 149(1-4), 133-154, doi: 10.1016/S0025-3227(98)00021-8.
- Mitra, A.K., B.K. Bose, H. Kabir, B.K. Das, M. Hussain (2002), Arsenic-related health problems among hospital patients in southern Bangladesh, *J. Health Population and Nutrition*, 20(3), 198-204.
- Morgan, J.P., and W.G. McIntyre (1959), Quaternary Geology of the Bengal Basin, East Pakistan and India, *Geological Society of America Bulletin*, 70, 319-342, doi: 10.1130/0016-7606(1959)70.

- Navas-Acien, A., E.K. Silbergeld, R.A. Streeter, J.M. Clark, T.A. Burke, and E. Guallar (2006), Arsenic exposure and type 2 diabetes: A systematic review of the experimental and epidemiologic evidence, *Environmental Health Perspective*, 114, 641-648.
- Navas-Acien, A., E.K. Silbergeld, R. Pastor-Barriuso, and E. Guallar (2008), Arsenic exposure and prevalence of type 2 diabetes in US adults, *Journal of American Medical Association*, 300(7), 814-822. doi: 10.1001/jama.300.7.814.
- Nath, B., J.-S. Jean, M.-K. Lee, H.-J. Yang, and C. C. Liu (2008), Geochemistry of high arsenic groundwater in Chia-Nan plain, Southwestern Taiwan: Possible sources and reactive transport of arsenic, *Journal of Contaminant Hydrology*, 99, 85-96, doi: 10.1016/j.jconhyd.2008.04.005.
- Nicholls, R.J., and A. Cazenave (2010), Sea level rise and its impacts on coastal zones, *Science*, 328(5985), 1517-1520, doi: 10.1126/science.1185782.
- Nicholls, R.J., N. Marinova, J.A. Lowe, S. Brown, P. Vellinga, D. de Gusmao, J. Hinkel, and R. S. J. Tol (2010), Sea-level rise and its possible impacts given a 'beyond 4° C world' in the twenty-first century, *Philosophical Transactions of the Royal Society*, 373(2039), 161-181, doi: 10.1098/rsta.2010.0291.
- Nohara, D., A. Kitoh, M. Hosaka, and T. Oki (2006), Impact of climate change on river discharge projected by multimodel ensemble, *Journal of Hydrometeorology*, 7, 1076-1089, doi: <http://dx.doi.org/10.1175/JHM531.1>.
- Penny, E., M.-K. Lee, and C. Morton (2003), Groundwater and microbial processes of the Alabama coastal plain aquifers, *Water Resources Research*, 39(11), 1320-1337, doi:10.1029/2003WR001963.

- Person, M.E., and G. Garven (1994), A sensitivity study of the driving forces on fluid flow during continental-rift basin evolution, *Geological Society of America Bulletin.*, 106, 461-475, doi: 10.1130/0016-7606(1994)106.
- Pethick, J., and J.D. Orford (2013) Rapid rise in effective sea-level in southwest Bangladesh: its causes and contemporary rates, *Global and Planetary Change*, 111, 237-245, doi: 10.1016/j.gloplacha.2013.09.019.
- Saunders, J. A., M.-K. Lee, A. Uddin, S. Mohammad, R. Wilkin, M. Fayek, and N. Korte (2005), Natural arsenic contamination of Holocene alluvial aquifers by linked glaciation, weathering, and microbial processes, *Geochemistry, Geophysics, and Geosystems*, 6(4), Q04006, doi:10.1029/2004GC000803.
- Saunders, J. A., M.-K. Lee, M. Shamsudduha, P. Dhakal, A. Uddin, M.T. Chowdury, and K.M. Ahmed (2008), Geochemistry and mineralogy of arsenic in (natural) anaerobic groundwaters, *Applied Geochemistry*, 23(11), 3205–3214, doi:10.1016/j.apgeochem.2008.07.002.
- Shamsudduha, M., A. Uddin, J. A. Saunders, and M.-K. Lee (2008), Quaternary stratigraphy, sediment characteristics and geochemistry of arsenic-contaminated alluvial aquifers in the Ganges-Brahmaputra floodplain in central Bangladesh, *Journal of Contaminant Hydrology*, 99(2008), 112-136, doi: 10.1016/j.jconhyd.2008.03.010.
- Shamsudduha, M., L.J. Marzen, A. Uddin, M.-K. Lee, and J.A. Saunders (2009), Spatial relationship of groundwater arsenic distribution with regional topography and water-table fluctuations in the shallow aquifers of Bangladesh, *Environmental Geology*, 57(7), 1521-1535, doi: 10.1007/s00254-008-1429-3.

- Smedley, P.L. and D. G. Kinniburgh (2001), A review of the source, behavior and distribution of arsenic in natural waters, *Applied Geochemistry* 17(2002), 517-568.
- Smith, A., E. Lingas, and M. Rahman (2000), Contamination of drinking-water by As in Bangladesh, *Bulletin of the World Health Organization*, 78(9), 1093-1103.
- Sohel, N., M. Vahter, M. Ali, M. Rahman, A. Rahman, P.K. Streatfield, and L.A. Persson (2010), Spatial patterns of fetal loss and infant death in an arsenic-affected area in Bangladesh, *International Journal of Health Geographics*, 9, 53, doi: 10.1186/1476-072X-9-53.
- Uddin, A., and N. Lundberg (1998), Cenozoic history of the Himalayan-Bengal system: Sand composition in the Bengal basin, Bangladesh, *Geological Society of America Bulletin*, 110, 497-511, doi: 10.1130/0016-7606(1998)110.
- United Nations Environmental Programme (2008), *Vital Water Graphics: An overview of the state of the world's fresh and marine waters*, 2nd edition, Nairobi, Kenya.
- United Nations Office for the Coordination of Humanitarian Affairs (2014), *Bangladesh Baseline Data*, Humanitarian Data Exchange version 0.7.3.
- Wheatcraft, S.W., and S.W. Tyler (1988), An explanation of scale-dependent dispersivity in heterogeneous aquifer using concepts of fractal geometry, *Water Resources Research*, 24(4), 566-578, doi: 10.1029/WR024i004p00566.
- Vahter, M., A., Akesson, C. Liden, S. Ceccatelli, and M. Berglund (2007). Gender differences in the disposition and toxicity of metals, *Environmental Research*, 104(1), 85-95.
- Vahter, M., M. Berglund, A. Akesson, and C. Liden (2002), Metals and women's health, *Environmental Research*, 88(3), 145-155.

- van Geen, A., Y. Zheng, R. Versteeg, M. Stute, A. Horneman, R. Dhar, M. Steckler, A. Gelman, C. Small, H. Ahsan, J.H. Graziano, I. Hussain, and K.M. Ahmed (2003), Spatial variability of arsenic in 6000 tube wells in a 25 km<sup>2</sup> area of Bangladesh, *Water Resources Research*, 39 (5), 1140, doi:10.1029/2002WR001617.
- Zahid, A., M. Q. Hassan, and K. M. U. Ahmed (2014), Simulation of flowpaths and travel time of groundwater through arsenic-contaminated zone in the multi-layered aquifer system of Bengal Basin, *Environmental Earth Sciences*, 73(3), 979-991, doi: 10.1007/s12665-014-3447-7.

## Appendices

### Appendix 1 – Basin2 Input File: Lateral Infiltration (NS3, 1 meter rise)

```
run = steady; start = 0 yrs
nx = 40; delta_z = 20 m
temperature = vertical; heat_flow = 1 HFU
salinity = full; salt_flux = 0
under_relax = 0.04

rock cl
  phi0 = 55%; phi1 = 5%; bpor = .85
  A_perm = 8; B_perm = -5 log_darcy; p_kxkz = 10; perm_max = 1
rock si
  phi0 = 45%; phi1 = 5%; bpor = .6
  A_perm = 12; B_perm = -2 log_darcy; p_kxkz = 10; perm_max = 1
rock cs
  phi0 = 40%; phi1 = 5%; bpor = .5
  A_perm = 15; B_perm = 3 log_darcy; p_kxkz = 10; perm_max = 1
rock ms
  phi0 = 40%; phi1 = 5%; bpor = .5
  A_perm = 15; B_perm = 1 log_darcy; p_kxkz = 10; perm_max = 1
rock fs
  phi0 = 40%; phi1 = 5%; bpor = .5
  A_perm = 15; B_perm = -1 log_darcy; p_kxkz = 10; perm_max = 1

width = 135 km
x_well (km)    0    16    31    33    40.5  40.6  40.8  47    61    71
               95   130   132   135

Strat 'Sand2'
t_dep = -16000 yrs
column      thickness(m)    X(fs) X(si) X(ms) X(cs) X(cl)
w(1)        155.49          .47  .08  .18  0    .27
w(2)        106.7          .93  .07  0    0    0
w(3)        106.7          .93  .07  0    0    0
w(4)        106.7          .93  .07  0    0    0
w(5)        39.63          1    0    0    0    0
w(6)        39.63          1    0    0    0    0
w(7)        39.63          1    0    0    0    0
w(8)        158.54         .48  0    .27  .08  .17
w(9)        51.83          .34  .06  .31  .17  .12
w(10)       106.71         .49  .05  0    0    .46
w(11)       79.27          .61  .23  0    0    .16
```

w(12)	121.95	.1	.04	.14	.34	.38
w(13)	121.95	.1	.04	.14	.34	.38
w(14)	134.14	.26	.53	.03	0	.18

Strat 'IB2'

t\_dep = -10500 yrs

column	thickness(m)	X(fs)	X(si)	X(ms)	X(cl)	X(cs)
w(1)	27.43	.47	.08	.18	.27	0
w(2)	30.49	.1	.9	0	0	0
w(3)	82.32	.05	0	.24	.59	.12
w(4)	82.32	.05	0	.24	.59	.12
w(5)	82.32	.05	0	.24	.59	.12
w(6)	36.58	.25	0	0	.75	0
w(7)	36.58	.25	0	0	.75	0
w(8)	36.58	.25	0	0	.75	0
w(9)	155.48	.38	.21	.16	.23	.02
w(10)	82.32	.19	.59	0	.22	0
w(11)	85.36	.21	.24	0	.42	.13
w(12)	103.66	.27	.05	.21	.33	.14
w(13)	103.66	.27	.05	.21	.33	.14
w(14)	48.78	.65	.03	0	.32	0

Strat 'Sand1'

t\_dep = -6000 yrs

column	thickness(m)	X(fs)	X(ms)	X(si)	X(cl)	X(cs)
w(1)	79.27	.98	.02	0	0	0
w(2)	158.53	.85	0	.15	0	0
w(3)	42.68	.74	0	.21	.05	0
w(4)	42.68	.74	0	.21	.05	0
w(5)	42.68	.74	0	.21	.05	0
w(6)	51.83	.84	0	.04	.12	0
w(7)	51.83	.84	0	.04	.12	0
w(8)	51.83	.84	0	.04	.12	0
w(9)	48.78	.61	0	.39	0	0
w(10)	18.29	.62	.08	.13	.17	0
w(11)	24.39	.6	.2	.15	0	.05
w(12)	6.1	.9	0	.1	0	0
w(13)	6.1	.9	0	.1	0	0
w(14)	0	1	0	0	0	0

Strat 'IB1'

t\_dep = -1000 yrs

column	thickness(m)	X(fs)	X(si)	X(ms)	X(cl)
w(1)	0	1	0	0	0
w(2)	0	1	0	0	0
w(3)	0	1	0	0	0
w(4)	0	1	0	0	0
w(5)	0	1	0	0	0
w(6)	0	1	0	0	0
w(7)	0	1	0	0	0
w(8)	0	1	0	0	0
w(9)	0	1	0	0	0

w(10)	60.97	0	.8	0	.2
w(11)	60.98	.47	.49	0	.04
w(12)	42.68	0	.67	0	.33
w(13)	42.68	0	.67	0	.33
w(14)	79.27	0	.92	0	.08

Strat 'TopClay'

t\_dep = 0 yrs

column	thickness(m)	water_depth(m)	X(cl)	X(si)	X(fs)
	surface_conc(molal)				
w(1)	6.1	-13	1	0	0
w(2)	12.2	-15	0	.95	.05
w(3)	12.2	-9	0	.95	.05
w(4)	12.2	-5	0	.95	.05
w(5)	12.2	-13	1	0	0
w(6)	12.2	-9	1	0	0
w(7)	12.2	-9	1	0	0
w(8)	24.39	-18	1	0	0
w(9)	12.2	-13	.1	.9	0
w(10)	6.1	-9	1	0	0
w(11)	18.29	-7	.67	.33	0
w(12)	6.1	0	1	0	0
w(13)	6.1	0	1	0	.5
w(14)	0	0	1	0	.5

## Appendix 2 - Basin2 Input File: Vertical Infiltration (EW1)

```

run = steady; start = 0 yrs
nx = 40; delta_z = 20 m
temperature = vertical; heat_flow = 1 HFU
salinity = full; salt_flux = 0
under_relax = 0.04

rock cl
  phi0 = 55%; phil = 5%; bpor = .85
  A_perm = 8; B_perm = -5 log_darcy; p_kxkz = 10; perm_max = 1
rock si
  phi0 = 45%; phil = 5%; bpor = .6
  A_perm = 12; B_perm = -2 log_darcy; p_kxkz = 10; perm_max = 1
rock cs
  phi0 = 40%; phil = 5%; bpor = .5
  A_perm = 15; B_perm = 3 log_darcy; p_kxkz = 10; perm_max = 1
rock ms
  phi0 = 40%; phil = 5%; bpor = .5
  A_perm = 15; B_perm = 1 log_darcy; p_kxkz = 10; perm_max = 1
rock fs
  phi0 = 40%; phil = 5%; bpor = .5
  A_perm = 15; B_perm = -1 log_darcy; p_kxkz = 10; perm_max = 1

width = 228 km
x_well (km)      0      41.5 66      114    117.9 118    118.5 118.6 138.5 138.6
                  142.8 142.9 147.4 147.5 148.3 148.4 165    228

Strat 'IB1'
t_dep = -30000 yrs
column      thickness(m)      X(cl) X(fs) X(si) X(ms)
w(1)        155.49             .86   .08   .06   0
w(2)        198.17             0     1     0     0
w(3)        158.54             0     .5    .05   .45
w(4)        164.63             .3    .4    .24   .06
w(5)        164.63             .3    .4    .24   .06
w(6)        164.63             .3    .4    .24   .06
w(7)        164.63             .3    .4    .24   .06
w(8)        164.63             .3    .4    .24   .06
w(9)        164.63             .3    .4    .24   .06
w(10)       164.63             .3    .4    .24   .06
w(11)       164.63             .3    .4    .24   .06
w(12)       164.63             .3    .4    .24   .06
w(13)       112.80             .11   .83   .04   .02
w(14)       112.80             .11   .83   .04   .02
w(15)       112.80             .11   .83   .04   .02
w(16)       112.80             .11   .83   .04   .02
w(17)       112.80             .11   .83   .04   .02
w(18)       158.54             .42   .47   .08   .03

Strat 'Clay1'

```

```

t_dep = -11500 yrs
column      thickness(m)      X(cl) X(si)
w(1)        21.34             .95   .05
w(2)         6.1              .8    .2
w(3)        30.48            .65   .35
w(4)         0                1     0
w(5)         0                1     0
w(6)         0                1     0
w(7)         0                1     0
w(8)         0                1     0
w(9)         0                1     0
w(10)        0                1     0
w(11)        0                1     0
w(12)        0                1     0
w(13)        0                1     0
w(14)        0                1     0
w(15)        0                1     0
w(16)        0                1     0
w(17)        0                1     0
w(18)       21.34            1     0

```

Strat 'Sand1'

```

t_dep = -10500 yrs
column      thickness(m)      water_depth(m)  X(fs) X(si) X(cl) X(ms)
w(1)        76.22            -9              .8    .2    0    0
w(2)        70.12            -14             .8    .2    0    0
w(3)        15.25            -9              .9    .1    0    0
w(4)        85.37            -12             .51   .39   .04   .06
w(5)        85.37            -19             .51   .39   .04   .06
w(6)        85.37            -19             .51   .39   .04   .06
w(7)        85.37            -13             .51   .39   .04   .06
w(8)        85.37            -13             .51   .39   .04   .06
w(9)        85.37            -8              .51   .39   .04   .06
w(10)       85.37            -8              .51   .39   .04   .06
w(11)       85.37            -8              .51   .39   .04   .06
w(12)       85.37            -8              .51   .39   .04   .06
w(13)       94.51            -5              .075  .84   .085  0
w(14)       94.51            -5              .075  .84   .085  0
w(15)       94.51            -9              .075  .84   .085  0
w(16)       94.51            -9              .075  .84   .085  0
w(17)       94.51            -14             .8    .07   0    .13
w(18)       54.92            -14             1     0    0    0

```

Strat 'TopClay'

```

t_dep = 0 yrs
column      thickness(m)      water_depth(m)  X(cl) X(si) X(fs)
surface_conc(molal)
w(1)  27.44      -9              .95   .05   0    0
w(2)  0          -14             1     0    0    0
w(3)  21.34     -9              .64   .36   0    0
w(4)  18.29     -12             .67   .33   0    0

```

w(5)	18.29	-19	.67	.33	0	0		
w(6)	18.29	-19	.67	.33	0	1/2		
w(7)	18.29	-13	.67	.33	0	1/2		
w(8)	18.29	-13	.67	.33	0	0		
w(9)	18.29	-8	.67	.33	0	0		
w(10)	18.29	-8	.67	.33	0	1/2		
w(11)	18.29	-8	.67	.33	0	1/2		
w(12)	18.29	-8	.67	.33	0	0		
w(13)	60.98	-5	.075	.84	.085	0		
w(14)	60.98	-5	.075	.84	.085	1/2		
w(15)	60.98	-9	.075	.84	.085	1/2		
w(16)	60.98	-9	.075	.84	.085	0		
w(17)	60.98		-14		.075	.84	.085	0
w(18)	12.20		-14		1	0	0	0